QUANTITATIVE STUDY OF FREQUENCY CONTROL OF LASER DIODES WITH EMPHASIS ON PHASE-LOCKING AND ABSOLUTE FREQUENCY MEASUREMENT OF THE A_{10} R(56)32-0 TRANSITION IN IODINE AND $^{87}RB/D_2$ D/F CROSSOVER

by

Stephen Swartz

B.S. Rensselaer Polytechnic Institute 1983

M.S. University of Colorado 1987

A thesis submitted to the Faculty of the Graduate School of the

University of Colorado

in partial fulfillment of the requirement of the

Doctor of Philosophy, Department of Physics

1996

Swartz Stephen D. (Ph.D., Physics)

Quantitative Study of Frequency Control of Laser Diodes with Emphasis on Phase-Locking and: Absolute Frequency Measurement of the a_{10} R(56)32-0 Transition in Iodine and $^{87}Rb/D_2$ d/f Crossover.

Thesis directed by Lecturer John L. Hall

The laser diode holds great promise as a new source of coherent light for atomic and molecular spectroscopy. Until recently the frequency stability and line-width of these diodes has limited their usefulness. Low speed frequency control schemes don't have the bandwidth required to affect the laser's linewidth. To assess the required servo, a quantitative study of the problem has been made. The chief sources of noise in the laser diode are assumed to be Schawlow-Townes noise and 1/f noise. The expected lineshape from typical frequency noise sources is calculated using the Weiner-Khintchine theorem. It is assumed that frequency noise is suppressed according to servo theory. Using phase-locking as an example it is shown that the servo-modified lineshape can be predicted. Good agreement between theory and experiment is shown in the prediction of a delta-like feature in the laser's output spectrum.

The R(56)32-0 transition in I_2 at 532 nm has shown great promise as a new optical reference in the visible. Identical spectrometers based on frequency doubled Nd:YAG lasers have shown fractional frequency fluctuations of $<10^{-13}$ and stability/reproducibility of <300 Hz. The absolute frequency of this transition has been determined to ±40 kHz using a frequency chain based on the 633 nm $HeNe/I_2$ reference and

the Rb/D_2 line at 780 nm. The chain takes advantage of the fact that 532 nm "Green" reference summed with the 780nm Rb reference lies just 263 GHz from twice the frequency of the 633 nm $HeNe/I_2$ reference. The 263 GHz gap is measured with a second IR laser and a Schottky diode driven by a frequency stabilized klystron.

Investigation showed the largest uncertainty in the measurement came from the uncertainty of the Rb/D_2 reference. To reduce this a second frequency measurement was made. The Rb/D_2 optical frequency was compared to the recently measured $5S_{1/2}$-$5D_{3/2}$ two-photon transition in ^{85}Rb. The measurement of this 1.014 THz beat frequency allowed a reduction in the uncertainty of the Rb/D_2 reference to $\pm$ 10 kHz.

In memory of

Alex and Esther Himmelfarb

Loving grandparents

ACKNOWLEDGMENTS

When I first came to graduate school I was under the mistaken, now almost humorous, illusion that it would be alot like undergraduate school. Four years of doing the assigned homework followed by the obligatory receipt of a diploma. Little did I know that while the course work was challenging the real challenge was in learning to think and solve problems without textbooks (or text book solutions). This should not be confused with the idea that all that I learned I taught myself. Nothing could be further from the truth. To that end I would like to extend my greatest gratitude to the following people who made my stay at the University of Colorado and JILA possible and profitable. I would also like to pre-apologize for anyone who feels they were inadvertently forgotten. If there are individuals who feel they were of help to me but not mentioned they are probably right as hardly a soul in JILA has not contributed in some useful way to my time here.

First and foremost I would like to thank my parents whose endless support, patience and love (and occasional infusions of cash) were absolutely essential. I would like to thank my brothers Ed, and Alan whose phone calls and e-mail help shorten the 1500 miles distance between Boulder and the rest of my family.

Most of the experimental results cited in this phase-locking chapters of this thesis can be traced to an era between 1989 and 1990. It is reassuring to report that in the intervening years a number of technological advances have made certain parts of this program easier to duplicate. Chief among these is the appearance of low cost high

speed op-amps which also boast low noise. Such devices make possible improved lower noise, higher bandwidth current controllers and faster, simpler loop filters. Similar devices acting as a high speed buffers might make possible the reduction of the triple loop servo system to a dual loop system.

The design, construction and operation of the frequency chain which produced the rewarding measurements of the iodine, a_{10} R(56)32-0 transition frequency was the product of hard work and dedication by many people. I would especially like to thank Peter Jungner, post-doc on this project, whose inspiration, hard work and organizational skills were an indispensable part of this endeavor. His work on the Ti-Sapphire laser, 3F Rb spectrometer, HeNe doubling cavity and Rb oven for the two-photon spectrometer were all critical parts of this experiments.

I would also like to give special thanks to Jun Ye, who worked very hard on all phases of this experiment. In particular, his skill at eliminating the systematic errors associated with both Rb saturation spectrometers as well as the two photon spectrometer allowed us to achieve an extra order of accuracy in our measurements. Additionally, his persistence in observing the unusual behavior of the Rb spectrometers allowed us to find operating parameters for them that were inherently more stable than the ones we started with.

Thanks are also certainly due to Zhu Miao who built the original Nd:YAG/I_2 frequency doublers and transfer spectrometers. Mark Eickhoff who bought these instruments to a state of high accuracy and stable operation clearly deserves recognition for these efforts as well as measuring the relative line splittings of the "green" I_2 transitions. Keeping the spectrometers operational while the chain was running was, of

course, another useful contribution.

Thanks are also due to Steve Waltman whose knowledge of microwave electronics and the operation of the Schottky detector were both essential and, absent from every other member of the experimental group.

J.M. Chartier and L. Robertson of BIPM are also deserving of thanks for performing the intercomparison of our HeNe/I_2 laser with the BIPM transfer standard.

Only slightly less, are the thanks owed to Mike Winters who did the early design and construction work on the Ti-Sapphire laser which provided light for our 3H-spectrometer. Similar thanks are owed to C. Chardonnet and S.Singh who worked with the other Ti-Sapphire laser in its earliest days. Included also in this group of Ti-Saph pioneers should be B. Kohler who wrote the first software which turned that laser into a serious research tool.

A serious debt of gratitude is owed to the entire support staff at JILA who keep it running phenomenally smoothly for such a large institution, space permits me to mention only a few by name. I would like to thank Ed Holliness and Doug Jackson who eventually did get everything I ever ordered to me. Thanks to John Andru, Blaine Horner and the entire JILA instrument shop. Their vast array of optical, and mechanical mounts, both standard and specially made, as well as other fixtures and "free" advice on all problems, machine-shop oriented have been indispensable. Thanks also to Hans Rohner who made our Rb cells for us. A special double helping of thanks goes to Terry Brown. His electronic handicraft and advice so pervade this electronically intensive project as to represent a substantial fraction all the construction done for this measurement.

Lastly, of course, I thank my advisor Jan Hall whose many years of patience and persistence in guiding my education have hopefully resulted in my becoming wiser and not just older.

TABLE OF CONTENTS

LIST OF TABLES

LIST OF FIGURES

Chapter I: INTRODUCTION AND THEORY

Quantitative Study of Frequency Control of Laser Diodes with Emphasis on Phase-Locking

Introduction

The invention of the laser had its 35th anniversary in 1995[1]. Without it the entire field of study of atomic and molecular physics would be hugely different and vastly smaller. The laser makes possible studies of the interaction between light and matter in domains of intensity and coherence that are not achievable by any other method. Another invention, low loss optical fiber, means that the laser launched photons will also be the primary carrier of electronic information in the coming years. Although it has been a relative late comer to the laser family the diode laser has already become the most widely produced form of laser. In this chapter a prototype diode laser frequency control system is presented. It is demonstrated by phaselocking two external cavity laser (ECL) diodes

The Importance Of Control Systems

A key problem in realizing these and other laser uses is the ability to precisely control the lasers output frequency in both an absolute and relative way.

The early days of laser stabilization were dominated by the gas laser epoch. One of the first approaches to laser stabilization was the Central Tuning Dip or Lamb dip as it came to be known in honor of Willis Lamb's contribution to the theory of the effect[2]. Such lasers were capable of $\approx 10^{-10}$ stability or better limited by mechanical vibrations. Long term stability was dominated by the gradual decrease in pressure in the HeNe gain cell which reduces the blue shift associated with He-Ne collisions[3]. In 1964 Bennet and Knutson[4] used a Ne laser operating at a much lower pressure (and without helium) to avoid many of those previous problems. A substantial leap forward was made in 1967 when the idea of using separated Ne discharge cells for the absorber and the lasing medium was introduced simultaneously by Lee and Skolnick[5] and Lisityn and Chebotayev[6]. Almost immediately several groups had the idea that saturated absorption in molecules would make excellent frequency references. Barger and Hall [7,8] demonstrated the advantageous coincidence of the 3.39 μ HeNe-CH_4 system at the same time as Bagaev, Kolomnikov, Lisitsyn and Chebotayev[9]. This combination which achieved stabilities in the range 10^{-11} to 10^{-13} in early experiments later was used to demonstrate stabilities to the 10^{-15} with the introduction of the external cell and other technique[10]. The same year Hanes and Dalstrom[11] took the high ground in visible region by demonstrating a HeNe-I_2 system at 633 nm. Since that time any number of laser/absorber systems have been studied, I_2 at 612nm, 594nm, 543nm, and 640nm, CO_2/CO_2, CO_2/SF_6, CO_2/SiF_4,and CO_2/OsO_4. In contrast to the gas laser case, progress in stabilizing solid state lasers was hindered by the quality of the pump source. Neither the flash lamp nor the plasma discharge lamp were well suited to the

job of building stable lasers. The Nd:YAG laser which was studied most intensely also suffered from a lack of coincidental atomic or molecular absorption lines, the notable exception being a line in Cs_2. The second harmonic of the Nd:YAG laser's radiation which falls at 532 nm does coincide with an I_2 band so it is this harmonic light that has been historically the center of solid state laser stabilization schemes[12]. Although gas lasers had already achieved 10^{-13} stability levels by 1979, real advances in solid state laser stabilization didn't occur till 1980 and 1985 with the introduction of laser diode (LD) pumping and the non-planar ring oscillator (NPRO). In that period the fast line-width of the YAG laser declined from 10^5 Hz to 10^2 Hz.

As the level of science that was being achieved was slowly ratcheted up, so were the demands on the systems which kept the lasers locked to their appropriate absorbers. Simultaneously the introduction of widely tunable lasers, in particular the dye jet laser, made observations of new species common place. The unfortunate price to be paid was that the dye laser also suffered from substantial, fast phase and frequency noise. The solution to these problems was, locking the laser to a stable interferometer. Unlike an atomic or molecular absorber, an interferometer responds in an essentially linear way to an increase in light. The detection noise on the other hand goes with the square root of the detected power. Thus more signal to noise is always available at the expense of more power.

Early laser cavity locking schemes tended to use fringe side locking technique. These were later replaced by FM sideband technique. With the use of reflection mode sideband detection, not only was high signal to noise discrimination of the cavity fringe possible, but servo bandwidth was no longer limited by cavity storage time[13].

The net effect has been that the design of frequency stable lasers of all types is no longer a question of designing the quietest laser structure, rather, it is the design of stable reference interferometers, low noise detection electronics and appropriate frequency servo electronics and transducers. The evolution of this type of system for a modern dye laser can be seen in references[13,14,15] where the relative linewidth between two lasers locked to independent cavities is reduced from several MHz free running to 0.49 Hz, dominated by shot noise from locking to the cavities. Using similar technology the relative linewidth between two Nd:GGG non-planar ring oscillator (NPRO) lasers has been reduced to 3 Hz[16]. Most impressively, a pair of HeNe lasers in our lab, using carefully constructed high finesse cavities kept in vacuum and temperature stabilized canisters have shown a relative linewidth of less than 50 milliHz.

Why Study Phase Locking?

The alert reader has by now noted that while a great deal has been said about laser frequency control, a discussion of phase locking has till now been absent. This is not because phase locking is not an important part of the laser scientist's art. Offset frequency/phase locked scanning has been a mainstay of precision spectroscopy for years. It not only guarantees that one laser is at a known frequency offset from another, it also enforces the requirement that one laser have the same linewidth characteristics as the other. The requirement that two sources be phase coherent is also at the heart of some Raman schemes used in optical pumping, see Moler,Weis,Kasevich and Chu[17] as an example. Proposals for advanced gravitational wave meters also rely on the idea

that the phase/frequency of a small master laser can be transferred by phaselocking technique to a large power laser.

Many proposed advanced fiber optic communications methods will also rely on the ability to achieve phase lock with diode lasers.

The Difference Between Frequency And Phase Control

Is there a difference between frequency and phase control? The answer is there is almost no difference between the two because they are related by time integration. When referring to a system of phase control, the error sensor is assumed to be one whose output is a function of phase. Frequency control systems usually detect and correct frequency errors. These cases are rarely pure, for instance the phase detector used in this experiment also uses frequency information to determine its output during its acquisition stage. The Fabry-Perot cavity used as a frequency discriminator in many laser experiments operates as a phase discriminator in some regimes[13]. The term phaselocked which is used throughout this paper is somewhat less ambiguous. Phaselocked systems are ones in which the root mean square phase difference between two oscillators is much less than one radian. The equivalent term frequency locked, while used occasionally, does not have as formal a definition, though it connotes a small and bounded frequency error. A moments thought will reveal that phaselocking is a more stringent requirement than frequency locking or equivalently frequency stabilizing. This is one reason why a demonstration of phase locking is such a powerful diagnostic in the world of frequency control.

Another reason to do phaselocking studies is purely practical. The experimental apparatus for obtaining a phase error signal is just two lasers, (it is helpful in assigning the sources of the relative phase noises if, they are of identical construction, or the phase noise of one, the "master laser" is already known) a beam splitter and a photodetector. The signal can be obtained at any point in optical frequency space where both lasers can operate simultaneously. In contrast, a frequency stabilization experiment require both the laser and its frequency reference such as high finesse cavity or atomics absorber. High finesse cavities can only provide a comb of locking points, atomic absorbers usually offer just a few transitions. Compared to a laser heterodyne beat signal, obtaining good signal to noise from either of these frequency references is more difficult and often involves extra oscillators, electro-optic crystals etc.

Another nontrivial point is any true measure of laser frequency stability will actually require **two** complete stabilized laser systems. This is because for one laser system the primary stability diagnostic is the error from frequency discriminator. It is considered unwise to use this alone to characterize the real frequency stability of a laser system. This is because the system error signal will not show an unstable frequency discriminator as long as the laser frequency stays locked relative to it. Another possible problem is noise in the frequency error signal. A high gain frequency servo can often reduce the apparent noise on such a signal by writing frequency noise onto the laser. The result is a quieter error signal at the expense of **more** noise on the laser.

A pleasant and intentional side effect of phaselocking experiments is that the understanding and technology developed during them are usually applicable to the problems of frequency stabilization.

In summary, we can see that increasing sophistication in the methods of spectroscopy, communications and other sciences have driven the needs for laser control systems to dizzying heights. Measurements of laser phase noise and phaselocking experiments are relatively simple ways to evaluate and develope the state of the art for any given laser system. Understanding of the phase control technique for a particular laser eases the development of other frequency control systems. It is with this intention that in 1989 a project in phase locking diode lasers was undertaken.

Experimental History

Laser folklore holds that it is possible to judge the ease or difficulty of phase/frequency control of any particular laser by its line width. Narrow line widths correspond to relatively slow phase diffusion times. Given this it is not surprising that HeNe lasers were the first to be phase locked, tentatively at first in the mid to late 60's and more robustly by the mid to late eighties. The line widths of 1 to 10s of kHz typical of the HeNe lasers correspond to diffusion times (for one radian) of 1 ms to 100's of microseconds. In contrast the dye jet laser can show one radian of phase excursion in a microsecond. Given this it not surprising that phase control for the dye laser was not reported until the eighties[14,15].

When the first room temperature near infra-red diode lasers became available in the early eighties, it was hoped that precision phase and frequency control would be just a short time away. Sadly, measurements showed that their phase diffusion times were on the order of 10-100 nanoseconds, much too fast for control by existing technologies.

The situation improved dramatically when experimenters began to notice that the linewidths of diode lasers could be dramatically reduced by optical feedback. The first report of electronic phase locking for a laser diode with optical feedback was by Steele in 1983 [18], who used feedback from a glass plate at several cm distance from his laser diode to optically narrow it. The reflection from a diffraction grating in Littrow or Littman orientation are also known to provide a reduction in the laser line width by a factor of 10-50 while providing frequency tunability. In 1987 B.Dahmani, L.Holberg and R.Drullinger[19] reported an even more dramatic line width reduction when the optical feedback field came from a resonant cavity. This approach can reduce the diode laser's line width by a factor of 100. By 1989 Laurent and Clairon[20] had used this technique to reduce the linewidth of a diode laser from 20MHZ to 4 kHz. Both these techniques are described in a recent review[21].

With the passage of time a variety of optical feedback methods have been used with diode lasers for both frequency control and linewidth reduction. These include use of folded figure-eight-style ring cavities for line width reduction, or simultaneous line width reduction and second harmonic generation, hybrid grating-cavity feedback and use of Littman or Littrow style grating cavities with ruled or holographic gratings.

In our lab the first experiments done on phaselocking diode lasers involved the use of external cavity lasers (ECLs) in Littrow configuration. Servo bandwidths for the phaselocking system were about 600kHz. The rms phase error was still larger than one radian with cycle skipping evident. No more than 67% of the laser's energy could be gathered into the central delta function of the laser beat signal. The system oscillation at 600kHz was also much lower than would have been anticipated based on time delay

alone. To solve these problems it was decided to undertake a detailed study of phase noise in laser diodes and their possible remedies. Particular attention was paid to learning how to estimate the effect of phase/frequency control systems on the energy distribution of the diode output.

Theory of Phase Noise and Suppression

Introduction

It is not unusual to find the experimentalist who works with diode lasers peering at a spectrum analyzer. This instrument can supply a visual representation of the power spectral density (PSD) of its input. The input source is often the beat note between two diode lasers or a test laser and another laser with known properties. The investigator is often hoping to find that the device under test outputs a single optical frequency free from drift and phase perturbations down to the limit of the instrumental resolution. Sadly, this is often not that case. For this reason it is necessary to study quantitatively how to identify, classify and remedy the imperfections in diode laser output fields.

This brings up an important point. What is the most useful way to quantify the performance of laser servos and oscillators in general? Characterization of oscillators is usually done in either the frequency domain or the time domain. The chief time domain measurement technique, the Allan Variance, is well suited to measuring slow changes in oscillator performance but not effects on the micro-second scale. In the past the RMS phase deviation of the loop error signal was a popular choice for diagnostics.

It has the advantage of being relatively easy to measure and once RMS phase error values are greater then 1 the experimenter can be sure that the loop is not well locked. A related and somewhat more useful measure is $S_{\Phi}(\omega)$ the power spectral density of the phase noise.

From the point of view of the physicist, what is often most interesting is to know how the laser oscillator energy is distributed. What fraction falls inside some atomic bandwidth, or, from one transition over to a nearby one. In practice all these measurements are related. In reference [22] pg 432 is a figure showing this experimental relation. These measures then define the nature of the phase/frequency control problem. How does one predict or understand the effective performance of the servo based on the measurement of the unperturbed diode laser?

The Perfect Oscillator

All oscillators have some oscillating variable that defines their time dependent behavior. For rf oscillators this is just their output voltage, for lasers and microwave devices it is the time dependence of the electric field. If the oscillator produced a true monochromatic field its output could be expressed as:

$$e = A \cdot e^{(-i\omega_0 t)} \qquad \text{Eq 1-1}$$

Oscillator With Phase And Amplitude Noise

However in order to allow for non-ideal behavior the expression is expanded to

$$e = E(t) \cdot e^{(-i\omega_0 t - i\phi(t))}, \qquad \text{Eq 1-2}$$

where E(t) represents the time dependent amplitude, ω_0 is some center frequency and $\phi(t)$ contains the instantaneous phase fluctuations. During the rest of this discussion we will assume the amplitude fluctuations are negligible. Given this, it is clear that instantaneous frequency can be defined as

$$\omega(t) = \omega_0 + \frac{d}{dt}\phi(t) \qquad \text{Eq 1-3}$$

Oscillator With Sinusoidal Modulations

Modulation of the oscillation frequency by periodic sources is a common situation and can be used to illustrate several important points. The field variable for a

sinusoidally modulated source can be expressed as:

$$e = E_0(t) \cdot e^{(-i\omega_0 t - i\beta \sin(\omega_m t))} \qquad \text{Eq 1-4}$$

where ω_0 is the oscillator center frequency, ω_m is the frequency of the modulating source and β is the modulation index. It is easily shown that β is equal to the modulation width divided by the modulation frequency. This equation can be expanded in Bessel functions to yield:

$$e = E_0 \sum_{n=-\infty}^{\infty} J_n(\beta) e^{-i(\omega_0 + n\omega_m)} \qquad \text{Eq 1-5}$$

One can see that the signal carrier will have strength $J_0(\beta)$. It is often useful to remember that for small β this corresponds to:

$$\text{carrier} \approx 1 - \frac{1}{2}\beta^2 \qquad \text{Eq 1-6}$$

Also worth remembering is that the carrier term, (J_0), disappears completely for the first time at β=2.4. Since the amplitudes $J_n(\beta)$ fall rapidly for $n \gg \beta$, frequency modulated oscillators tend to have one of two distinct types of field spectrum. These two cases are shown in figure 1-1 as they might appear on a spectrum analyzer. To illustrate, two carriers of unity amplitude at 20 MHz and 60 MHz with small and large modulation indexes, respectively. Signals in which the modulation index $\beta \ll 1$ have large distinct carriers and a few sidebands of rapidly declining strength. Alternatively if $\beta \gg 1$ there is no distinct carrier and sidebands remain relatively large over a frequency interval of plus or minus the modulation width from the carrier. When viewed with a real spectrum analyzer systems with large modulation amplitudes often appear as distributions rather then discrete lines.

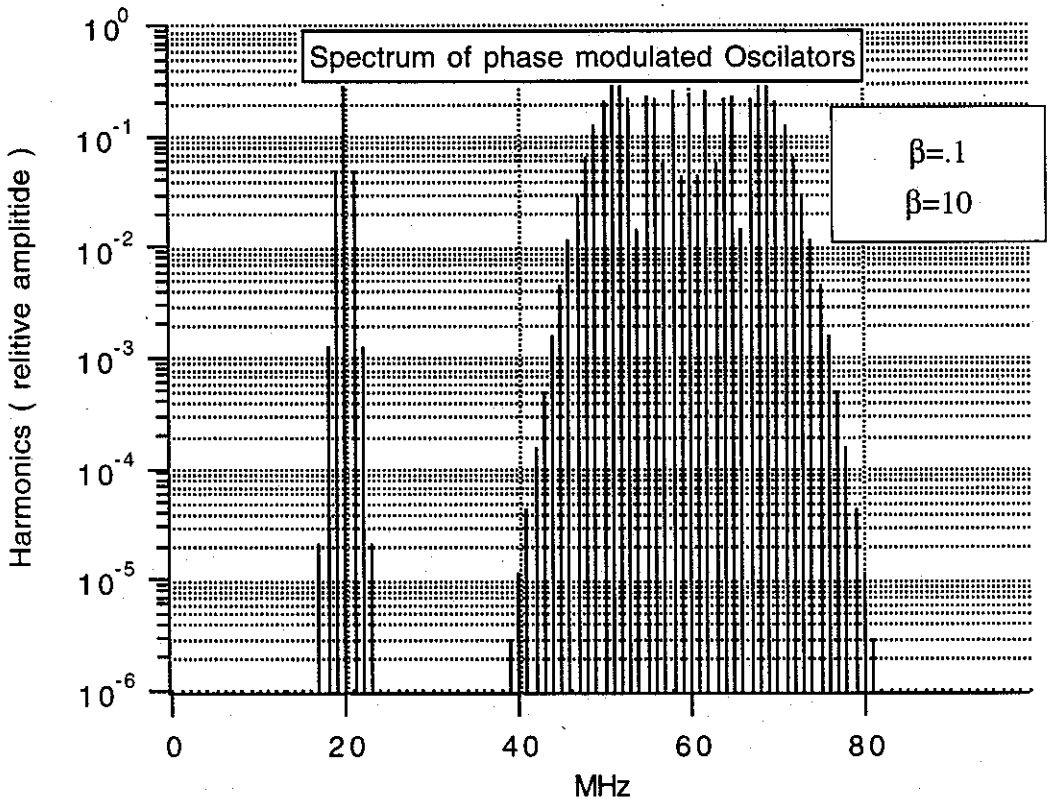

Figure 1-1 Simulated Spectra For Beta = 0.1 and 10

Oscillator With Noise Modulations

Introduction

The beauty of equations 1-4 describing the phase modulated oscillator and Eq 1-5 of Bessel's expansion is that they are quite versatile. Using a combination of linearity properties and properties of exponentials they can be used to calculate spectra for sources with multiple modulation frequencies and multiple modulation indices. When combined with the theory of AM modulation, they can predict the size of unequal sidebands, such as may arise from current modulated diode lasers. With the aid of Fourier methods they can also be used to estimate spectra from sources which are modulated by periodic but non sinusoidal sources.

Stochastic Sources

Mental extensions of these discrete frequency methods can lead to insight into noise driven situations, but, the rigorous treatment of oscillating systems where phase disturbances are driven by stochastic processes requires an expanded vocabulary.
If we allow the phase as defined in equation 1-3 to be re-written as:

$$\phi(t) = \int_{t_0}^{t} \omega(t')\,dt' \qquad \text{Eq 1-7}$$

and we require that $\omega(t)$ be a Gaussian variable, Then we can define

$$P_x(\omega) = \left|F_v(X(\omega(t)))\right| \qquad \text{Eq 1-8}$$

Where $F(x)$ indicates the Fourier transform of $X(\omega(t))$, and thus $P_X(\omega)$ is the power spectral density of the frequency fluctuations of some function $X(t)$, $P_E(\omega)$, the power spectral density of the laser's electric field can often be measured directly, either with a Fabry-Perot cavity or by heterodyning a laser of interest with another sta-

ble laser.

By convention, the power spectral density of the frequency fluctuations are labeled as $S_\nu(f)$. It also can be measured directly by heterodyne techniques and processing the beat signal with a frequency to voltage (FV) converter, or by using an optical cavity, or atomic or molecular transition as a frequency discriminator.

In general we can also define an autocorrelation function $R_x(\tau)$ for the time varying field $X(\tau)$ as:

$$R_x = \langle X(t) \cdot X(t+\tau) \rangle \qquad \text{Eq 1-9}$$

where the angle brackets denote an ensemble average, which is equal to a time average in the ergotic stochastic process.

Wiener-Khintchine Theorem

If one knows the autocorrelation function for the electric field of the laser (or other oscillator) then one can apply the Wiener-Khintchine (WK) theorem:

$$P_E = \frac{1}{2\pi} \int_{-\infty}^{\infty} R_E(\tau) \exp(-\omega\tau)\, d\tau \qquad \text{Eq 1-10}$$

to extract the PSD of the electric field.

This leaves just one last step in our quest to predict the laser line shape based on our knowledge of the PSD of its frequency noise and the effect that our phase/frequency control system is going to have on it.

If we knew the relationship between $P_E(\omega)$, and the autocorrelation function of the laser output $R_E(\omega)$, then we could know in advance the effect that modifying the first one would have on the second.

This is the heart of the phase/frequency control question. Because all that a frequency control servo does is allow the experimenter to modify $R_E(f)$ with the hope that some target $P_E(\omega)$ can be achieved.

Unfortunately, the derivations involved in this last, important, relationship are not trivial and it is not the purpose of this paper to review in detail the subtleties of this derivation or the necessary and sufficient conditions which must be satisfied. Interested readers can find the details in references[23] or [24]. The paper by Hall[23] also discusses the assumptions involved in ignoring coupled AM and FM noise. A final working form for the WK theorem relating laser lineshape and $P_\omega(\omega)$ is:

$$P_E(\omega) = \frac{E_0^2}{2}\frac{1}{2\pi}\int_{-\infty}^{\infty} d\tau \exp(-i(\omega-\omega_0)\tau)\exp\left(-\frac{1}{\pi}\int_{-\infty}^{\infty} d\omega S_v(\omega)\left[\frac{Sin\left(\frac{\omega\tau}{2}\right)}{\omega}\right]^2\right) \qquad \text{Eq 1-11}$$

The coefficient $E^2_0/2$ reflects the physical nature of the equations but will be normalized to unity for the remainder of the chapter.

Unmodulated Carrier.

The simplest case to which this WK formalism can be applied is the case where $S_V(\omega)=0$. This causes the integral in the exponent to collapse to zero and $e^{(0)}=1$. This means the autocorrelation is unity and independent of time. Since the Fourier transform of 1 is $2\pi\delta(0)$ we have recovered the original carrier as a delta function.

Spectrum For Lorentzian

The simplest non-trivial case for which the integrals can be done analytically is for $S_V(\omega)=2D$, a constant. The results calculated by Elliot et al.[24] are

$$R(\tau) = \exp(-D|\tau|) \qquad P_E(\omega) = \frac{E_0^2}{2}\frac{D}{\left(\frac{D}{2}\right)^2 + \omega^2}, \qquad \text{Eq 1-12}$$

in agreement with the prediction by Schawlow and Townes that the output line shape for a laser would be Lorentzian. From Winters,[25] we can see that the full width at half maximum (FWHM), D, of the Lorentzian is just the phase diffusion constant for the free running laser:

$$D = \frac{2\pi h\nu(\Delta\nu)^2}{P_{\text{Laser}}}\frac{N_2}{N_2 - N_1} \qquad \text{Eq 1-13}$$

where h is Planck's constant, ν is the laser optical frequency, $\Delta\nu$ is the cold cavity linewidth, P_{laser} is the output power of the laser, and N_1 and N_2 are the populations of the lower and upper states respectively

Spectrum For Gaussian

Another illuminating case for which the WK can be solved exactly is the case of low-passed frequency noise. If the frequency noise $P_\omega(\omega)$ can be expressed in the form of flat frequency noise of power spectral density 2b, after it has been filtered by a lowpass filter with a corner frequency of β

$$S_\nu(\omega) = \frac{2b}{1 + \left(\frac{\omega}{\beta}\right)^2}, \qquad \text{Eq 1-14}$$

then according to Elliot:

$$P_E(\omega) = \frac{{E_0}^2}{2}\int_{-\infty}^{\infty} \exp(-i(\omega - \omega)\tau)\exp\left(-b|\tau| + \frac{\exp-\beta|\tau| - 1}{\beta}\right), \qquad \text{Eq 1-15}$$

which can be broken down into two distinct regions of interest.

If $\beta >> b$ then the "corner" frequency for the system is at a "high" frequency compared with the modulation level and Eq 1-15 reduces to Eq 1-12, the formula for

the Lorentzian as seen previously. On the other hand, if b>>β then the system is driven by large low frequency excursions and Eq 1-15 reduces to:

$$P_E(\omega) = \frac{E_0^2}{2}\left(\frac{2\pi}{b\beta}\right)^{1/2}\exp\left(-\frac{(\omega-\omega_0)^2}{2b\beta}\right), \qquad \text{Eq 1-16}$$

which is a Gaussian shape with FWHM equal to $\{8(\ln 2)b\beta\}^{1/2}$. This is in agreement with the fact that beat notes between free running HeNe lasers appear to be Gaussian. This is because under free running conditions the dominant sources of frequency noise are large, low frequency mechanical and acoustic vibrations.

A comparison of these three cases is shown in figure 1-2. Note that in the case of the unperturbed carrier the autocorrelation as τ approaches infinity is non-zero and a constant. This is the hall mark for systems where there a is central carrier. It is easy to understand why. If the autocorrelation is separable into two parts, a constant and distribution, then its Fourier Transform will also have two parts: a part proportional to a delta function and a part which is the transform of a continuous distributions.

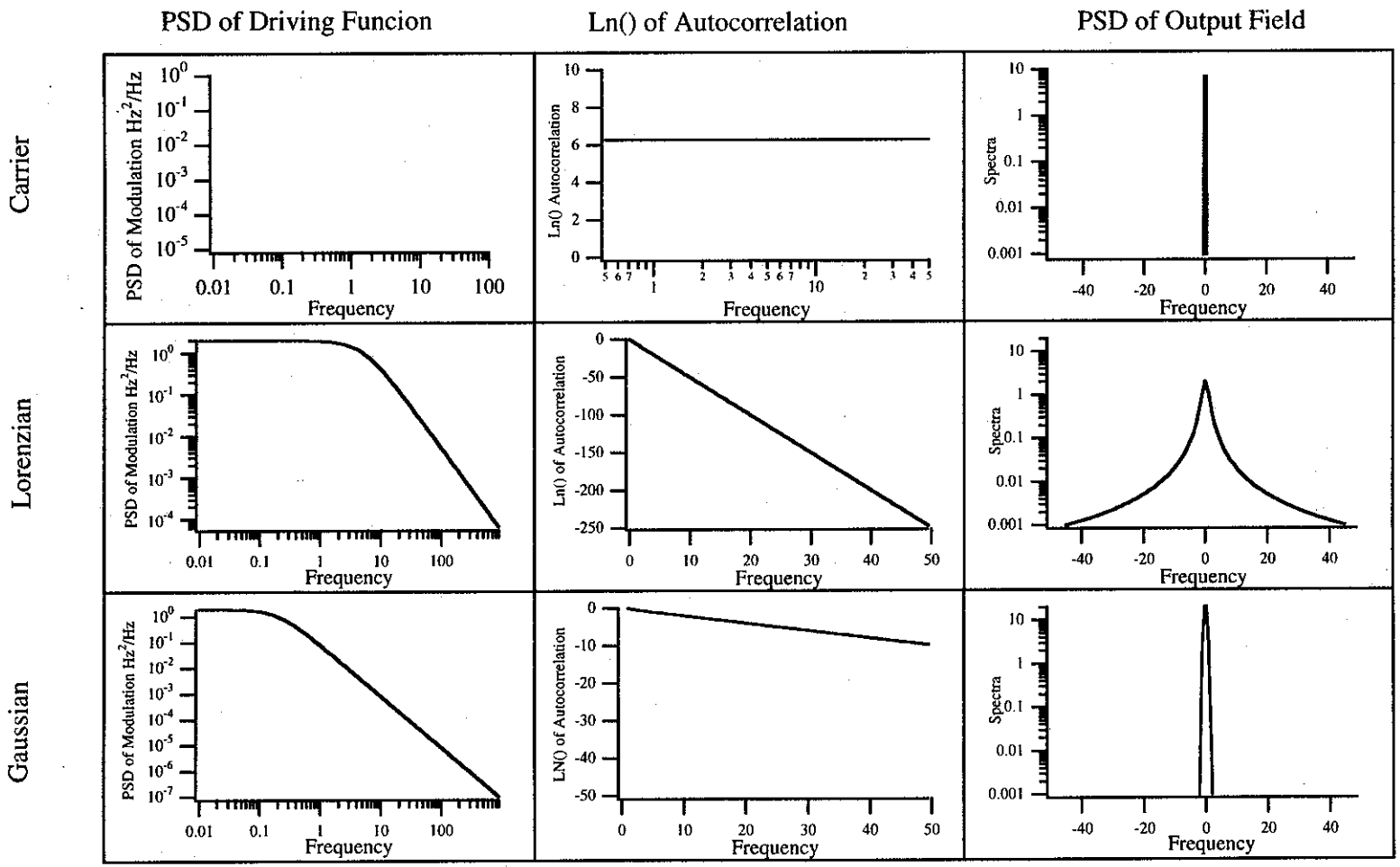
PSD of Driving Funcion
Ln() of Autocorrelation
PSD of Output Field
Carrier
Lorenzian
Gaussian
PSD of Modulation Hz²/Hz
Ln() Autocorrelation
Ln() of Autocorrelation
LN() of Autocorrelation
Spectra
Frequency

Spectrum For Sum Of Sources

A useful feature of the WK equation is that if $S_v(\omega)$ can be represented as the sum of noise sources for which the solutions to equation 1-11 can be found then the entire spectral profile can, at least, be reduced to a series of convolutions. This can be seen by noting that if $S_v(\omega)$ is a sum, then the inner integrand of eq. 1-11 will also be a sum and it's exponentiation a product. The convolution theorem states that the Fourier transform of a product of two functions is the convolution of the transforms of the individual functions.

An example of using this property is when $S_v(\omega)$ consists of two terms. One a large low frequency component which fulfills the previously stated requirement for generating a Gaussian field, the other a broad-band noise source of the type which will produce a Lorenzian. The result will, of course, be the convolution of a Gaussian and a Lorenzian which is called a Voigt profile.

Another example of using this property is to help understand "real world" systems. It will be shown in the next section that it is possible to construct a phase control servo such that its associated line shape has a delta function in it. While this is gratifying, since it nearly mirrors what is observed, mathematically pure delta functions are not often seen in the laboratory. To fix this we assume (or observe) that the driving noise in the system really consists of the theoretical model plus a small amount of broadband flat electronic noise. Then the "real" lineshape can be seen to be the convolution of a "narrow" Lorenzian and the otherwise pure delta function leaving the Lorenzian as an acceptable "real world" component in the observed line shape. Since

multiple convolutions are acceptable if the electronic or detection noise also had a large low frequency content, then we can see the delta function would have acquired the already discussed Voigt profile instead. In this way it is sometimes possible to build up a lot of information about the line shape of the oscillating system without having to perform exact and tedious calculations.

Spectrum For Phase Locked System

Introduction

There are other cases in which the WK theorem can be solved in closed form, and some are the interesting cases for phaselock and frequency servo designers. One is the case of "white" frequency noise after the application of a "high pass" characteristic. This characteristic can result from a servo system reducing the frequency/phase noise at low frequencies.

Basic Servo Model

Figure 1-3 shows a simplified schematic of a phase-locked loop (PLL) servo system. The phase detector gain is K_d and the voltage controled oscillator (VCO) gain factor is K_0. F(s) is the open loop transfer function of any system components between the phase detector and the VCO. According to conventional PLL theory we define the open loop transfer function:

$$G(s) = \frac{K_0 K_d F(s)}{s} \qquad \text{Eq 1-17}$$

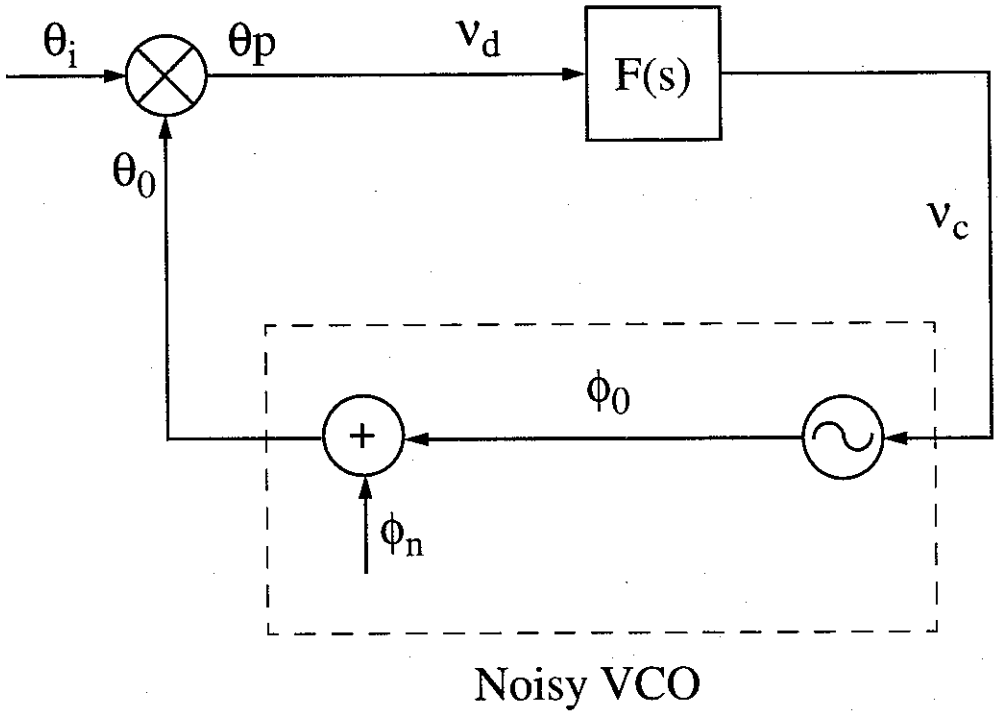

Figure 1-3 Oscillator Noise Model

And the closed loop transfer function:

$$H(s) = \frac{G(s)}{1+G(s)} \qquad \text{Eq 1-18}$$

The oscillator is taken to be a perfect jitter-free oscillator with phase output ϕ_0 which is followed by an internal disturbance source that adds phase jitter ϕ_n. The resulting phase external to the oscillator output is $\theta_0 = \phi_0 + \phi_n$. If we take the phase of the incoming reference to be θ_i then the phase error in the closed loop system is defined as $\theta_p = \theta_i - \theta_0$. This phase error (θ_p) results in an output from the phase detector of $v_d = K_d(\theta_i - \theta_0)$. If the input frequency (θ_i) is taken to be noise free, then Gardner[26] chapter 2 shows that the phase error is:

$$\theta_p(s) = [1 - H(s)]\,[\theta_i(s) - \phi_n(s)] \qquad \text{Eq 1-19}$$

Thus we have the relationship between the Laplace transform of the phase error, the closed loop gain, and the phase noise. Gardner points out that strictly speaking stochastic variables such as ϕ_n do not have Laplace transforms and the variables should be discussed in terms of their power spectral densities. Two accomplish this we define the variable $S_\phi(f)$ as the single sided power spectral density of the phase-error and $S_v(f)$ the PSD of the oscillator frequency fluctuations, similar to the definition in the section on stochastic sources.

$$S_{\phi p}(\omega) = [1 - H(\omega)]^2 S_{\phi 0}(\omega) \qquad \text{rad}^2/\text{Hz} \qquad \text{Eq 1-20}$$

It is more common to speak of the PSD of the frequency fluctuations of the phase-error and the phase-noise defined by:

$$S_{vp}(\omega) = [1 - H(\omega)]^2 S_{v0}(\omega) \qquad (\text{rad/sec})^2/\text{Hz} \qquad \text{Eq 1-21}$$

These equations have similar forms because of the general relationship between the PSD of frequency noise ($S_\nu(f)$) and phase-noise ($S_\phi(f)$)

$$S_\nu(f) = \omega^2 S_\phi(f) \qquad \text{Eq 1-22}$$

Assuming that the PLL is a first order loop:

$$H(s) = \frac{1}{1+\frac{s}{K}} \qquad \text{where} \qquad K = K_0 K_d F(0) \qquad \text{Eq 1-23}$$

Then plugging into equation 1-23 to equation 1-21 and using $S_\omega(\omega)=2D$ as in the case of a Lorentzian where D is the laser phase diffusion constant, yields

$$S_{\omega p}(\omega) = \frac{\omega^2}{\omega^2 + K^2} S_{\omega 0}(\omega) \qquad (\text{rad/sec})^2/\text{Hz}$$
$$S_\omega(\omega) = 2D\frac{\omega^2}{\omega^2 + b^2} \qquad \text{Eq 1-24}$$

We insert equation 1-24 into the WK and carry out the first integration

$$P_E(\omega) = \frac{1}{2\pi}\int_{-\infty}^{(\infty)} e^{(-i\omega'\tau)} \exp\left[-\frac{D}{b}(1-e^{-b|\tau|})\right] d\tau \qquad \text{Eq 1-25}$$

We can then remove the common multiplier:

$$P_E(\omega) = \frac{1}{2\pi} e^{-\frac{D}{b}} \int_{-\infty}^{(\infty)} e^{(-i\omega'\tau)} \exp\left[-\frac{D}{b}(e^{-b|\tau|})\right] d\tau \qquad \text{Eq 1-26}$$

And expand the exponential in a series:

$$P_E(\omega) = \frac{1}{2\pi} e^{-\frac{D}{b}} \int_{-\infty}^{(\infty)} e^{(-i\omega'\tau)} \left(\sum_{n=0}^{\infty} \frac{1}{n!}\left(-\frac{D}{b}\right)^n e^{-nb|\tau|} \right) d\tau \qquad \text{Eq 1-27}$$

Reversing the order of the summation and integration:

$$P_E(\omega) = e^{-\frac{D}{b}} \{\delta(\omega') + \frac{1}{\pi}\left[\left(\frac{D}{b}\right)\frac{b}{\omega^2+b^2} + \frac{1}{2!}\left(\frac{D}{b}\right)^2 \frac{2b}{\omega^2+(2b)^2} \cdots\cdots\right]\} \qquad \text{Eq 1-28}$$

The first, $\delta(\omega)$ term represents the original recovered "carrier" term. The coefficient exp(-D/b) indicates height of the carrier. If D/b << 1 then:

$$e^{-D/b} \approx 1 - D/b \qquad \text{Eq 1-29}$$

and D/b can be seen to be the fraction of the carrier that was lost.

As we have already seen, if D were the FWHM of the Lorentzian's observed $P_\omega(\omega)$ for the free running laser of unity power, then 2D is the magnitude of the power spectral density of the white frequency noise driving the system. We can also see that the remaining profile consists of a sum of Lorentzians of ever increasing width and lower height. This picture is shown in figure 1-4 for values of b of 0.5, 2, 10, and 50 with D held constant at one. As is obvious for b=0.5 there is little effect on the expected profile but by b=10 a prominent carrier has formed on the on top of the spectral distribution. The lowering and broadening of the distribution is quite clear by b=50.

Spectrum For Double Pole At F=0

Another situation in which the WK equation can be solved in closed form is the case of a servo with two poles at zero frequency. Persons familiar with servo theory will recognize that this type of system is inherently unstable. Therefore in this case it is more useful to imagine the perfect VCO driven by high passed noise. The high pass filter is chosen to have the same frequency response as a stable second order servo would.

The closed loop transfer function then becomes:

$$H(s) = \frac{k^2}{k^2 + \omega^2} \qquad \text{Eq 1-30}$$

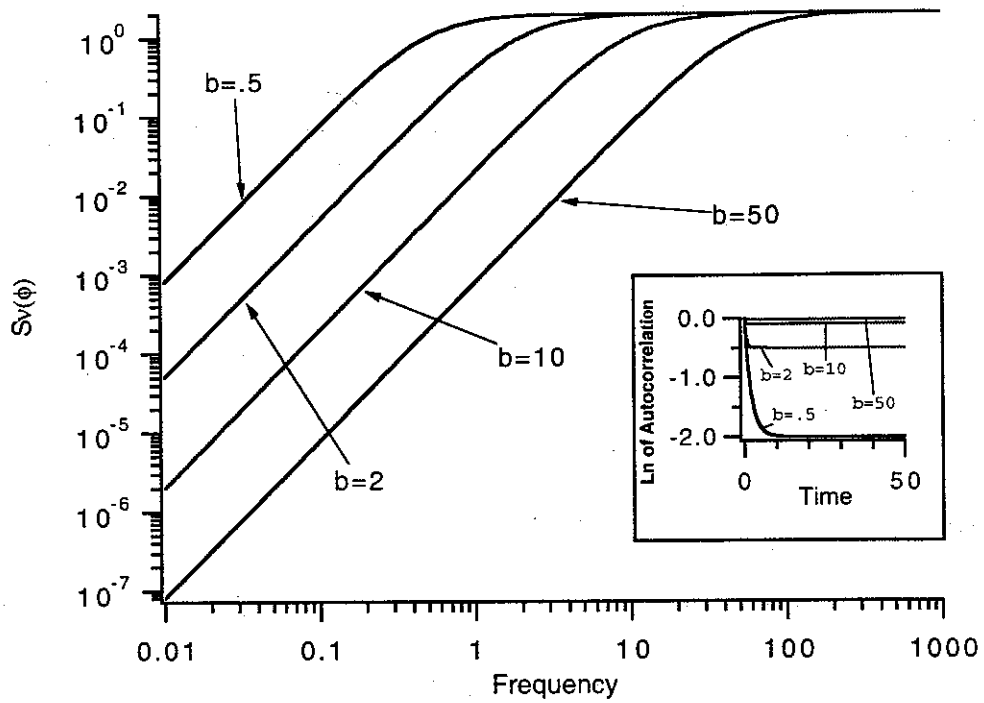

Figure 1-4 PSD of $S_v(\phi)$ versus Bandwidth b for D=1

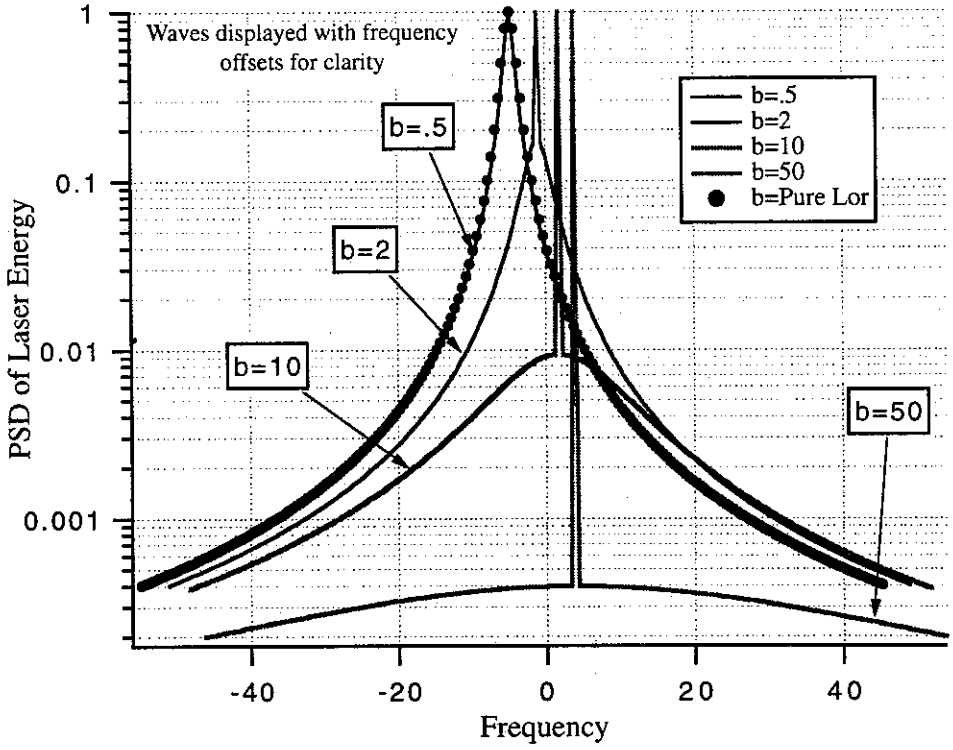

Lineshape prediction for different values of b when D=1

This yields the frequency noise in the loop as:

$$S_{p\phi}(\omega) = [1 - H(\omega)]^2 S_{0\phi}(\omega) \Rightarrow S_{p\phi}(\omega) = \frac{\omega^4}{(\omega^2 + k^2)^2} S_{0\phi}(\omega) \qquad \text{Eq 1-31}$$

Once again plugging the above equation into the WK theorem and setting $S_{0\phi}(\omega)=2D$ and equating k^2 with b^2 from the previous calculation yields the first integration of:

$$\text{integral} = 4D \cdot \int_0^\infty \frac{\omega^2 \sin\left(\frac{\omega\tau}{2}\right)}{(\omega^2 + b^2)^2} d\omega \ , \qquad \text{Eq 1-32}$$

where one factor of 2 has come from using the symmetry of the integrand to change the limits of integration. Performing the integration and plugging back into the WK theorem:

$$P_E(\omega) = \frac{1}{2\pi}\int_{-\infty} e^{-i\omega\tau} \exp\left[\frac{-D}{2b}(1 + e^{-b|\tau|} + b|\tau| e^{-b|\tau|})\right] d\tau \ . \qquad \text{Eq 1-33}$$

The integral at first looks daunting, but exp(-D/2b) is a common multiplicative factor. The remaining Fourier transform of the double exponential can handled by a combination of expansion as before and use of the convolution theorem, which states[27] the fourier transform of the product of two functions is the convolution of their transforms

$$\int_{-\infty}^{\infty} e^{-i\omega t} f(t)\, g(t)\ dt = F(\omega) \otimes G(\omega) \qquad \text{Eq 1-34}$$

So we split the transform to two parts:

$$\text{Part 1:} \qquad P_E(\omega) = \frac{1}{2\pi} e^{\frac{-D}{2b}} \int_{-\infty}^{\infty} e^{-i\omega\tau} \exp\left[\frac{D}{2b} e^{-b|\tau|}\right] d\tau \qquad \text{Eq 1-35}$$

Comparing this integral with the one from the last case we already see they have common forms. One difference is that in front of the integral is exp(-D/2b) which we know will end up multiplying a delta-like function. The other is the scale for the sum of Lorentzian widths, which will also be set by D/2b. From apendixsection Appendix A: on page 193 we have the final result.

$$\text{Part1:} \qquad P_{E1}(\omega) = e^{\frac{-D}{2b}}\left\{\delta(\omega) + \frac{1}{\pi}\left[\frac{1}{1!}\left(\frac{D}{2b}\right)\frac{b}{b^2+\omega^2} + \frac{1}{2!}\left(\frac{D}{2b}\right)^2\frac{2b}{(2b)^2+\omega^2}\cdots\cdots\right]\right\} . \qquad \text{Eq 1-36}$$

The second part of the integration looks like:

$$\text{Part 2:} \qquad P_E(\omega) = \frac{1}{2\pi}e^{\frac{-D}{2b}}\int_{-\infty}^{\infty} e^{-i\omega\tau}\exp\left[\frac{-D}{2}|\tau|e^{-b|\tau|}\right]d\tau . \qquad \text{Eq 1-37}$$

As before, this will be done by writing the exponential as a sum

$$P_{E2}(\omega) = \frac{1}{2\pi}e^{\frac{-D}{2b}}\int_{-\infty}^{\infty} e^{-i\omega\tau}\left(1 + \sum_{n=1}^{\infty}\frac{\left[\frac{-D}{2}|\tau|e^{-b|\tau|}\right]^n}{n!}\right)d\tau . \qquad \text{Eq 1-38}$$

And doing the integration part by part after separating the n=0 term. The result is (See Appendix A)

$$P_{E2}(\omega) = e^{\frac{-D}{2b}}\left\{\delta(\omega) + \frac{1}{\pi}\sum_{n=1}^{\infty}\left(-\frac{D}{2b}\right)^n\left\{\frac{\left(\cos\left[(1+n)\operatorname{atan}\left(\frac{|\omega|}{bn}\right)\right]\right)}{\left(1+\left(\frac{|\omega|}{bn}\right)^2\right)^{\frac{n+1}{2}}n^n}\right\}\right\} . \qquad \text{Eq 1-39}$$

We can see without doing the convolution explicitly that it will have four parts. The first part is a delta function of height Exp(-D/b). This is similar to the one pole case which had also height of Exp(-D/b). The second and third terms in the convolution come from the respective delta functions acting on the continuous portions of the functions $P_{E2}(\omega)$ and $P_{E1}(\omega)$. The last term will contain the actual convolution of $P_{E1}(\omega)$ and $P_{E2}(\omega)$

Sources Of Noise Modulation

The study of phase and frequency noise in electronic and microwave oscillators has a long history. As mentioned, there are a large number of methods for quantifying oscillator noise and its effect on the oscillator output. One which has evolved over the years is to assume $S_\phi(\omega)$ (the power spectral density of the phase noise) and consequently $S_\nu(\omega)$ (the power spectral density of the frequency noise) will obey power law statistics. This is illustrated in figure 1-5. The alert reader will have noticed that all the proceeding examples for calculating lineshapes have begun with the assumption $S_\nu(\omega)$ that is a constant which was modified by a filtering action. We shall now discuss this assumption and the relevant situations under which it needs modification

Schawlow-Townes Noise

Equation 1-13 gives an expression for the Lorenzian linewidth of a HeNe laser. Even a "weak" HeNe which emits only a few 10s of μW potentially has a quantum limited linewidth in the milli-hertz range. It is interesting to try to apply the same formula to a typical diode laser. The power of a laser diode maybe one thousand times larger than a HeNe's, but, the HeNe's cavity linewidth will be much smaller. A typical value for a HeNe is about $1*10^6$Hz . Absorption in the laser diodes limits its cold cavity linewidth to $1.5*10^{11}$Hz which is about the free spectral range of the diode chip.Without including any population inversion effects we can see the diode laser threatens us with a linewidth of 10^5-10^6Hz.

When Flemming and Mooradian[28] measured the line width of a free running

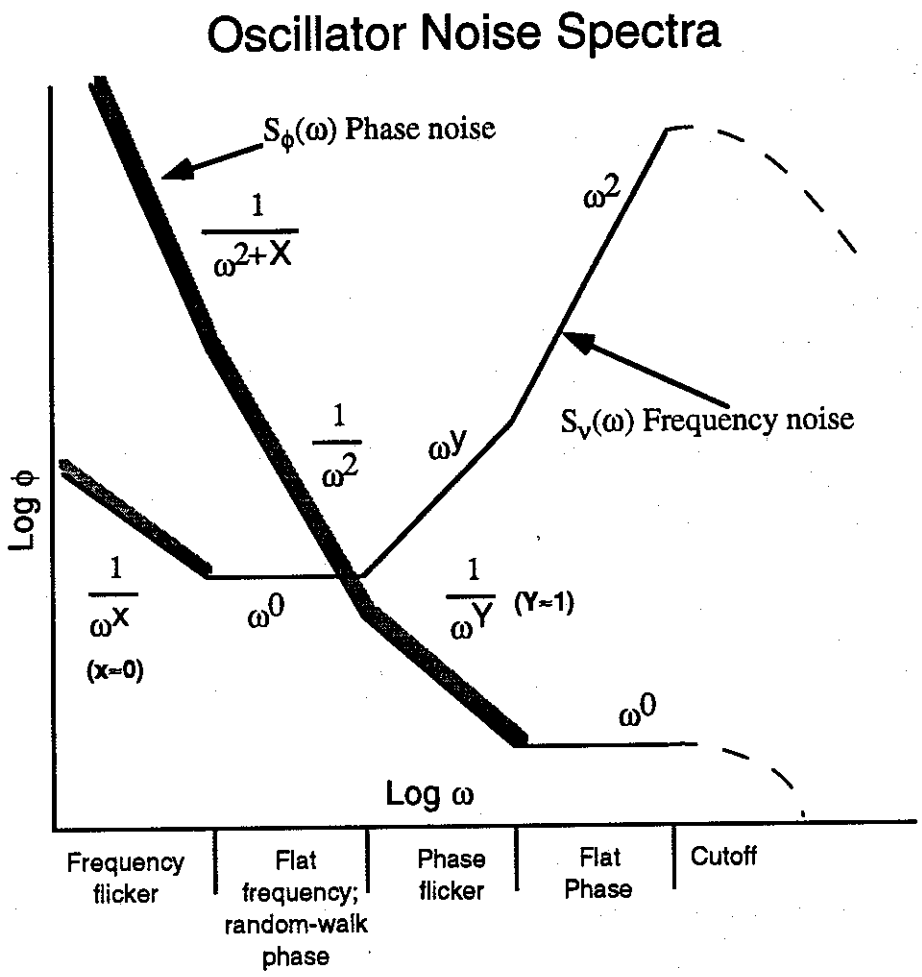

Grey marks indicate regions of nonstationary or nonexistent autocorrelation

Figure 1-5 Oscillator Noise Spectra

diode in 1981 it was found that the linewidth was actually much worse then expected based on standard calculations by Lax. The reason for this was found by Henry[29] to be a coupling between the quantum intensity noise and effective index of the diode's gain material. This coupling coefficient (called α) is defined such that:

$$\alpha = \frac{\Delta\chi'}{\Delta\chi''} \qquad \text{Eq 1-40}$$

where $\Delta\chi'$ and $\Delta\chi''$ are the changes in the real and imaginary complex susceptibility due to quantum mechanical fluctuations of the internal photon fields. Including this term and assuming the quantum fluctuations are approximately "white" in spectrum it is possible to express the field profile for the solitary mode diode laser as a Lorentzian with a FWHM by using the *Modified Schawlow Townes Formula* [30]

$$\Delta\nu = \frac{h\upsilon_l}{8\pi P_0}\left(\frac{c}{n_i L}\right)^2\left(\alpha_i L + \ln\left(\frac{1}{R}\right)\right)\left(\ln\left(\frac{1}{R}\right)\right)n_{sp}(1+\alpha^2) \qquad \text{Eq 1-41}$$

$$n_{sp} = \frac{1}{1 - e^{[(h\nu_l + E_{Fv} - E_{Fc})/kT]}} \qquad \text{Eq 1-42}$$

where ν_l=laser output frequency, P_o= laser output power, n_i=refractive index of the laser, α_i= the optical density, L is the length of the diode and R is the facet reflectively (assuming both facets are equally reflective), and in Eq 1-42 n_{sp} is the spontaneous emission factor where E_{Fv} and E_{Fc} are the quasi-Fermi levels of the valance and conduction band respectively. For a solitary laser $\Delta\nu$ usually lies between 10-50 MHz and α between 4-6. The new generation of quantum well and multiple quantum well lasers show α's on the order of 2-3, giving them a substantially reduced linewidth at the same output power.

1/f Noise

Even with the correction for amplitude/frequency coupling, the linewidth of the laser diode as defined by the -3db points was much larger then expected. Surprisingly, Welford and Mooradian also measured a power-independent component to the linewidth. Kikuchi and Okoshi[31] observed that the laser diode has a power-independent 1/f component in its frequency noise. Then Ohtsu and Shinichi [32]carefully measured the 1/f noise along with the spectral profile of several 0.8 μm lasers and showed the correspondence between the magnitude of 1/f noise and the predicted line shape. This, from ref.[32] has also been confirmed for an optically narrowed diode by Laurent[20]. It has also been shown that this 1/f, noise driving thermal heating of the diode chip, results in a still further amplification of low frequency large excursion noise.

The line profile for 1/f noise is proportional to $1/f^3$ for a tuning offset far from the line center, and the linewidth scales as:

$$(A_{-1})^{1/3} \qquad \text{if the noise is defined as} \qquad P_\omega = \frac{A_{-1}}{\omega} \qquad \text{Eq 1-43}$$

regardless of whether it is defined by:

$$\Delta\nu = \int_{\frac{\nu}{2}}^{\infty} S_\phi = .69 \qquad \text{or} \qquad \Delta\nu = \pm 3\text{db} \qquad \text{Eq 1-44}$$

See Walls and deMarchi[33] for additional discussion

The Real Problem

This leads to the doubly unfortunate result for the ECL that while the linewidth

contribution from the Schawlow-Townes (see Eq. 1-13) noise is falling off with the square of the cavity length (in association with a reduction in $\Delta\nu$), the contribution from 1/f noise is only falling off proportional to the cavity length. This makes reducing the frequency fluctuations in an ECL by lengthening it a case of diminishing returns, because mode control problems build up quickly in long ECL lasers. The result is that hopes about how much bandwidth is needed to gather a certain fraction of energy into the carrier are optimistic. This is because until the diode's 1/f noise is strongly suppresses no carrier-like feature will appear. It also indicates that the loop gain should be at least second order in ω out to some frequency beyond the cross-over between 1/f and flat noise. This noise picture is illustrated in the beatnote in figure 1-6, for which two diodes are frequency locked with a minimum servo bandwidth so as not to affect the laser's energy distribution. When the line is fit with a Voigt profile, the Lorentzian is about 72 kHz HWHM but the Gaussian shows almost 540 kHz HWHM. This is why early attempts to phaselock this system with 600 kHz PLL proved to be unsuccessful. In retrospect it can be seen that this was due to the 1/f noise. In figure 1-7 is the graph of S_ϕ for a typical laser diode, (after Ohtsu [29]) which illustrates this from another perspective. The line labeled "A" indicates the classic Schawlow -Townes frequency noise and B indicates the modified Schawlow -Townes noise due to Henry's α^2 factor. The extra thermally driven noise is "C" and the 1/f noise is labeled as "D". The resulting sum is labeled "E". Pictured on the graph but not discussed is the relaxation resonance around 1GHz which does not affect servo performance.

Beatnote between two laser diodes using the minimum servo bandwidth needed for a stable measurement.

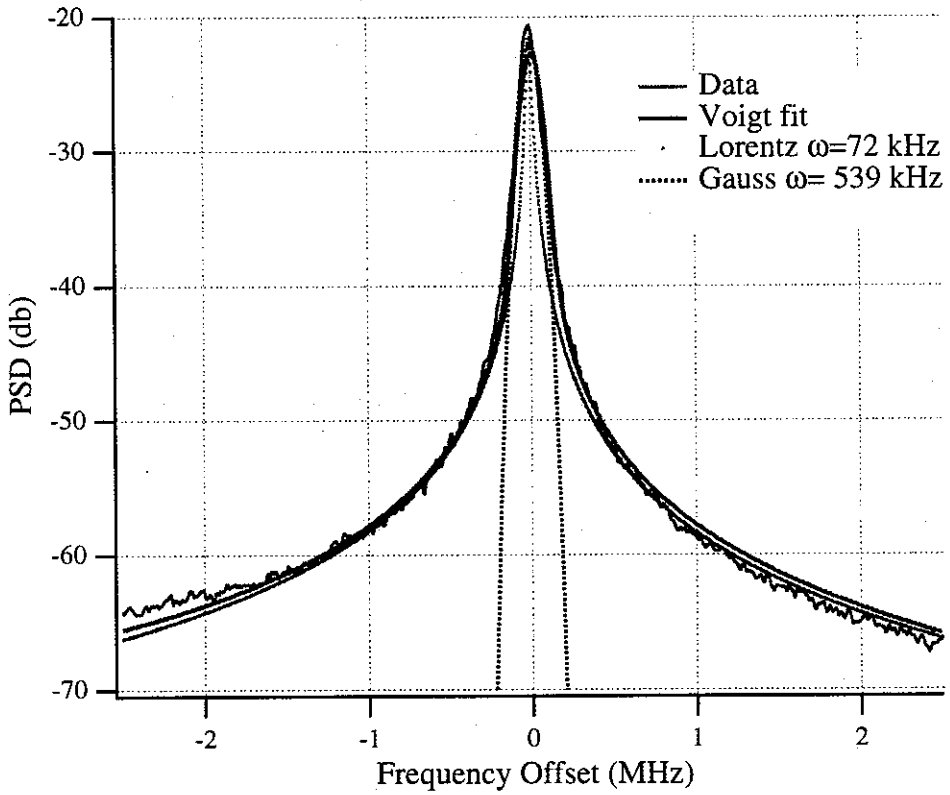

Figure 1-6 Beatnote between two diode lasers

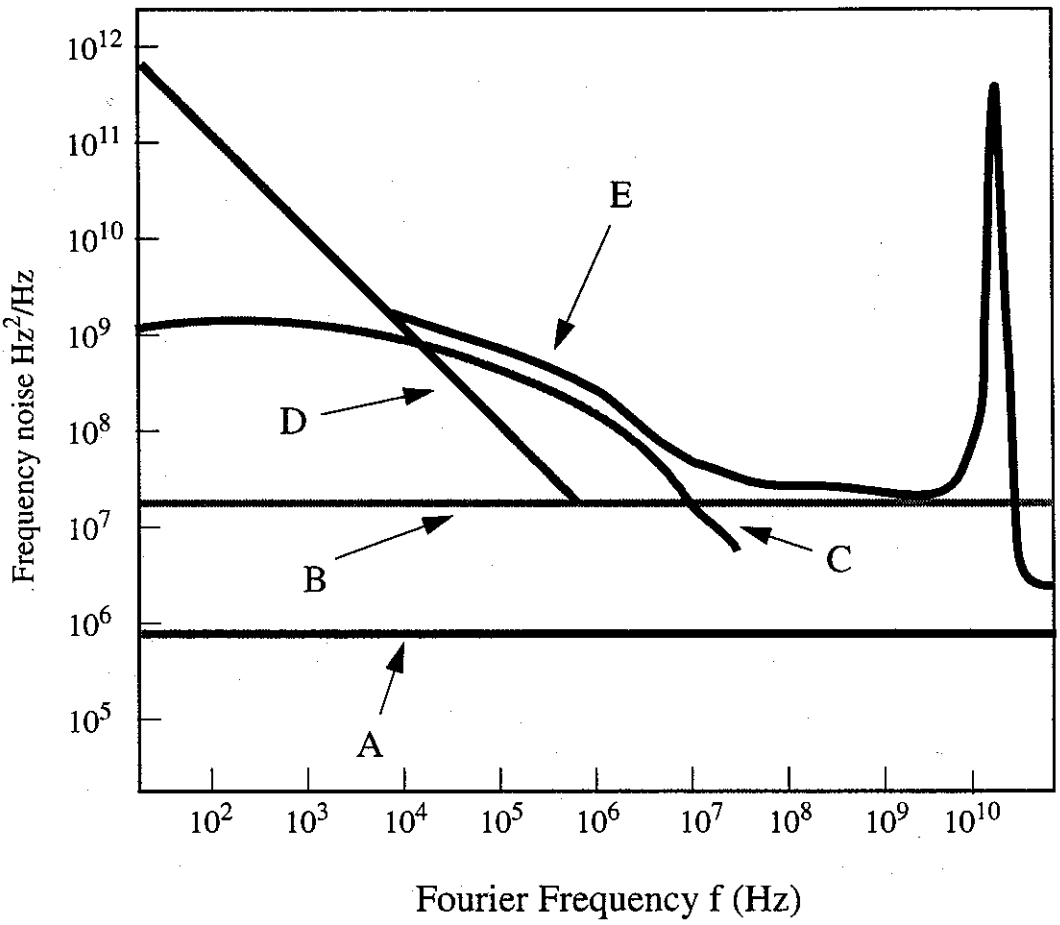

Figure 1-7 Noise Density in Typical Laser Diode

References

[1]Joan Lisa Bromberg, "The Birth of the Laser," Physics Today , October (1988): 26-33.

[2]W.E. Lamb,"Theory of an Optical Maser," Phys. Rev. 134, (1964): 1429.

[3]John L. Hall, "Frequency Stabilized Lasers - A Parochial Review," in Frequency-Stabilized Laser and Their Applications, ed. M. Ohtsu, Leo Hollberg, and Chung (Boston: SPIE, 1992), Vol 1837 2-15.

[4]W.R. Bennett Jr, and J.W. Knutson Jr ,"Simultaneous Laser Oscillation on the Neon Doublet at 1.1523 μ," Proc. of the IEEE 52, (1964): 861.

[5]P.H. Lee and M.L. Skolnick, "Satuarated Neon Absorbtion Inside a 6328 A Laser," Appl. Phys. Lett. 10, (1967): 303-305.

[6]V.N. Lisityn and V.P. Chebotayev, ZH. Eksper. Teor. Fiz. 54, (1968): 419.

[7]J.L. Hall, "P-1 The Absolute Wavelength Standard Problem," IEEE J. of Quant. Electr. 4, 10 (1968): 638-631.

[8]R.L. Barger and J.H. Hall, "Pressure Shift and Broadening of Methane Line at 3.39 micron Studied by Laser Saturated Absorbtion," Phys. Rev. Lett. 22, (1969): 4-8.

[9]S.N Bagaev et al., IEEE J. of Quant. Electr. 4, (1968): 868.

[10]Yu G. Rastorguev and A.N. Titov, "Increase in Frequency Stability and Reproducability of HeNe Standard using E component of Methane.," Sov. J. Quantum Electron. 21, (1991): 348-351.

[11]G.R. Hanes and C.E. Dahlstrom, "Iodine Hyperfine Structure Observer in Saturated Absorption at 633 nm," Appl. Phys. Lett. 14, (1969): 362-364.

[12]R.L. Byer and et al, "Optical Pumped Moleculer Iodine Vapor Phase Laser," Appl. Phys. Lett. 20, (1972): 463-466.

[13]R.W.P. Drever et al., "Laser phase and frequency stabilization using an optical resonator," Appl. Phys. B B31, (1983): 97-105.

[14]J. Hough et al., "Dye- Laser Frequency Stabilization Using Optical Resonators," App. Phys. B 33, (1984): 179-185.

[15]Zhu Miao and John L. Hall, "Stabilization of Optical phase/frequency of a laser system: application to a commercial dye laser laser with an external stabilizer.," JOSA B 10, May (1993): 802-816.

[16]T. Day, E.K. Gustafson, and R.L. Byer, "Active frequency stabilization of a 1.062 mm Nd:GGG, diode-laser-pumped nonplaner ring oscillator to less than 3 Hz linewidth," Opt. Lett. 15, 4 (1990): 221-223.

[17]Moler, K. Weis, D. Kasevich, M., Chu, S, "Theoretical analysis of velocity-selective Raman transistions," Phys.Rev. A 45, 1 (1992): 342-348

[18]R.C. Steele, "Optical Phase-Locked Loop Using Semiconductor Laser Diodes," Electron. Lett. 19, 2 (1983).

[19]B. Dahmani, L. Hollberg, and R. Drullinger, "Frequency Stabilization of Semiconductor Lasers by Resonant Optical Feedback," Opt. Lett. , (1987).

[20]P. H. Laurent, A. Clairon, and CH. Breant, "Frequency Noise Analysis of Optically Self-Locked Diode Lasers," IEEE J. of Quant. Electr. 25, June (1989): 1131-1142.

[21]Carl E. Weiman and Leo Hollberg, "Using diode lasers for atomic physics," Rev. Sci. Instrum. 62, January (1991): 1-19.

[22]J.L. Hall, Ma Long-Sheng, and G. Kramer, "Principles of Optical Phase-Locking: Application to Internal Mirror He-Ne Lasers Phase-Locked via Fast Control of Discharge Current.," IEEE J. of Quant. Electr. QE-23, 427-437 (1987).

[23]John L. Hall and Zhu Miao, "An Introduction to Phase-Stable Optical Sources.," in Proceedings of the International School of Physics 'Enrico Fermi', ed. E. Arimondo, W.D. Philips, and F. Strumia (North Holland, 1992), 671-701.

[24]D.S. Elliot and S.J. Smith, "Experimental Synthesis of phase-diffusing optical fields," JOSA B 5, Sept (1988): 1927-1939.

[25]Michael Philip Winters, "Correlated Spontaneous Emission in Zeeman Laser and High Resolution Optical Spectroscopy" (Ph.D, University of Colorado, 1990).

[26] Gardner Floyd M., Phaselock Techniques , 2nd ed. (New York:John Wiley & Sons,1979).

[27]Ronald N. Bracewell, The Fourier Transform and Its Applications, 2nd ed. (New York: McGraw-Hill Book Company, 1986).

[28]M.W. Flemming and A. Mooradian, "Fundamental line broadening of single-mode (GaAs)As diode lasers," Appl. Phys. Lett. 38, (1981): 511.

[29]Charles H. Henry, "Theory of the Linewidth of Semiconductor Lasers," IEEE J. of Quant. Electr. QE-18, Feb (1982): 259-264.

[30]Motoichi Ohtsu, Highly Coherent Semiconductor Lasers, 1st ed. (Boston: Artech, 1991): pg 40

[31]K. Kikuchi, "Effect of 1/f -type FM Noise on Semiconductor Laser Linewidth Residual in High-power Limit," IEEE J. Quant. Electr. 25, #4, April 1989 (1989): 684-688.

[32]Motoichi Ohtsu and Shinichi Kotajima, "Derivation of Spectral Width of a 0.8 micron AlGaAs Laser Considering 1/f Noise," Jap. J. Appl. Phys. 23, 6 (1984): 760-764.

[33]F.L. Walls and deMarchi A., "RF spectrum of a signal after frequency multiplication. Measurement and comparison with a simple calculation.," IEEE Trans. Instrum. Meas. IM-24, (1975): 210-217.

Chapter II: TRANSFER FUNCTION MEASUREMENT

Experiment

Introduction

In this chapter we describe the experimental apparatus and techniques used in the laser diode phase locking experiments. The laser sources for the experiments are external cavity lasers (ECLs) based on commonly available diode lasers. The diodes used were chosen based largely on their commercial availability at a "reasonable" cost,$180-$250, and on the ability to have them delivered at hand selected wavelengths that were matched, and of spectroscopic interest. That the laser diodes used generate a reasonable (20- 40 mW) amount of power and can be constructed with their front facets anti-reflection coated were also important considerations.

Incidental to the rest of the diode laser phase locking experiment was the development of a current source to drive the diode lasers. It will be described later in this chapter. Though it may no longer represent state-of-the-art performance its design has been published [1] and it has been a work horse of laser diode driven research at JILA with over one hundred copies having been made since its introduction.

The experimental section of this chapter is divided into roughly three parts. In the first part experimental equipment will be described when it is of unusual construction or when knowledge of its details is pertinent to understanding of the experiments.

In the second part the measurement of the laser diode's transfer function will be described. Lastly the operation of the ECL phase locking system will described.

External Cavity Laser

Diode Mount

In order to conduct the experiments first two nearly identical ECL diode lasers were built. In order to facilitate temperature stabilization the laser diodes (either Sharp LT-24 or Mitsubishi ML-6702) were mounted on a small copper pyramid with a knurled plastic ring. A thermistor was also glued into a hole in the pyramid with heat conductive epoxy. The same epoxy was used to attach a peltier cooler to the "bottom" of the pyramid. This whole assembly was then glued to a aluminum disk of about 1" diameter and one quarter inch thickness which had a 10-24 thread in it's back.

This whole unit could then be attached or removed from a special version of the "L" type JILA mount which had a large area of its aluminum back relieved to accept the copper disk. (See figure 2-1). In order to focus the laser diode a special aspheric lenses (chosen to have a numeric aperture of 4.0 or higher) were mounted in a plate, which was held to the front of the JILA mount with "D" washers so as to make it possible to center the lens by hand in front of the LD. The usual 80 pitch screws on the JILA mount then give three non-orthogonal degrees of freedom to adjust the focus of the LD or compensate for astigmatism.

ECL Body

In order to form the ECL the LD mount was fastened with five minute epoxy to either a 1/4"*2"*6" strip of Zerodur or a quarter inch thick 6 inch diameter piece of

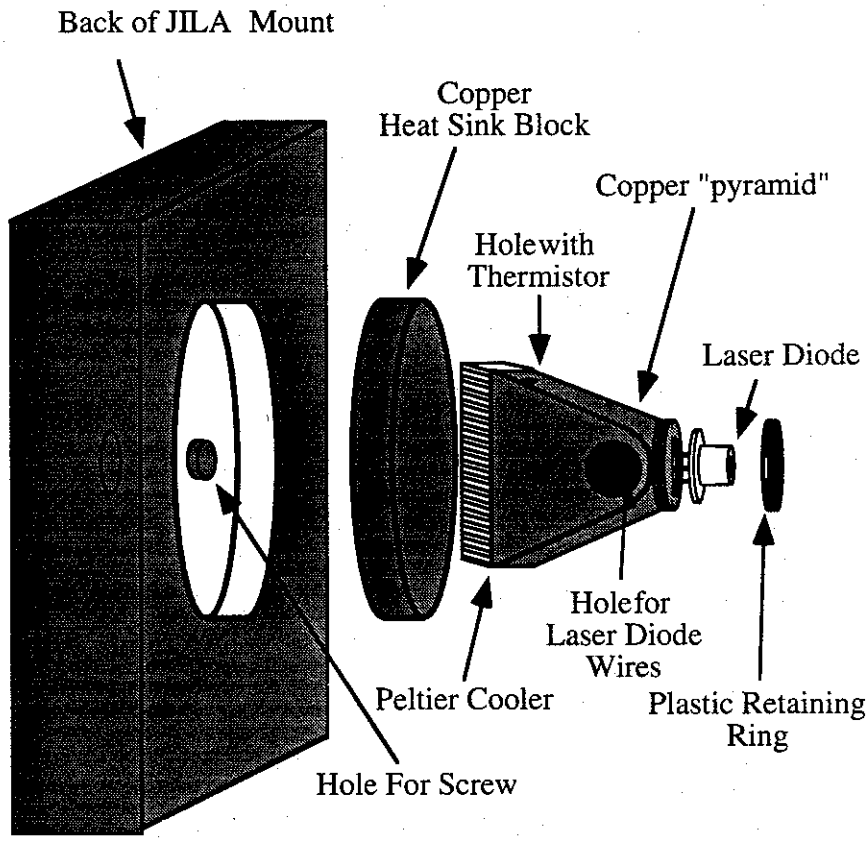

Figure 2-1 Laser Diode Mount

Pyrex glass. In order to provide cavity tuning for the ECL a 1 mm thick glass plate at Brewsters angle on a General Scanning model G108 galvo was placed about one cm in front of the LD lens. Another centimeter beyond the lens plate was placed a second JILA mount which held a diffraction grating. The grating, made by ARIES, with 1200 lines/mm and 750 nm blaze was mounted at Littrow orientation. The polarization of the LD output and grating rulings are chosen perpendicular so that 60% of the light was returned to the LD and 25% was taken as output (the remainder is lost in unwanted orders of the grating or absorbed by the grating's aluminum coating). The second JILA mirror mount also held a small mirror at a right angle to the diffraction grating. This mirror acts in concert with the diffraction grating and a pick off mirror to compensate any rotation of the grating and so keep the output angle of the ECL laser constant. See figure 2-2

ECL Can

After construction or modification, the completed ECL is placed in a sealed container. This is because previous experience had shown that even under quiescent conditions the air flow in the lab was enough to cause severe perturbations of the laser frequency. This is not surprising given that tests of the ECL showed more than 350 MHz/°C tuning rate. The container was designed jointly with Kurt Gibble and built in the JILA instrument shop (See figure 2-3). It consists of three pieces all cylindrical and 8 inches in diameter. One piece is the bottom piece in which the ECL rests on vibration dampening foam. It also has all the input and output connections for electronic connections. A second piece is the top which also has a side arm with a vacuum flange for the ECL output. Lastly a matching flange fitting with a small tube cut at Brewsters

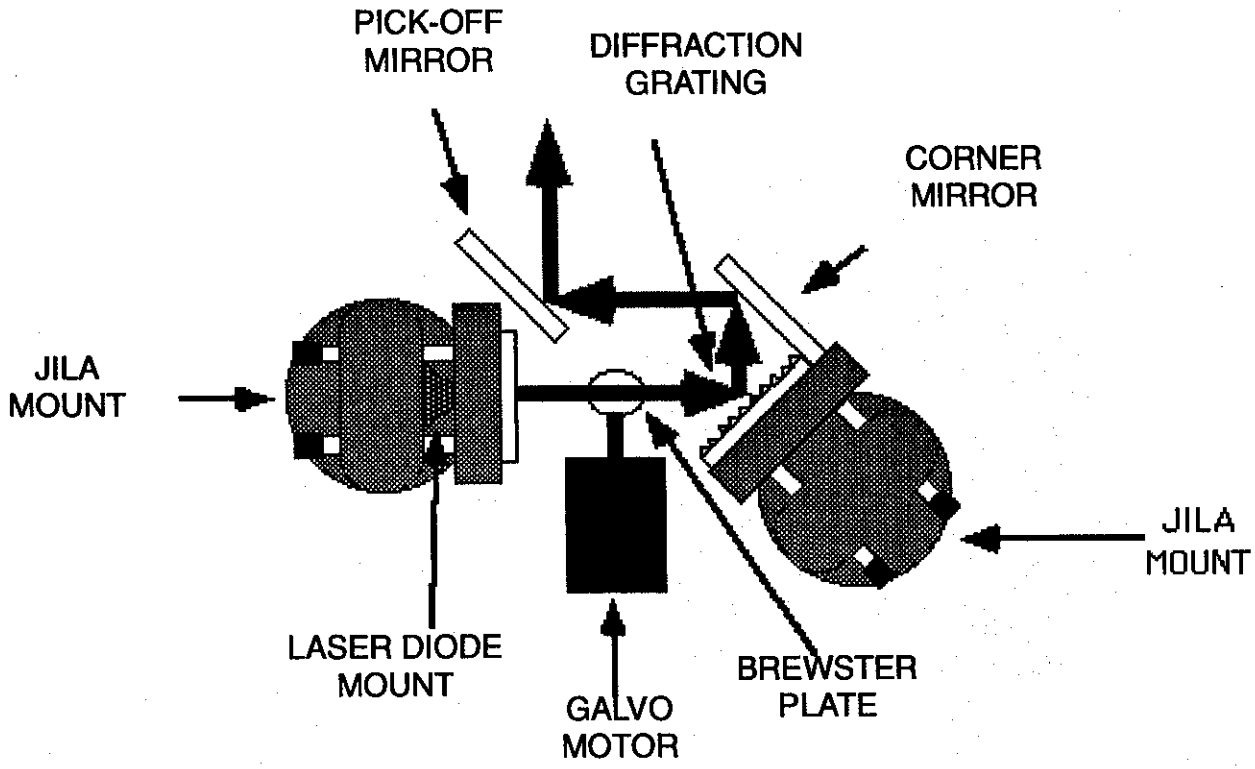

Figure 2-2 Configuration of ECL Laser

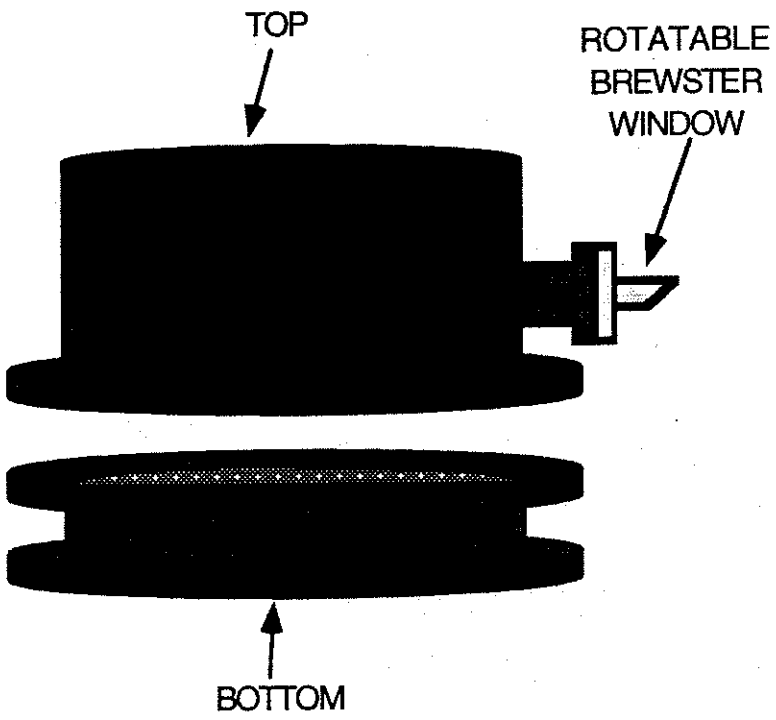

Figure 2-2 Laser Diode Container

angle served to carry an output window for the ECL. This arrangement allows the Brewster output window to be rotated for either horizontal or vertical output polarization.

The entire container is hermetically sealed and also is equipped with gas inlets and outlets for purging water vapor and O_2 from the optical path.

High Speed Phase Comparator

For this phase locking experiment it was thought at first that a limiting factor would be the speed of the phase comparator. It was also thought that a type 4 phase/frequency (FFL)[a] detector would be optimum to aid in the acquisition phase of the lock-in process due to the fact it can provided frequency steering in a large domain of frequency error [2] . Since this type of digital detector exhibits an inherent delay of at least one clock cycle it is obvious that a detector capable of high clock rate be should be used. At the time, emitter coupled logic (ECL) was one of the fastest technologies available so an FFL detector based on Motorola MECL[3] was built.

The circuit consists of four parts. A 45 MHz oscillator provides the reference against which the laser diode beat note is compared. A combination input filter, diode limiter and ECL comparator conditions the beat-note signal before injection into the FFL. An MC12040 integrated circuit was used as the phase/frequency discriminator. The output of this chip passes a notch filter to remove any 45MHz components and is then amplified and buffered by a NE5539 high speed op-amp.

---

a. A type of digital phase/frequency detector providing frequency correction information over the full range of ω_1-ω_0 and phase correction information over the range -2π to 2π. See ref [2] pg 7-14

Measuring Diode Transfer Function

Set Up

The transfer functions of the laser diodes used in this experiment were measured with a Michelson interferometer using a technique that was adapted from D. Welford and S.B Alexander [4] to measure the transfer functions of diode lasers for passive equalization in communication systems. This technique uses the linear portion of the sinusoidal fringe of a Michelson interferometer as an optical frequency discriminator.

The light path can be seen in figure 2-4. The output of the "bare" (no optical feedback) diode was first collimated then focused through a Hoya miniature optical diode which uses the Faraday rotation effect to provide isolation of the laser diode from back reflections and scattering. The laser beam is then recollimated and a small portion of the beam extracted for use in a 10 cm Fabry-Perot cavity. This cavity was used occasionally to calibrate the free spectral range of the Michelson.

The majority of the laser beam is coupled into the Michelson interferometer. The arm difference is chosen so the linear portion of the cavity fringes were much bigger then the expected maximum frequency deviation in any given experimental run. The maximum arm difference size is constricted by the coherence length of the diode laser output. In practice this translates to a system with about 5 cm arms and path length differences chosen to give FSRs between 1-3 GHz. One mirror of the Michelson was mounted on a piezo tube which allowed it to be moved back and forth so that the interferometer could always be operated in the linear portion of its fringes.

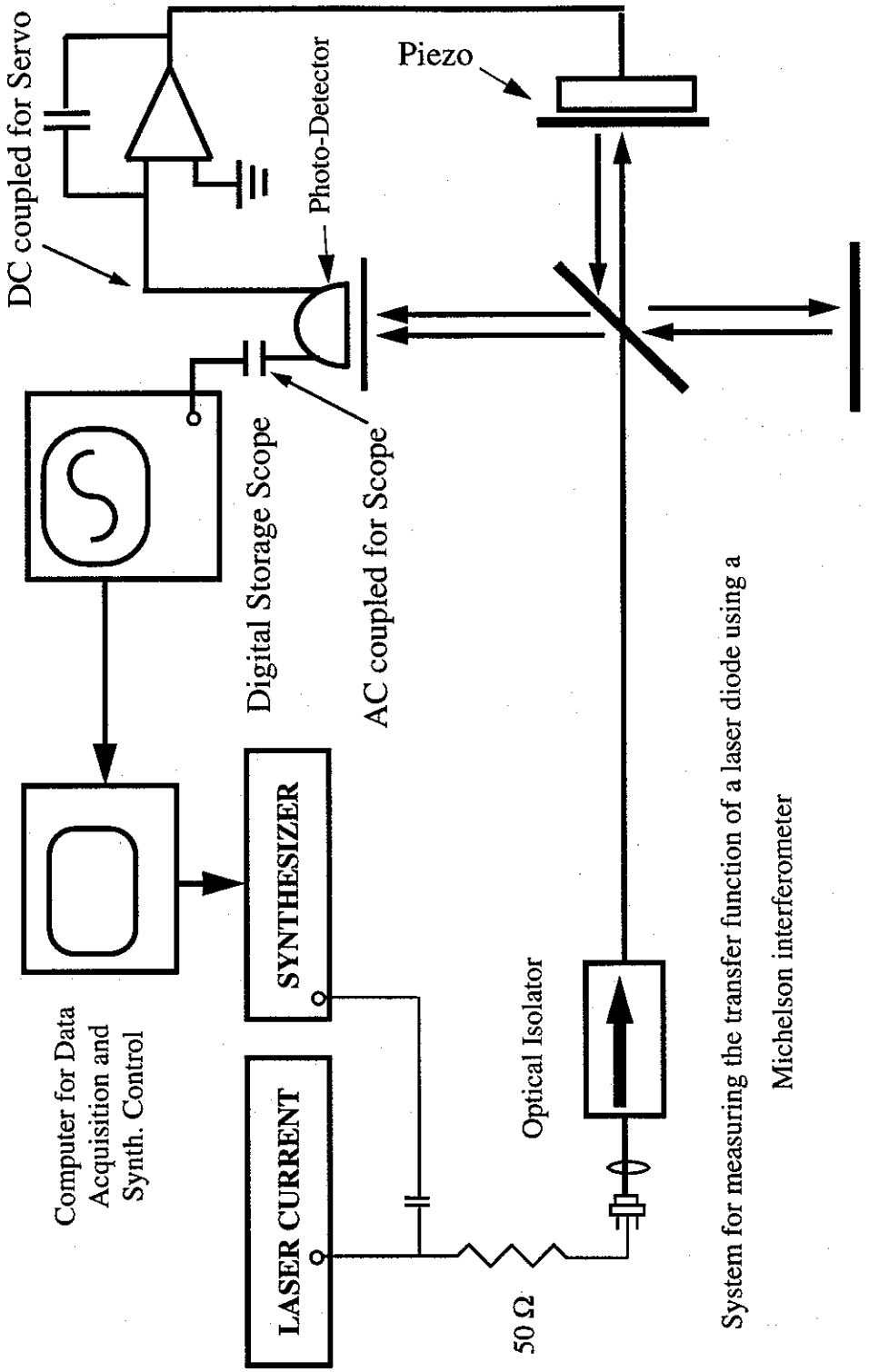

Figure 2-3 System for measuring diode laser transfer functions

The output of the Michelson is monitored with one of two photo detectors depending on the frequency range being tested. Both detectors also provide DC coupled output.

Experimental Procedure

At the beginning of an experimental run the DC coupled output from the photo detector is used to lock the Michelson interferometer to a point where its output intensity is one half its maximum. This is done by subtracting the photo detector output from a stable DC source and then using this difference to drive a slow servo loop which controls the piezo mounted mirror. The servo loop is designed so that its unity gain frequency is only a few hertz. This low unity gain frequency guarantees that the servo does not interfere with the rest of the experiment.

After the interferometer servo is locked, either an HP 8660c or HP 3325A digital synthesizer is summed with the current from the diode driver to induce a small amount of AM and FM modulation on the LD's output. While the transfer functions of the diode lasers were being measured a fifty ohm resistor was placed in series with the diodes to provide a proper termination for the signal generators

The response of the interferometer to the AM and FM of the LD, as detected by the photo detector, is digitized using an HP 54200 digital oscilloscope. The scope is triggered by a separate synchronization signal which is available on either generator. This assures good synchronization of the scope as it is used in its averaging mode during the experiment. When a sufficient number of averages are collected to achieve good signal to noise the output wave form is downloaded to a computer for further processing

In order to disentangle the FM from the AM and FM combination two more measurements are done. They are identical to the first except that in each case one arm of the Michelson interferometer is blocked with a dark card so that what is measured is the AM from the LD as transmitted through one arm of the Michelson. The digitized signals from each arm were then summed in a computer and this used as the total " AM only" signal. This AM signal was then subtracted from the AM plus FM signal to yield the FM only signal. This entire portion of the experiment runs under computer control and only requires human intervention when a change from high frequency to low frequency synthesizer is needed.

The digitized AM or FM signals are then numerically fitted on a personal computer using a linear least squares fitting routine. This is possible for the special case of fitting sinusoidal waves of known frequency because the phase and magnitude of the of the wave can be extracted from the linear fitting of the sin and cosine coefficients of the wave.

Transfer function measurement results

Introduction

If the change in laser diode output frequency were proportional to the current and free from time-history dependencies, then the phase locking of diode lasers would hardly have been a subject worthy of study. However application of time varying currents to the diode laser results in a host of effects interacting on different time and spatial scales. Ohtsu [5] pg. 94 suggests the diodes behavior can be general characterized by:

$$\Delta\nu = -\nu_l\left[\left(\frac{A_c}{n_i}\right)\Delta N(I) + (\alpha_T + \beta_T)\Delta T(I)\right] \qquad \text{Eq 2-1}$$

$$\text{Where: } A_c = \left(\frac{e^2\lambda^2}{8\pi^2 n_i \varepsilon_0 c^2}\right)\left(\frac{1}{m_e} + \frac{1}{m_h}\right)$$

where the first term in $\Delta\nu$ represents the change in refractive index due to the carrier density charge plasma effect. In the term Ac, m_e and m_h are the masses of the electron and hole respectively. The second and third term contributing to $\Delta\nu$ represents the temperature dependent change in cavity length and refractive index.

Low Frequency Behavior.

A typical example of the data is shown in figure 2-5 A&B which shows the magnitude and the phase of the AM vs. FM signal as measured for three different diodes. The Sharp LT-24which uses a VSIS structure, the Mitsubishi ML-6702 which uses a TJS and the Hitachi 7806G which uses as CSP type structure. In the region where the modulation frequency is less than 100 kHz to 1 MHz, the diode's behaviors are dominated by the thermal effect of bulk heating of the diode chip. The effects can be analyzed by either a lumped parameter or a continuous model, but the net result is the prediction that the thermal response is relatively flat out to some corner frequency and then falls off proportional to $\omega^{1/2}$. The large differences in the magnitude of the low frequency behaviors of different lasers are due to the laser chip size, the laser threshold current (the measurements are often normalized against % AM not % current), size, and the method by which the chip is mounted to block, and especially as to whether the laser chip is mounted N or P side down, as much of the heat is thought to originate in the P side contact. The results are similar to those of other authors who have made similar measurements. [4,6,7]

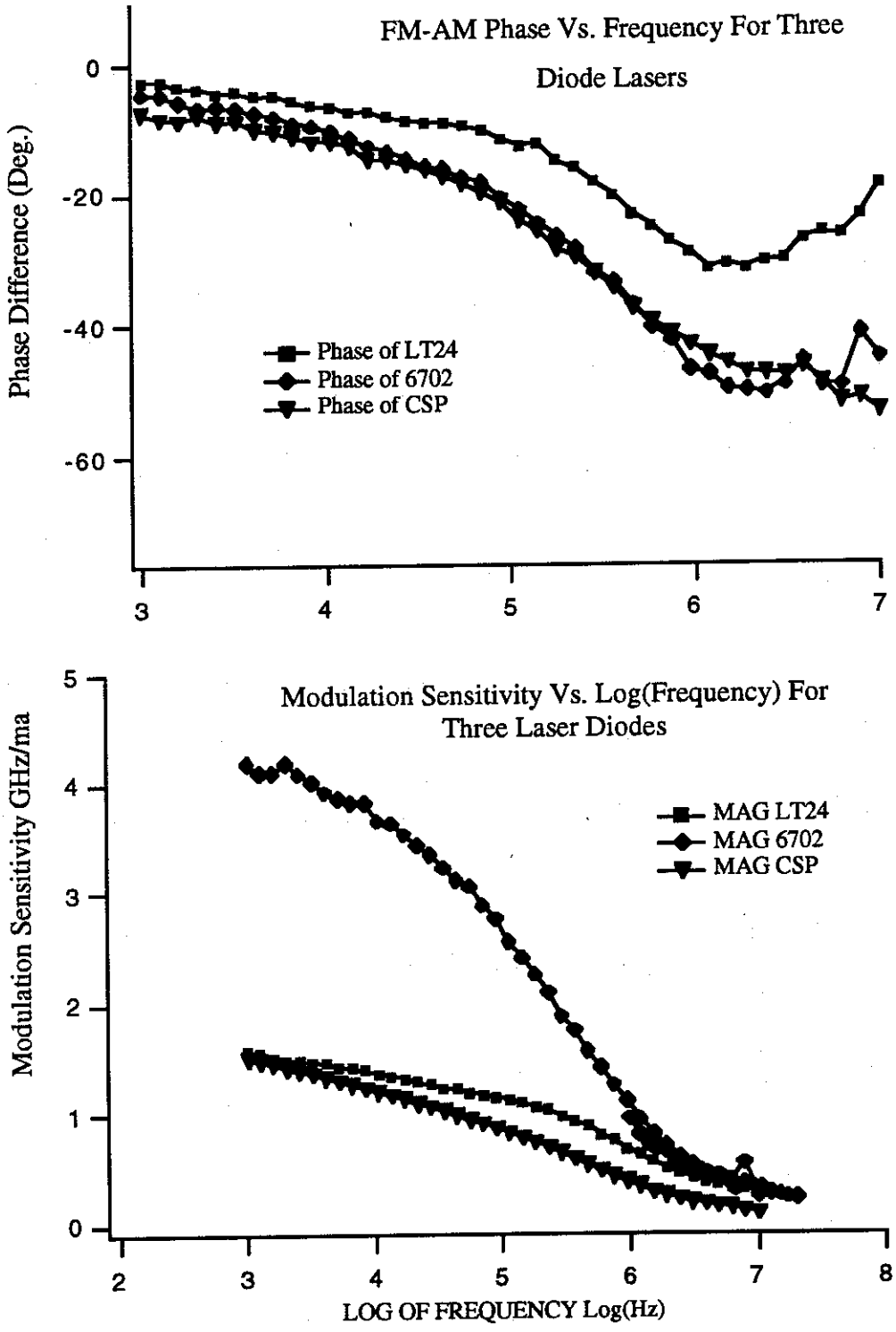

Figure 2-4 Measurement of the transfer function of three types of laser diodes

References

[1]Carl E. Weiman and Leo Hollberg, "Using diode lasers for atomic physics," Rev. Sci. Instrum. 62, January (1991): 1-19.

[2]Roland Dr. Best, Phase-Locked Loops: Theory Design & Applications, 1st ed. (New York: McGraw-Hill Book Company, 1984).

[3]Motorola, MECL DEVICE DATA (1985).

[4]D. Welford and S.B. Alexander, "Magnitude and phase characteristics of frequency modulation in directly modulated GaAlAs semiconductor diode lasers," J. Lightwave Technol. LT-3, (1985): 1092-1099.

[5]Motoichi Ohtsu, Highly Coherent Semiconductor Lasers, 1st ed. (Boston: Artech, 1991).

[6]Masaaki Imai and Koji Kawakita, "Measurementt of direct frequency modulation characteristics of laser diodes by Michelson Interferometry," Appl. Opt. 29, 3 (1990): 348-353.

[7]S.B. Alexander, D. Welford, and D.L Marquis, "Passive Equalization of Semiconductor Diode Laser Frequency Modulation," J. Lightwave Technol. 7, Jan (1989): 11-23.

Chapter III: EXPERIMENTAL DESCRIPTION

Demonstrating Phase Locking

In order to demonstrate that an improved knowledge of the laser diode transfer function coupled with the theory of wideband PLL design would enable the hybrid optical-electronic phase locking to work better, the experiment shown in figure 3-1 was constructed.

Multi-loop Servo

As can be seen the resulting experiment looks somewhat complicated. This is because of the multi-loop topology that was used. It splits the feedback signal into three frequency domains to provide the optimum feedback signal in each.

For reasons already discussed, it was anticipated that a servo with a unity gain bandwidth of several megahertz would be needed. In order to reduce delay time to a minimum it is desirable to use a double balanced mixer (dbm) as a phase detector in the high frequency region of the PLL system. The dbm was chosen because as a passive and simple device it has a minimum time delay[1]. The output of the dbm feeds a filter which compensates for the diode transfer function in the highest frequency range

While the mixer system provides the fastest part of the laser diode phase correction, the MCL12040 based phase detector provided all the feedback for frequencies

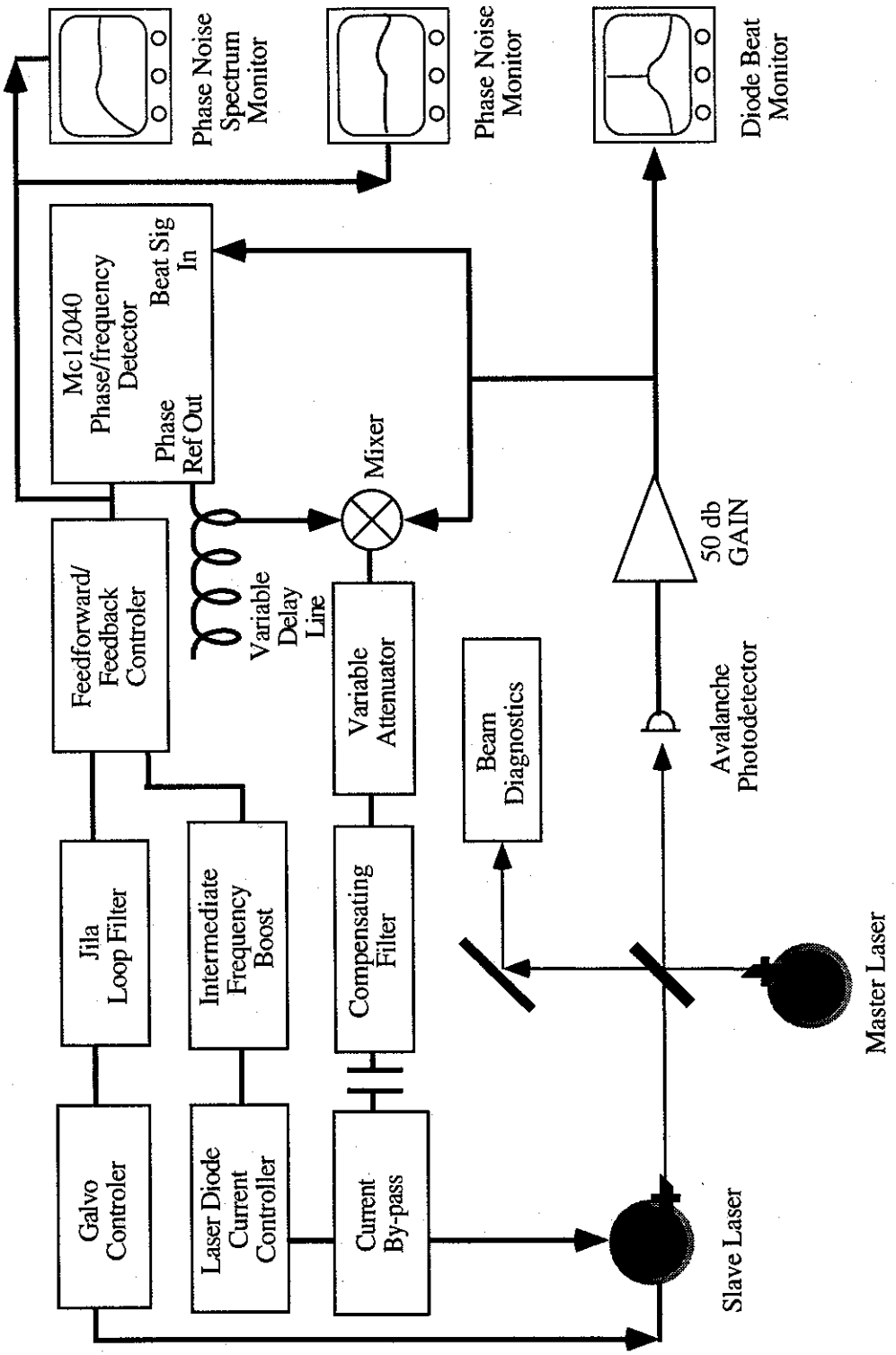

Figure 3-1 Experimental Setup for Phase Locking

below several hundred kHz. This is because the dbm type phase detector is much more prone to cycle-skipping due to it's limited (phase) dynamic range. The MCL-12040 also has the advantage of a much larger frequency pull-in range and therefore helps in phaselock acquisition and provides a more robust lock.

In the frequency range from several hundred kilohertz to several hundred hertz the feedback signal is routed through the laser diode current controller. At these (relatively) lower frequencies the extra delay due to two op-amps is acceptable.

In the frequency range below a few hundred Hertz the servo relies on feedback to the ECL's galvo-mounted Brewster-angled plate. The transfer function for the galvo feedback is obtained by routing this signal through a standard JILA low frequency feedback loop filter. The loop filter allows a number of different choices for integration order and corner frequency.

Experimental Apparatus

For practical reasons the slave laser must be easily tunable so that it can be brought to the same frequency as the master. In order to accomplish this a feedforward/feedback controller circuit was constructed. The purpose of the controller is to allow the experimenter to synchronously tune the laser's galvo plate and the laser diode current. It was found experimentally that tuning of the galvo plate alone would allow only 500-700 MHz of tuning range before a mode hop occurred, but that synchronous tuning with the current would extent this to 10 GHz. Provisions were also made on the controller for input of sweep and slow feedback error signals. See figure 3-2.

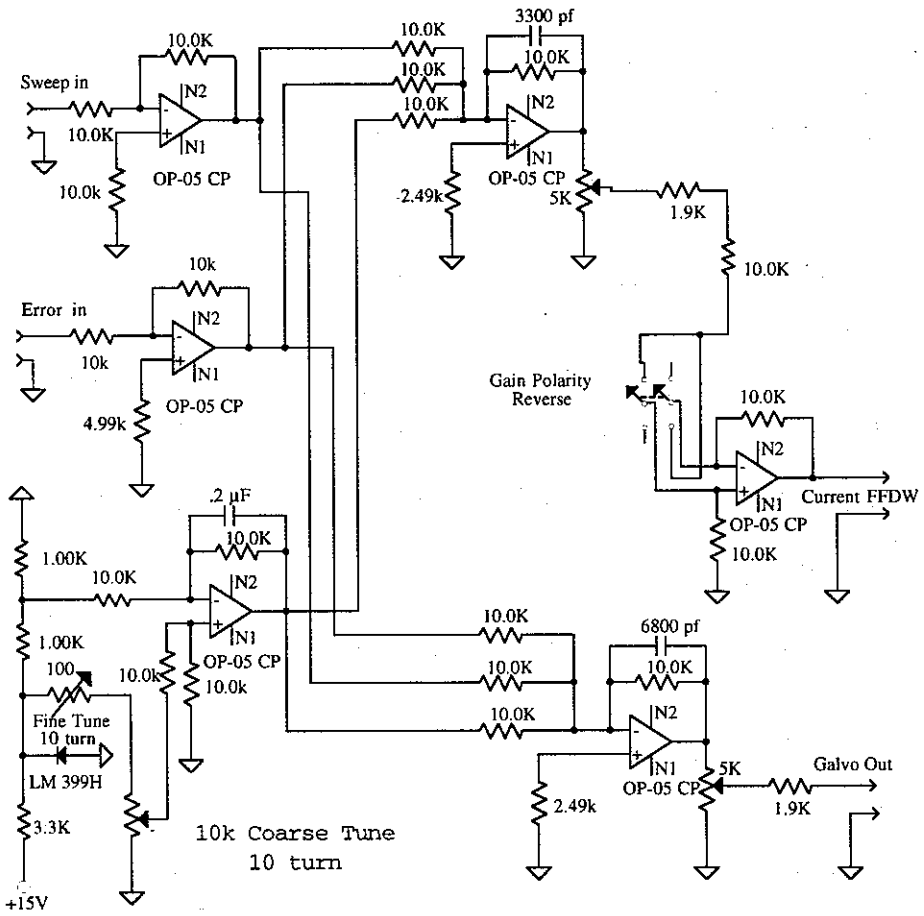

Figure 3-2 Feedforward/feedback controller for diode laser

Filter Synthesis

Because the transfer function of the diode laser is not a simple integer power of ω, it isn't a trivial matter to pick an inverse function filter. Alexander proposed [2] several topologies based on a series expansion of the transfer function which he measured. Several other authors have also discussed possible filters [3].

Since each diode differs in its transfer function the compensating filters and the diodes need to be matched. For this experiment the Sharp LT-24 was chosen.

As a starting point for building the servo, the topology in figure 3-3 was used and a short basic program was written that calculates its transfer function and it's error in compensating the diode laser. Initial and subsequent component values were chosen by hand and tested with the program. It was decided not to use the full power of a non-linear least squares inverting algorithm because past experience had shown "hand tuning" of the component values in a fast servo was usually necessary. This suspicion was confirmed as can be seen by the fact that the final filter has a different topology as well as component values. (see figure 3-3)

It was also decided that, rather than let the output of the buffer amplifier drive the diode directly, it would drive a "current bypass". This bypass was designed so it could only take current away from the laser diode. This ensures that an unexpectedly large transient from the locking system only results in the loss of current to the diode and not damage due to excess current.

The bypass was implemented as a current mirror based using a CA3028 integrated circuit. The current mirror works by drawing a few milli-amps of current away from the diode laser during no-input conditions. The amount of current taken by the

Initial Topology for Current Bypass

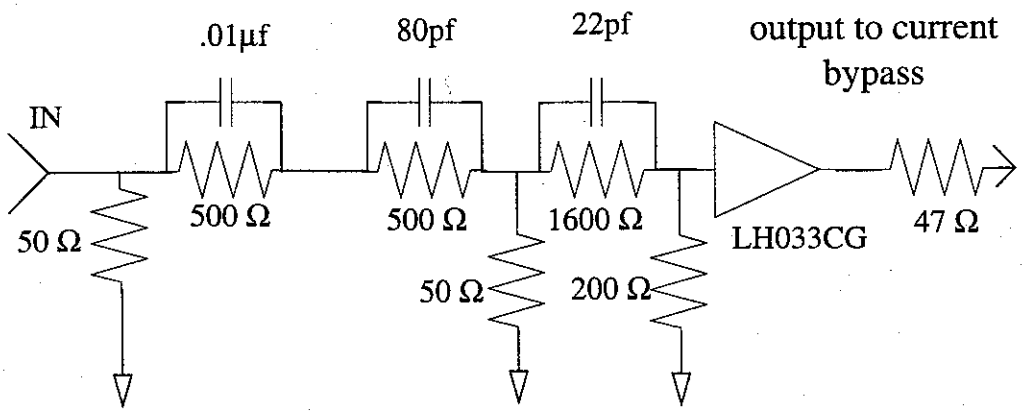

Final Topology for Current Bypass

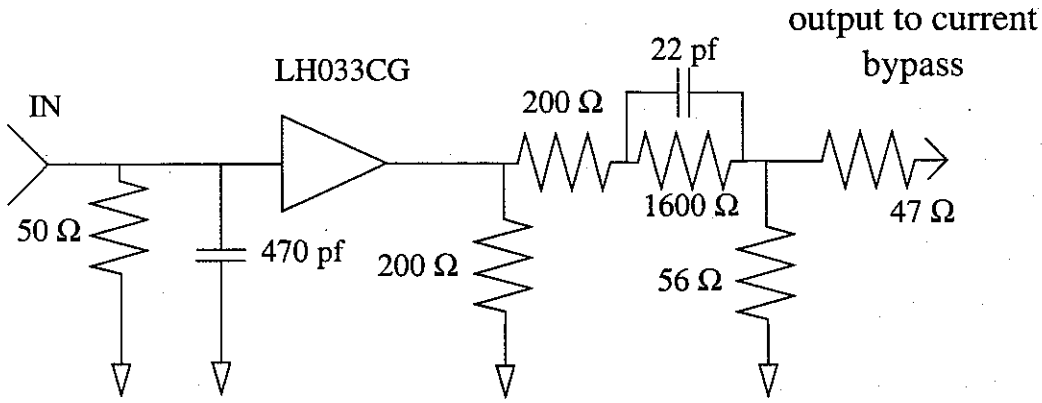

Figure 3-3 Initial and Final Topology for Diode Compensator

current mirror is then modulated by driving current into or out of the current mirror control port. The current mirror gets its name from the fact that the current taken from the laser diode is equal and opposite the current at its input. Figure 3-4 show the current mirror's layout. Tests of the current mirror showed that its -3db point was well beyond 30 MHz, so it was assumed that it's delay time was small enough not to affect the over all servo speed.

The filter and bypass are driven from the dbm. The phase comparison frequency was 45 MHz and the reference was supplied from the MC12040 PLL box. An adjustable delay line between the PLL box output reference and the mixer LO port was used to bring both phase-detection systems into agreement on where the τ=0 point was. A variable attenuator between the a signal splitter and the dbm served to control the level of feedback through the current bypass. At first a fourth order Butterworth filter with -3db at 15 MHz was used after the mixer to remove harmonics of the mixing frequencies, but this was later changed to a series of notch filters at 45 and 90 MHz when the lowpass filter was found to have a large detrimental effect on the loop performance.

Current Controller Servo

Initially the transfer function for the phase detector to current controller was a simple bandpass filter with corner frequencies at 8.8kHz and 680 kHz. The lower frequency allows a JILA loop filter to servo the ECL's galvo plate without interference from the current controller. The high frequency corner does the same for the dbm to current bypass system. Early results from the phase locking experiments clearly showed a problem in the region from DC to 400 kHz so a more elaborate transfer func-

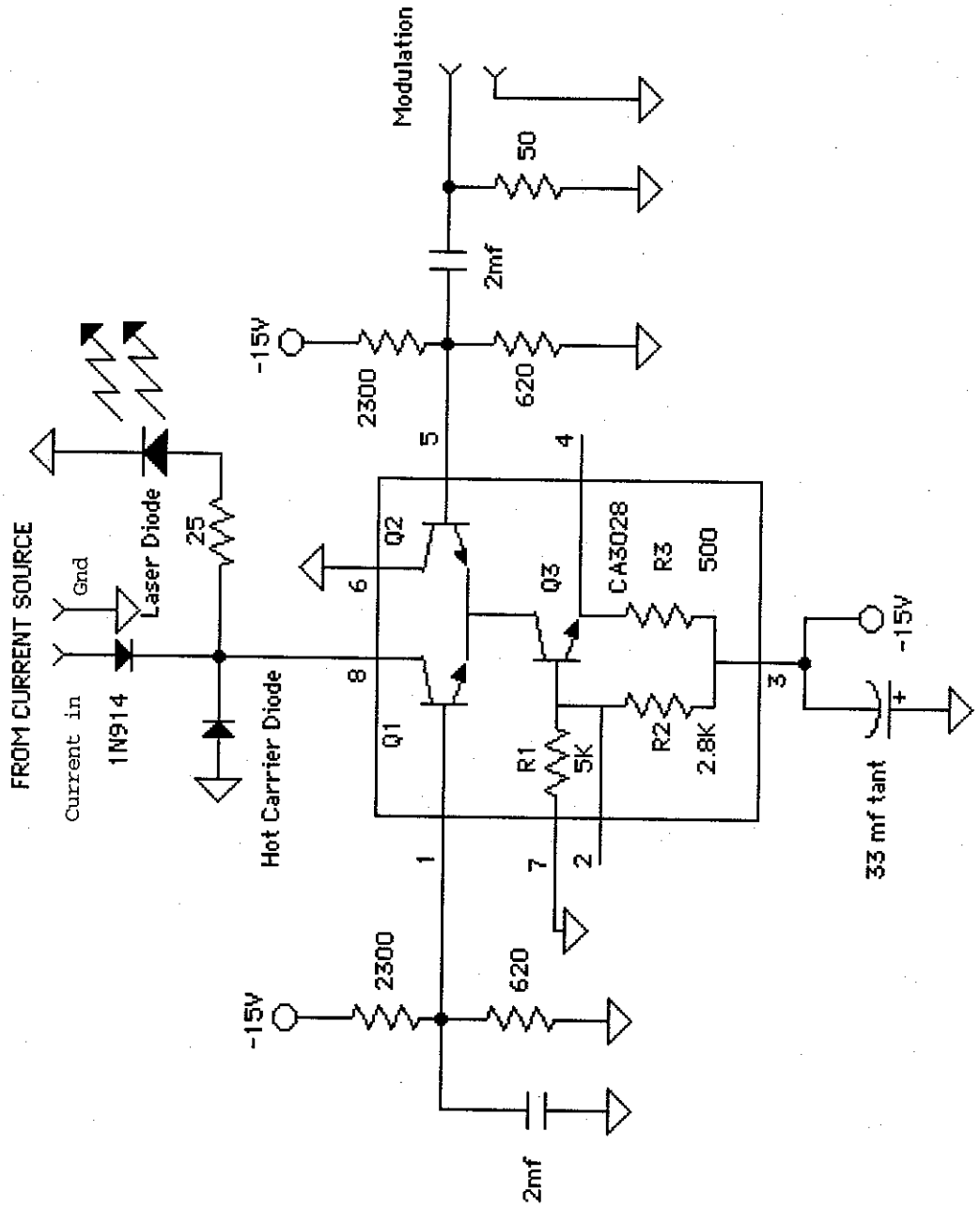

Figure 3-4 Schematic of Current Bypass

tion was used and a switch was installed in the circuit that let the two choices be compared. Figure 3-5 shows the circuit and figure 3-6 the two transfer functions. Figure 3-7 shows the relative effect on the quality of the diode beatnotes in the region within 1 MHz of the lock point.

Results From Phase Locking Measurements

Actual operation of the equipment is very straight forward. The system is started with all the feed backgains off. The master laser is set to any frequency in the range over which the phase locking laser can be tuned. This was at first done with a grating spectrometer and later with a lambdameter. Then both laser beams are overlapped on the avalanche photodiode. The output of the photodiode is sent to the phase locking electronics and monitored with a spectrum analyzer. When the laser beatnote is seen it is adjusted to F=45MHz by the feedfoward/feedback controller. At this point the gain of the JILA loop filter and the gain of the current controller are increased in an iterative fashion till they show signs of impending oscillation. The "fast loop" gain is then also increased to an optimum setting. Careful adjustment of the reference delay line is then made to be sure all the servos agree on where zero phase is. Tests of the servo's performance were made by numerically examining the beatnote with a spectrum analyzer to determine what fraction of the diode beatnote energy was in the delta-function and what fraction was in the pedestal. The shape of the pedestal was also examined to see if it conformed with the expected shape. Typical result is shown in Figure 3-8 . The graph is a composite of three measurements taken with the analyzer's

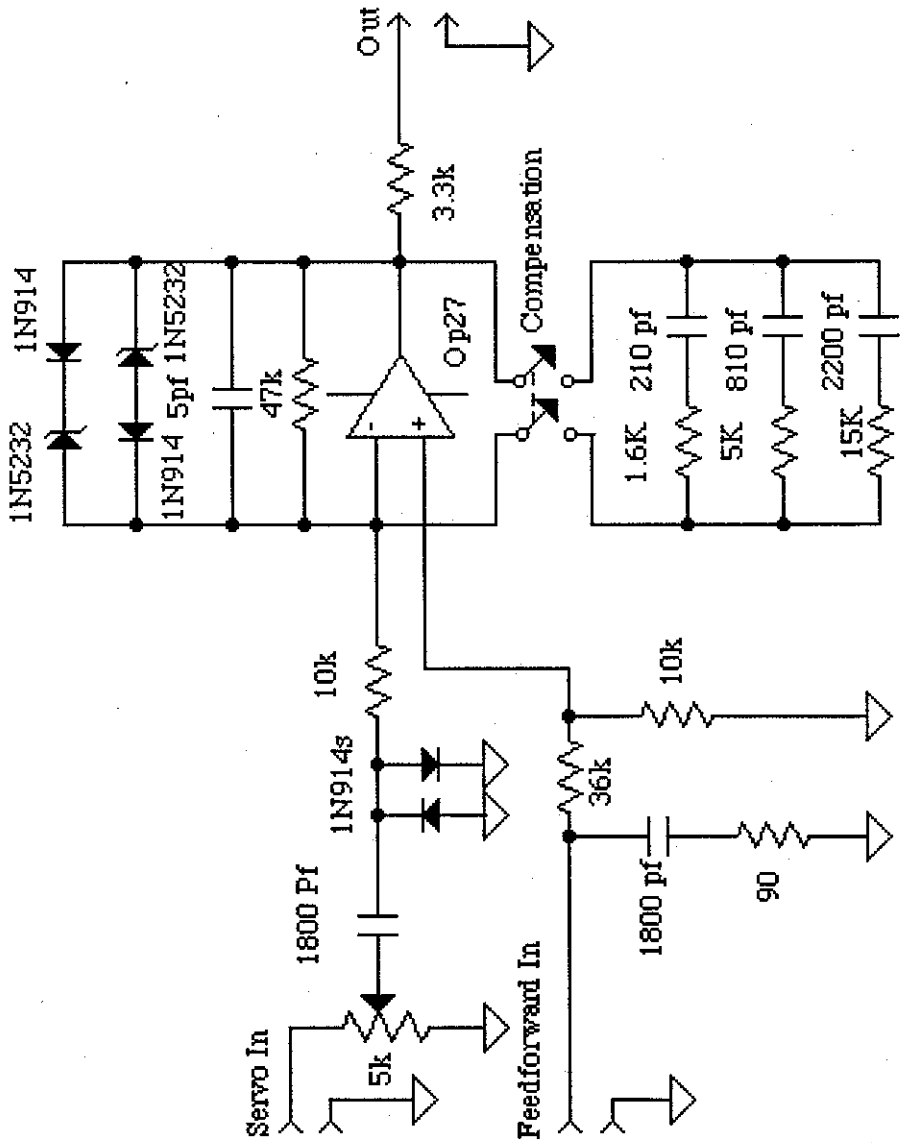

Figure 3-5 Schematic of Current Controller Compensator

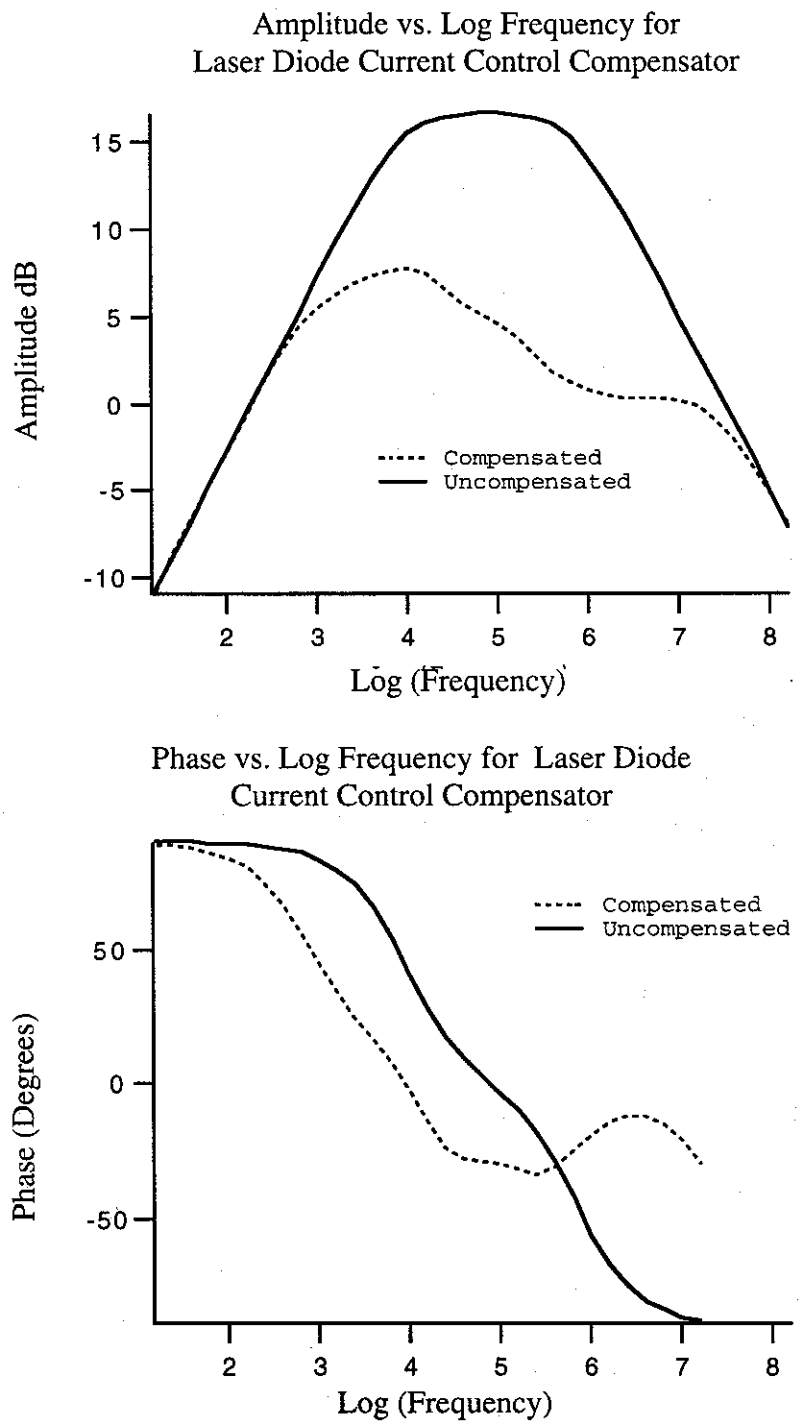

Figure 3-6 Transfer function of current control compensator

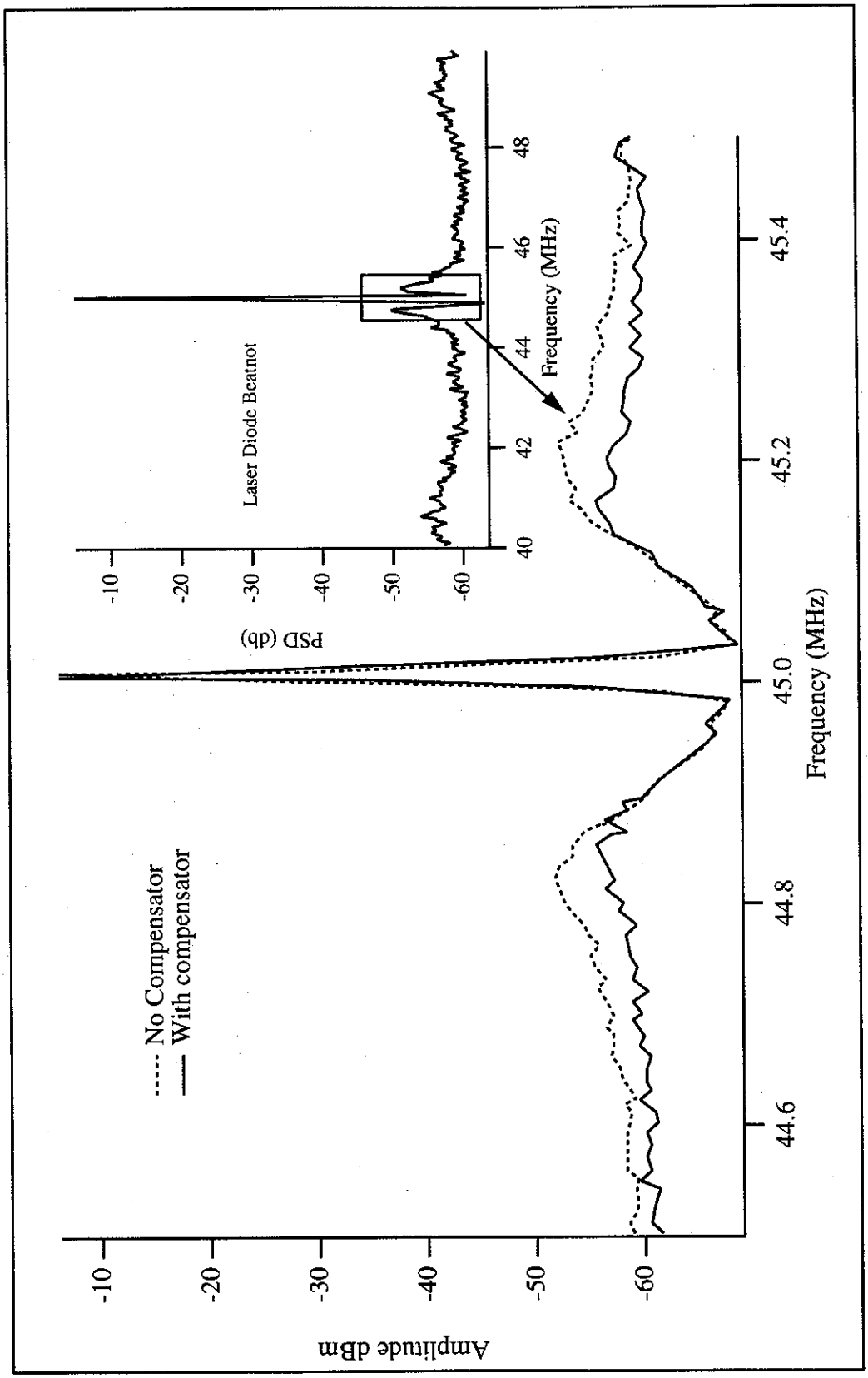

Figure 3-7 Central Feature of laser diode beatnote

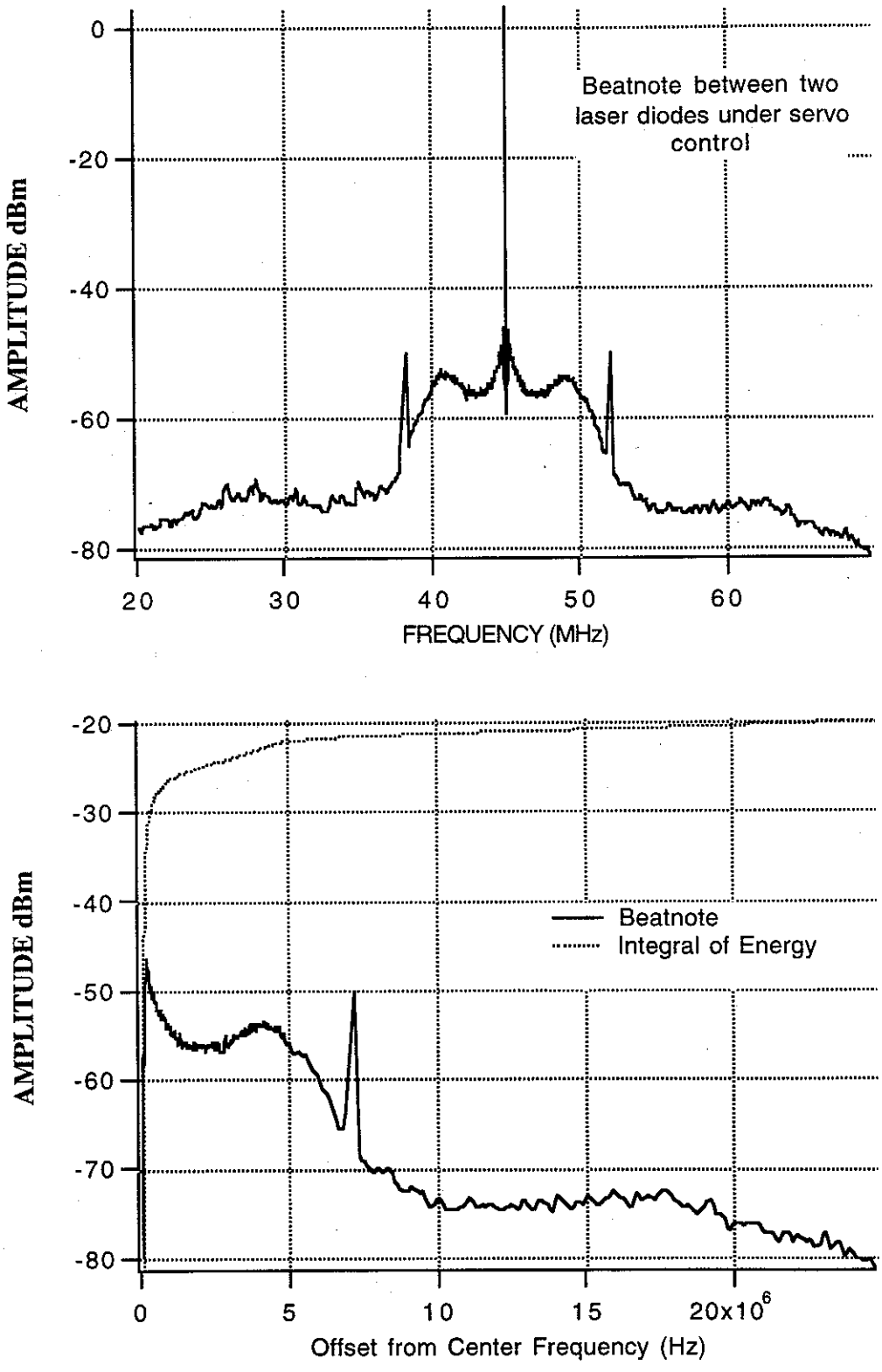

Figure 3-8 Beatnote and Energy integral of for diode beatnote

span set to 50MHz,10MHz and 1 MHz respectively. This is necessary because no single setting has both the span and the resolution needed. The delta like functions at 45MHz ± 7 MHz are rf pick up from a nearby experiment and do not affect the results of measurements significantly.

Overall the performance of the system is quite good. The fraction of energy in the pedestal is 0.49% and the system shows a unity gain bandwidth of about 4MHz. The energy integral is shown in graph 3-8 b. As can be seen, a large part of the integral comes from the region within 500kHz of the central core. This shows the cross over region between the current controller servo and the fast mixer servo is almost as critical as the ultimate servo band width and should probably be given more attention if this region is considered critical to the particular experiment at hand

Possible improvements to existing system

One improvement which is possible is moving the comparison frequency for PLL systems to a higher frequency. In the current system the choice of 45MHz was made based on the maximum operating frequency of the MC-12040 phase detector. A faster alternative, the Analog Devices AD-9901 is now available. This chip can operate at comparison frequencies up to 200 MHz and provides a more linear transfer function then the MC-12040[4]. The technology of fast rf frequency divider chips also provides a possible improvement. A fast divider chip can be placed between the photodetector and the phase/frequency detector, but not the mixer/phase detector. This would results in the phase/frequency detector having a much wider frequency range for acquisition purposes, but without it having to operate at any faster clock speed. The mixer would still see the full frequency content of the beat signal and enjoy the reduced its time delay. It is not hard to imagine a system with a 100 MHz comparison clock for the frequency/phase detector proceeded by a divide by 16 pre-scaler. Such a system would have over 1 GHz acquisition range and less then 1 ns delay in its mixer stage. A drawback to this idea is that the constraints on keeping phases in both channels of such a system in agreement may be difficult.

Ultimate Limits

Shot noise

According to Hills [5] the frequency noise density (Δ) for a laser with power P and photodetector quantum efficiency η locking to a cavity with sidebands of modulation index β is:

$$\Delta^2 = (\Delta\nu)^2 \frac{[1 - [J_0(\beta)^2 (2\sqrt{D} - D)]^2]}{D} \frac{e}{4J_0(\beta)^2 J_1(\beta)^2 P\eta} \qquad \text{Eq 3-1}$$

Where the resonant efficiency is D and resonant linewidth FWHM=$2\Delta\nu$. Using as an example a system in which β=1, D=0.1, P=300μw and $2\Delta\nu$=1 MHz we get $\Delta\nu$=24 milli-Hertz/Hertz$^{1/2}$! It should be noted that this in no way represents an extraordinary cavity. As derived in the previous sections if the noise spectra were flat as expected from shot noise, the central (delta-like) feature of laser under would have a linewidth of $\pi\Delta^2$ or 7.5 milli-Hertz. This level of performance would be difficult to attain due to amplitude noise in the laser, but, anything even close is not bad for a diode laser that starts out with 10 MHz linewidth and costs a few tens to hundreds of dollars and should have a minimum working life in the tens of thousands of hours[a].

a. Methods for suppressing the intensity noise of the laser exist, as due detection methods which are less sensitivite to the laser intensity noise, however the laser current alone cannot make fast corrections to the intensity noise and the frequency noise because their correlation function is not a constant.

References

[1]William Egan, "Sampling Delay- Is it Real?," RF Design , Febuary (1991): 114-116.

[2]S.B. Alexander, D. Welford, and D.L Marquis, "Passive Equalization of Semiconductor Diode Laser Frequency Modulation," J. Lightwave Technol. 7, Jan (1989): 11-23.

[3]Linlin Li, "The Optimal Loop Gain for the Spectral Linewidth Reduction in an Electrical Feedback Simeconductor Laser," IEEE J. of Quant. Electr. 27, 8 (1991): 1975-1980.

[4]Allen Hill and JIm Surber, "The PLL Dead Zone and How to Avoid it," RF Design , March (1992): 131-134.

[5]D. Hils and J.L. Hall, "Ultra-Stable Cavity-Stabilized Lasers with Subhertz Linewidth," in Frequency Standards and Metrology, ed. A. DeMarchi (Berlin,Hiedelberg: Springer-Verlag, 1989).

Discussion

Introduction

Attempting to look very far into the future of an emerging technology (like laser diodes) can be seriously dangerous. It is asking to be remembered for ones contributions to the list of fool's predictions such as "if man were meant to fly he would have wings, or, "I don't believe there is any reason anyone would want a computer in their house". That said, I shall restrict my comments as much as possible to the near future of laser diode technology and frequency control issues.

In the here and now there is one factor which makes nearly all laser diodes (LDs) difficult to use for atomic and molecular experimentation, that is, they were not designed for it. Most of the available diodes were designed with telecommunications, information storage and retrieval (including CD players), or optical pumping of other lasing mediums like Nd:Yag in mind. This means that the available LD's wavelengths are not the one's which would necessarily be chosen for scientific purposes. Similar problems involving beam power, astigmatism, ellipticity, LD packaging etc. abound. This is not to say that beautiful work has not already been done with laser diodes. The recent demonstration of Bose-Einstien condensation is one example[1]; another is the work on the Rb two-photon optical reference [2], which previously required a Ti:Saphire laser and has already been moved to the laser diode domain through the use of build-up cavities. Because the build up cavity guarantees the mode-matching of the forward and backward running waves the repeatability of this reference is now < 200 Hz.

Many of the current laser diode's shortcomings have already been sidestepped.

With regards to available wavelength a number of schemes have been devised that involve heating or cooling the LD or using frequency selective optical feedback to "pull" the diodes off their natural lasing wavelength. Odd beam geometries can be largely compensated with optics and true Gaussian modes can be obtain by filtering the LD output through a Fabry-Perot etalon. Unfortunately, maximum power is still something over which the scientific community has little say[a], although higher power diodes at some wavelengths have become much cheaper.

This brings us back to the question of whether frequency control is now a "solved" problem. The answer without a doubt is a qualified maybe. The "maybe" of course comes from the challenge of what level of frequency control is required by any given experiment. We have shown in this paper that a 780 nm LD in an external cavity of typical dimensions exhibits a Voigt-like profile in which the Gaussian of 500-200 kHz HWHM and the Lorenzian ≈70 kHz HWHM. This lineshape is fine for some optical pumping experiments in allowed transitions like the D_2 line in Rubidium (unless the energy in the far wings is problematic). As a method for observing hyperfine splitting in overtones of simple gases (requiring a HWHM of few kHz) it would not work.

As a method of assessing the effects of a frequency/phase control servo we have developed the idea of measuring the fraction of the laser's energy which is gathered into a central delta like feature. For the simple case of a pure Lorenzian lineshape a theory has been derived showing this fraction of energy can be quickly estimated if the HWHM of the Lorenzian is known and is much smaller then the servo unity gain bandwidth. This formula is:

---

a. The emergence of MOPA or master oscillator power amplifier technology from Spectra Diode is a very good sign.

$$\text{Fraction of energy in Carrier} = 1 - \frac{\text{HWHM of Lorenzian}}{\text{Servo untiy gain bandwidth}} \qquad \text{Eq 3-2}$$

It has also been shown that the finite servo gain or the frequency measurement noise can be taken into account by approximating the frequency noise as an ideal system plus a frequency independent lower noise floor. The line shape for the lower noise floor can then calculated separately (choosing a flat noise floor produces a Lorenzian) and this line shape can then be convolved with the ideal one from the servo. For most practice cases this should have no real effect except to assign a finite width to the inner delta function.

The existence of 1/f noise was shown to significantly degrade the predicted performance of the servo action and to reduce the expected linewidth versus length gain in an external cavity laser. In order to overcome this, a servo of at least second order is recommended, at least until the 1/f noise and the constant $1+\alpha^2$ enhanced Schawlow-Townes noise are of equal magnitude. From equation 3-2 it can then be estimated if the required fraction of energy in the central delta feature can be met by the hybrid optical plus electronic feedback methods discussed in this paper. The 5 MHz bandwidth achieved in this demonstration should by no means be considered the maximum possible; in 1991 a 134 MHz optical phase-locked-loop was reported although using a special diode[3].

There are still other remedies that can be used to improve spectral purity of the laser diode if those discussed are not sufficient. One choice is filtering of the LD's output through a high finesse cavity. An obvious implementation is to lock the LD to the

cavity using the high speed electronic methods described earlier. This will narrow the LD's linewidth, allowing the use of a cavity which is much narrower than the diode's initial linewidth, while loosing little power and removing the residual phase noise pedestal. In figure 3-9 is a graph comparing the spectrum generated in the phase-locking experiments with a theoretical one generated by multiplying it with the transfer function of a 500 MHz cavity that has a finesse of 1000.

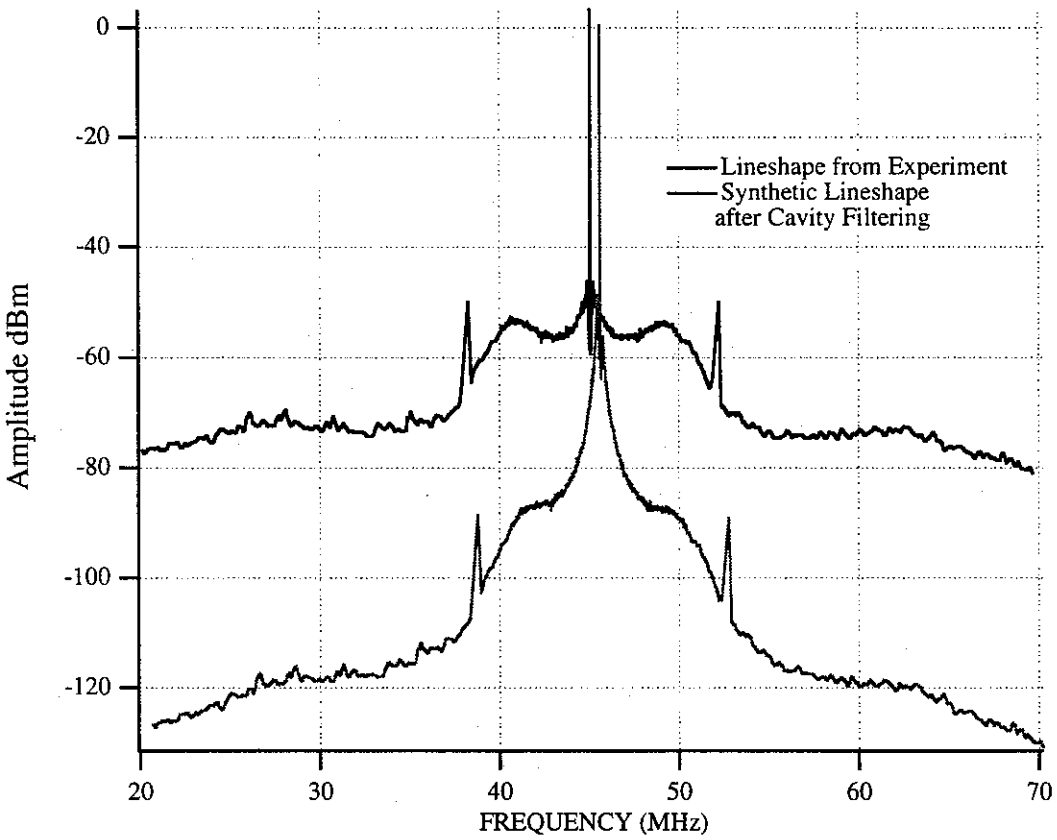

Figure 3-9 Lineshape before and after cavity filtering

(A small frequency offset has been introduced to make the graph more clear)

Two of the easiest possible steps that can be taken to reduce frequency noise in any laser diode system may have already been taken by the average experimenter

without even knowing it. These are using higher power, and switching to a quantum well laser diode. The modified Schawlow-Townes equation (Eq 1-41) like the unmodified (similar to Eq. 1-13) one predicts a drop in quantum noise that goes as 1/power in the laser cavity. Since ECDLs have low finesse[a], and this cannot be changed, simply using a higher power diode can lower the broadband frequency noise. In most cases experimenters tend to want the most optical power they can easily afford, so this is not difficult advice to follow[b]. Quantum well lasers typically have α factors of 2-3, lower then the 3-6 double heterostructure lasers have. Since this factor contributes as $(1+\alpha^2)$ to the fast line width, a factor of 4 can be gained here. The good news is that quantum well lasers are also favored for use in high power diodes and ones with low threshold currents. The bad news is that because they are more difficult to fabricate they are not available at all wavelengths.

It is natural to be skeptical that this demonstration of phase locking translates easily into multiple diode types or frequency control, as opposed to phase control. In order to allay skeptics, rather then present mathematically argued formalism, I offer Figure 3-10. This figure shows the beatnote at 633 nm between an ECLD in Littman configuration and a HeNe Laser which is stabilized by offset phase-lock to an iodine stabilized HeNe[c]. The figure shows that a servo bandwidth of 2 MHz is conveniently attainable. It is worth noting that LD used to obtain this figure can easily tune plus or minus five nanometers, the same cannot be said for the HeNe lasers which were used.

---

a. Internal loss in a typical AlGas diodes is $\alpha_l \approx 10 cm^{-1}$ where transmission $= e^{-\alpha_l * 300 \mu m} = e^{-3} = .05$

b. This does not help reduce the power independent 1/f noise, but it is the broadband quantum noise that requires multi-MHz servos to suppress.

c. Thank you to Pierre Dube for use of this data

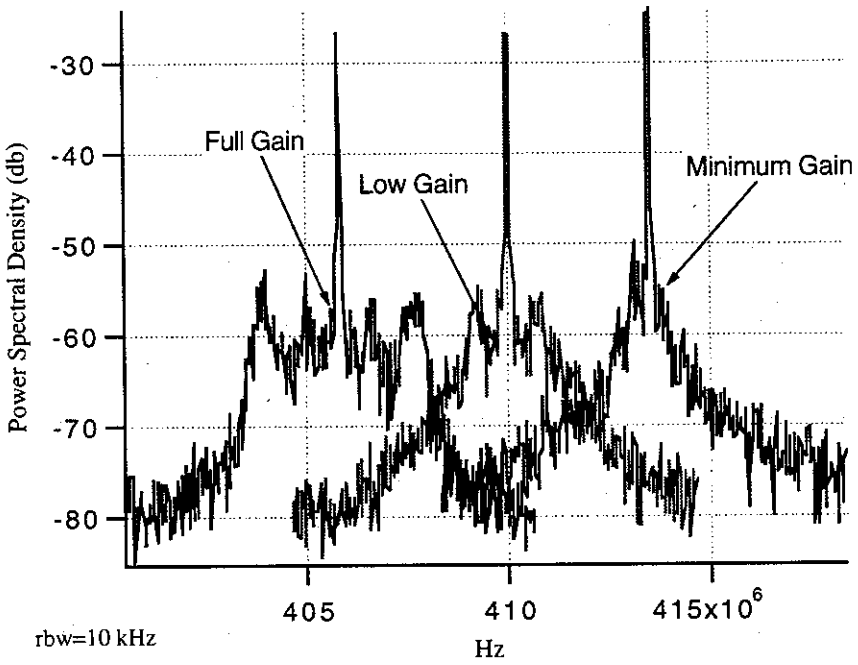

Heterodyne beat between 633 nm HeNe/I_2 laser and EC diode laser. Three beat curves are shown to illustrate the effect of increasing gain on red ECDL. The apparent loss of carrier energy with increasing gain may be a measurement artifact caused by relative jitter between the lasers. The relative stabilities between these lasers did not allow for precision measurement of the feature.

Figure 3-10 Heterodyne beat between 633 nm LD and HeNe/I_2 laser

Flights of Fancy

New developments in laser diode technology are taking place at a phenomenal pace. Sadly, many devices that look useful from a scientific point of view have not merited commercial interest. One intriguing laser diode that had made part of the journey from laboratory curiosity to commercial product is the three-section DBR laser[4]. In this laser one section, the active section, is located at the back of the laser chip. It functions just like any other laser diode, that is, it provides optical gain and a back reflecting facet. In front of this is fabricated a phase-control section. It uses the electro-optic coefficient of GaAs for fine frequency/phase control of the laser diode and for phase matching of the back section to the front section. This is the distributed Bragg reflector section. It acts as a wavelength selective reflector inside the diode much as a diffraction grating does in an ECDL. This DBR section is also fabricated to take advantage of the electro-optic coefficient of GaAs. Unlike the phase control section the changing index of the DBR section affects the apparent spacing of the DBR groves and thus causes large scale tuning of the laser diode. Thus with three sections one can affect the laser's power (with the active section), obtain high speed frequency/phase control with out affecting the power (with the phasing section), and tune the device **electronically** over several tens of nanometers. A very enticing promise indeed.

At the moment few spectroscopists can have lasers diodes made to order or fabricated on site. It is interesting to consider what would be possible if this could be

done[a]. The first improvement would be the availability of a variety of new wavelengths. For material reasons it may not be possible to design LDs with wavelengths radically different then those which are currently available, however, the relaxation of some commercial restrictions such as expected yield or life time should allow the edges of some wavelength bands to be explored. Another fabrication technique which would likely be employed quickly is the application of anti-reflection coatings to the front surface of laser diodes. While many commercial diode lasers claim to have AR coatings, these are usually in the 3-5% reflectance range. This is still high enough to form an etalon with the LD's back facet, that can reduce its controllability in an external cavity configuration. The importance of an AR coat with R<1% cannot be overstated. Several research groups have found them so indispensable that they have learned to open commercially-made laser diodes and apply the AR coating themselves! Several companies now make this service available for a fee.

If one AR coated facet seems like a good idea then two is even better, but, only if both are accessible. This is based on idea that building a laser-diode-based ring laser would suppress spacial hole burning in the diode in the same way that it does in a dye or Ti-Sapphire laser. With all the gain going into the dominant mode, and with mode competition much stronger[b], it should be possible to make the laser cavity much longer without it going multi-mode (after the inclusion of standard mode control parts such as etalons, optical diodes etc.). A 1.3 μm diode ring cavity based on a tilted (to

---

a. This is not entirely far fetched. Several universities have on or near site silicon foundries, usually in association with their Electrical Engineering Dept. If LD based computing or telecommunications becomes common place, GaAs foundries at or near universities will likely follow.

b. See any standard text on laser physics such as "Laser Physics" by Murry Sarget III Marlan O. Scully and Willis E. Lamb, Jr (Addison Wesley Publishing Inc., Redwood City Ca., 1974)

avoid back reflection) diode geometry has already been built[5]. The author claims that the ring achieved 4000:1 suppression of the next cavity mode and, that it remained in single mode operation while being tuned approximately 35 nm. Self homodyne measurements made on this ring indicated a linewidth of less than 50 kHz. Although it has been pointed out several times that a long-ring configuration will not have the hoped for proportional-to-length^2 reduction in total linewidth, it should have this effect on the Lorentzian part of the lineshape. This should reduce much of the demand for extra broadband frequency servos. It should also diminish the size of the Lorentzian "wings".

The surface emitting laser (SEL) diode is another candidate for the scientists special wish list. Originally developed in an attempt to cut diode production costs by designing a diode that can be fabricated vertically, this diode holds out some special promises. Usually the SEL is made by fabricating an HR back facet from a stack of GaAs alloy multiple-elements of slightly differing indexes (similar to the way normal HR optical coatings are made). On this a single or multiple quantum well gain stack is grown, its thickness is only a few nm. This quantum well construction already gives the SEL the earlier mentioned advantage of smaller α and the accompanying reduced linewidth. Unfortunately, at this point, another HR stack is currently grown on top of the gain block with the resulting laser cavity being rarely more then one or two wavelengths long! The result is an ample supply of quantum noise due to the very small photon storage number.

A more interesting alternative would be an anti-reflection coating instead. Whether this could be made to work or not depends on the available gain as well as the

ability to make low loss AR coatings. The resulting device could now be made to lase with aid of an external mirror. This adds a flexibility not available in any existing LD scheme. One property the resulting device should have is high resistance to multiple-frequency operation in spite of it's standing wave nature. This is because the gain medium is less than one percent of one wavelength long. This means all longitudinal lasing modes essentially compete for all the lasing medium i.e. no spacial hole burning is possible. This, of course does not apply to a case in which multiple transverse modes are allowed to coexist. This SEL external cavity laser might still need some external cavity elements for frequency selection. An interesting if only imaginary improvement could be the replacement of the AR stack with a GaAs stack that has high loss except at one frequency (for lasing) that can be tuned with the GaAs electro-optic coefficient[a]. Another possible benefit of this type of device (if it is possible at all) is that it would vastly reduce quantum frequency noise. Bulk GaAs junctions have such a high internal loss that in "normal" diode lasers the cold cavity photon storage time does not include the possibility of multiple passes inside the LD cavity. In contrast, in the SEL only a few nm of junction are traversed, thus it may still be possible to build a cavity of high finesse ($10\ cm^{-1}*2nm = 2*10^{-4}$ loss if the quantum well has the same loss as bulk GaAs). Given the possibility of building a multi-cm cavity with a finesse on 100-1000 and a few mw output, the SEL ECDL laser would have about 3-5 (kHz-100 Hz) fast linewidth. For the majority of experiments this would be ignorable or easily handled with opamp-speed servos.

---

a. This device bares some resemblance to a similar device, which I have recently become aware of. In it a VSEL is fabricated with an electronically moveable HR back mirror. The device can tune electronically more than 20 nm[6]

Colors of the Future

One of the most exciting features of working in the diode laser field, both in the past and in the future, is the rapidly changing choice of wavelengths. Not long ago this was restricted to the regions near 780 nm, 830 nm, 1.3 μm, 1.5 μm and the longer wavelength Pb-salt diodes. Now a cursory examination of "The1994 Laser Focus Buyers Guide" shows a great proliferation of choices. These are summarized in table 3-1

Table 3-1 Summary of Available Laser Diodes

Wavelength nm	Power mw	Threshold ma
633	.5-3	≈30
635	1-3	60-95
650	1-5	60-100
670	1-10	30-70
670-690	-500	multi-mode
680	5-30	
685	10-40	50-80
690	30	50
750	3-5	
780	1-100	5-60
790	3-40	40-100
790-840	250-20000	250-12000*
830	1-200	40-170
850	3-10 50-100	20-30 200*
875	30-170	80
900	25	60
980	1-50	5-25
1.06	50	20-35
1270-1310	1-40	20-40
1480	70-90	40-60
1520-1580	.005-1	20-30
1550	.3-20	15-50
1650	10	20-40

More exciting yet are the promises of laser diodes to come. Blue and blue-green laser diodes based on Zinc Selenide have already been demonstrated in laboratories, lifetime issues currently prevent their commercialization . Stimulated emission from diodes based on InGaN-AlGaN[7] producing blue and blue-green have also been recently announced. Also demonstrated are multiple quantum well lasers in which the quantum wells have different energies and the diode lases on the energy difference between the wells[8,9]. Since this energy is fixed by the physical dimensions of the wells it will allow substantial new flexibility in providing laser diode wavelengths

Closing remarks

In the course of doing this research and in the years following it has been a great reward to see diode lasers become a mainstream tool of atomic and molecular research. It has also been pleasing to see the methods for diode laser frequency control come into regular practice. This is especially so because the reduction of linewidth obtained with hybrid electro-optic feedback is so great. It is also pleasing to know that as a tool the diode laser is very economical compared to some of its competition. It is expected that in the future technology and economics will continue to drive the cost of doing experiments with diode lasers down, while providing the means for ever more effective and convenient frequency control.

References

[1]M.H. Anderson et al., "Observation of Bose-Enstein Condensation in a Dilute Atomic Vapor," Science 269, 14 July (1995): 198-201.

[2]Y Millerioux et al., "Towards an accurate frequency standard at λ=778 nm using a laser diode stabilized on a hyperfine component of the Doppler-free two-photon transitions in rubidium," Opt. Commun. 108, May (1994): 91-96.

[3]M. Kourogi, C.H. Shin, and M. Ohtsu, "A 134 MHz Bandwidth Homodyne Optical Phase-Locked Loop of Semiconductor Lasers," IEEE Photon. Techol. Lett. 3, 3 (1991): 270-272.

[4]Y. Kotani et al., "Tunable DBR Laser with Wide Tuning Range," Electron. Lett. 24, 8 (1988): 503-505.

[5]Peng, En T. et al.,"Properties of an external-cavity traveling-wave semiconductor ring laser" Opt. Lett 17, 1 (1992): 55-57

[6]M.S. Wu, "Tunable micromachined vertical cavity surface emitting laser," Electron. Lett. 19, (1995): 1671.

[7]"Stimulated Emission from Current Injected InGaN/AlGaN Diode," Coumpound Semiconductor Nov/Dec, (1995): 8.

[8]J. Faist et al., "Quantum Cascade Lasers," Science 264, 22 April (1994): 553.

[9]J. Faist et al., "Quantum Cascade Lasers: Temperature Dependence of the Performance Characteristics and High T_0 Operation," Appl. Phys. Lett. 65, 23 (1994): 2901.

Chapter IV: FREQUENCY MEASUREMENT OF THE A_{10} COMPONENT OF I_2 R(56)32-0

Introduction

The frequency of the (532 nm) a_{10} I_2 hyperfine line in the transition R(56)32-0 of the Iodine has been measured. The measurement is referenced to the (780 nm) working standard for the Rb/D_2 d/f crossover line, as measured at the National Physical Laboratories(NPL) in the U.K[12].

The measured frequency of the a_{10} component was determined to be 563,260,223.471 MHz ± 70 kHz. This provides a secondary frequency standard within the tuning range of a doubled Nd:YAG laser.

As a follow on to this experiment, the frequency of the (780 nm) Rb/D_2 hyperfine lines were measured relative to the (778 nm) $5S_{1/2}$-$5D_{3/2}$ two-photon transition in Rb using frequency difference methods. This allowed a reduction in the uncertainty of D_2 transitions frequencies and an overall reduction in the uncertainty of the R(56)32-0 a_{10} frequency from our first measured value of 563 260 223.480 MHz ± 70 kHz. The improved value for the transition's frequency is 563 260 223.471 MHz ± 40 kHz. Excellent stability for two independent spectrometers on this line have been observed ($<10^{-13}$ for $\tau>1$s).

Four possible frequency chains were considered for this measurement. The first, which was actually used, takes advantage of the fact that:

$$263\ \text{GHz} + F_{req.}(I_2)|_{532nm} + F_{req}(Rb/D_2)|_{780nm} = 2*F_{req}(HeNe)|_{633nm} + \delta\nu_1$$

The second uses:

$$1.27\ \text{THz} + F_{req}(I_2)|_{532nm} + F_{req}(\text{two-photon})|_{778nm} = 2*F_{req}(HeNe)|_{633nm} + \delta\nu_2$$

The third was:

$$1.27\ \text{THz} + F_{req}(CH_4)|_{3.39\mu} + F_{req}(HeNe)|_{633nm} = F_{req}(I_2)|_{532nm} + \delta\nu_3$$

The last was:

$$1.22\ \text{THz} + 2*F_{req}(CH_4)|_{3.39\mu} + F_{req}(\text{two-photon})|_{778nm} = F_{req}(I_2)|_{532nm} + \delta\nu_4$$

These relationships are illustrated graphically in figure 4-1.

Motivation

The most obvious requirement for an optical standard is that its frequency of operation should be well measured and that the accuracy and precision of that measurement should be understood. It is also important that the standard should be reproducible. This is not to imply that to replicate the frequency standard an identical apparatus should be required, only that proper preparation of critical components and careful use of experimental techniques should yield the same laser frequency within expected limits.

Generation of laser beams with well defined optical frequencies is rarely an end in itself. It is the use of these lasers in further experiments and measurements that is the motivating force for construction and characterization of these devices. The need to have these devices available in the laboratory and in field experiments means that hey are also subject to practical constraints.

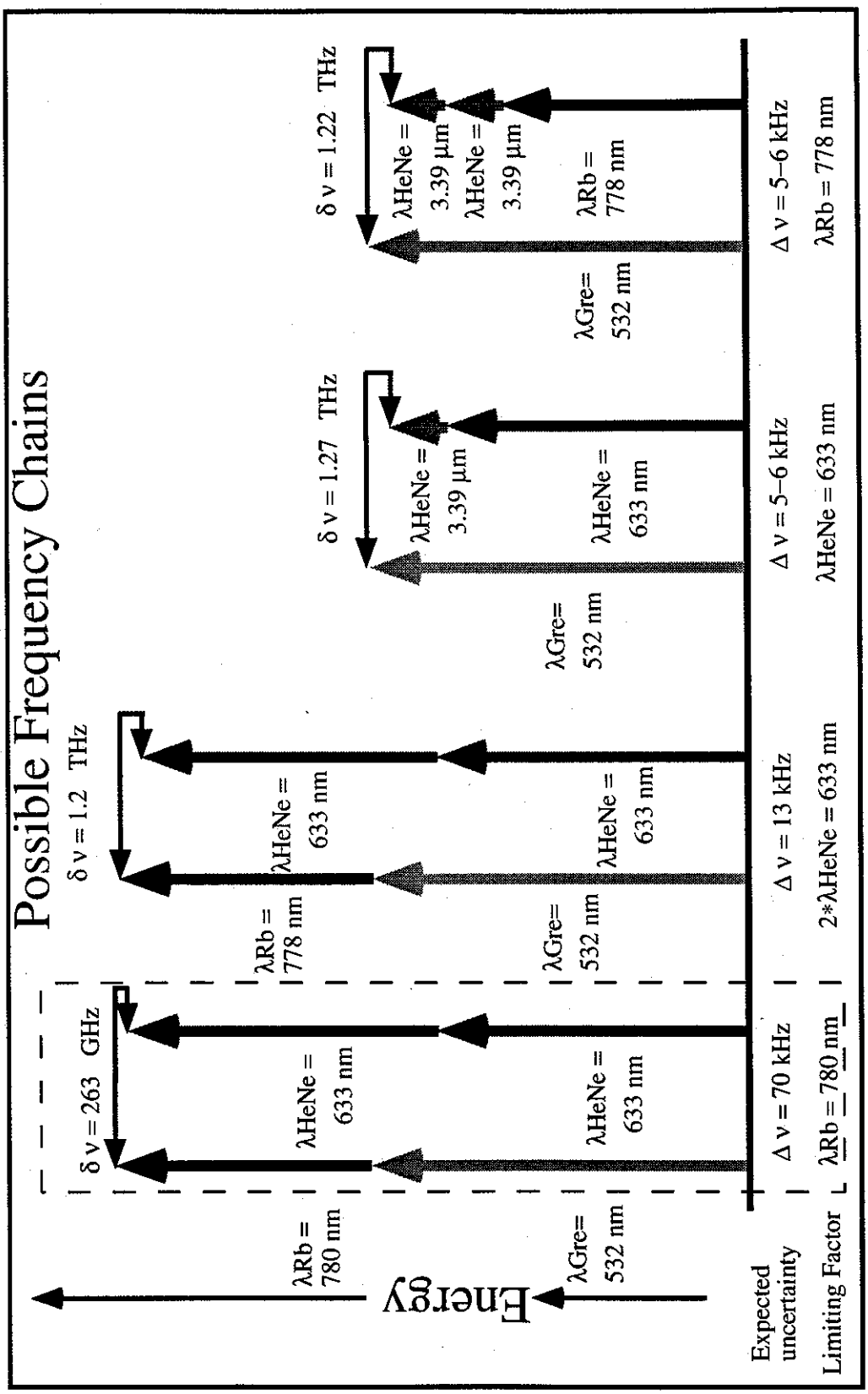

Figure 4-1 Possible Frequency Chains

The doubled YAG I_2 stabilized laser already possesses one of the most important "real world" qualities. It is reliable. During the course of these experiments both the lock for the doubling crystal cavities and the lock to the I_2 spectra functioned for hours at a time with no intervention. When this type of reliability is available from measurement prototypes it seems likely that more refined versions of the I_2 stabilized doubled YAG laser will easily match the reliability of other standard frequency sources.

I_2 as a Frequency Standard

The HeNe/I_2 633 nm standard is one of the elderly statesmen of the frequency standard world. The earliest observations of resolved hyperfine structure in I_2 were by Ezekiel and Weiss [3], using an I_2 beam at frequencies near the Ar^+ 514.5 nm line. This in combination with an early paper by White [4] set the stage for most of the work which is now the lore of laser frequency stabilization. It is interesting to note that in his paper White not only discussed stabilizing lasers to an atomic or molecular resonance lines, but also foresaw the use of high finesse optical cavities to provide short term frequency stability. The introduction of intracavity saturation spectroscopy by Lee and Skolnick in 1967 made frequency stabilization a "practical" idea by eliminating the need for a beam machine [5]. In 1969 the first hyperfine spectra at 633nm was observed by Hanes and Dahlstrom[6], who put their Iodine cell inside their laser as a saturable absorber. The modern HeNe/I_2 633 nm stabilized laser does not differ much from their laser configuration except in details.

It was during the ensuing years that it was discovered that, when compared to

each other, the so-called "standard" lasers did not quite operate on the same frequencies! Thus began a slow refinement of what the idea of standard meant (and thus the need for ongoing research such as this document). The HeNe/I_2 633 nm frequency standard has been one of the most extensively studied of frequency standard systems. The transition used, the R(127)11-5 is pre-dissociating and so shows a linewidth of $\approx$ 6 MHz, which is much wider than the $\approx$ 500 kHz R(56)32-0 "green" transition being measured in this paper. The 633 nm transition is also "weakly" populated due to its ground state being in the fifth vibrational state, causing it to have a low signal-to-noise ratio. Figure 4-2 illustrates these relationships. In order to compensate for this the I_2 cell is placed inside the laser cavity. This however, aggravates the problem of the broad transition by adding power broadening as well. In spite of these difficulties the precision and accuracy of the HeNe/I_2 633nm laser are very respectable. In the latest document on laser standards published by BIPM[7] the estimated standard uncertainty for a 633nm reference laser using the appropriate recipe (see the aforementioned ref.) is $\sigma=2.5*10^{-11}$ ($\approx$12 kHz). The HeNe/I_2 633nm laser had a milestone year in 1993 when a frequency chain was constructed by Acef et al[8], which connected the "f" component of the R(127)11-5 transition with a CO_2/OsO_4 laser, thus reducing the uncertainty in the absolute frequency of this line to $\Delta\nu/\nu = 1*10^{-11}$ and placing ν firmly at ν = 473,612,353,586.9 $\pm$ 5 kHz. This figure is essentially the limit of the HeNe/I_2 laser's reproducibility.

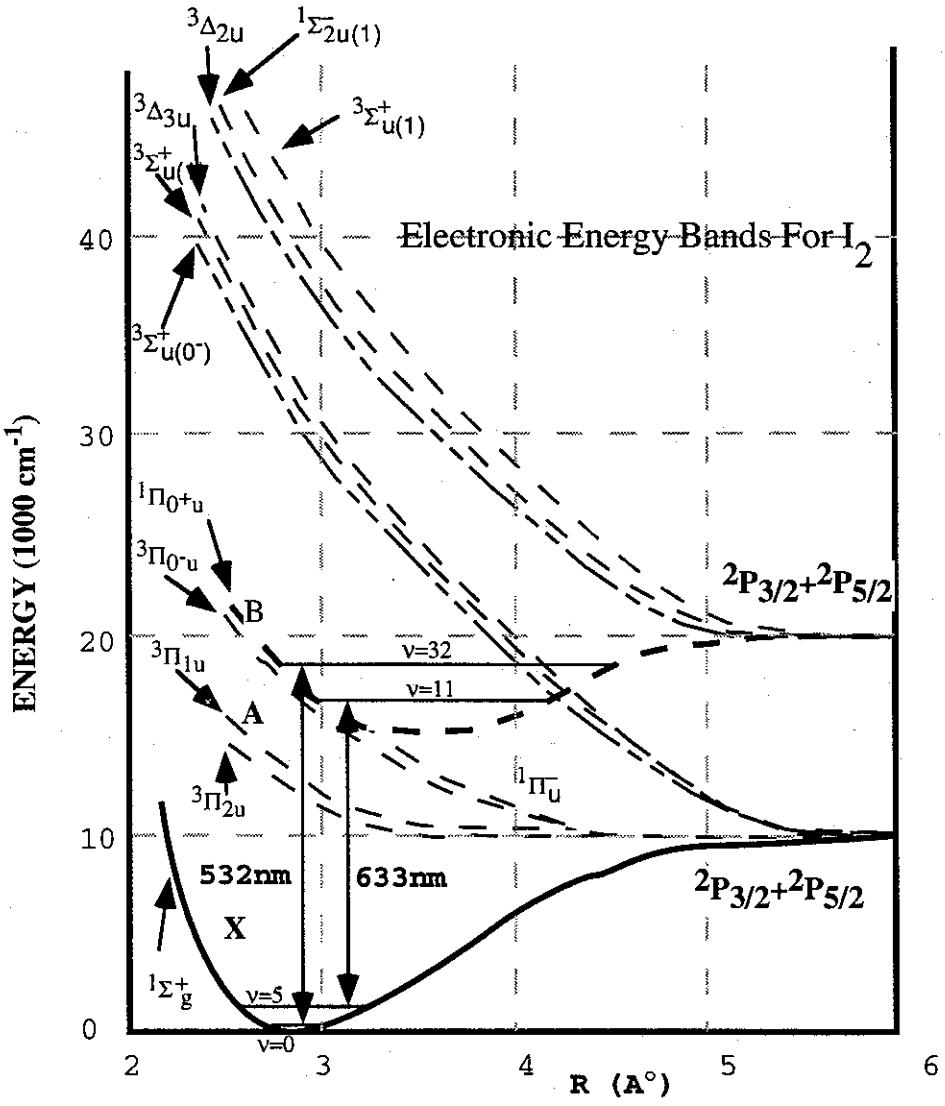

Figure 4-2 Electronic Energy Structure of I_2

Rb/D_2 Line as a Frequency Standard

An obviously critical part of the measurement of the 532 nm I_2 line is the knowledge of the absolute frequency of the D_2 line in Rb. This measurement has been carried out at the National Physical Laboratory(NPL) in Teddington England by G.P. Barwood, P. Gill and W.R.C. Rowley. For discussion, in this paper the labeling convention from these experiments is adopted. Figure 4-3 shows the hyperfine transitions in the D_2 family and their letter assignments. To conduct these measurements Barwood et al[2] used saturation spectroscopy to lock an external cavity laser diode laser (ECDL) to the d/f crossover hyperfine component of the Rb D_2 transition. With an NPL-designed wavemeter the uncertainty of the laser frequency was reduced to less than 30 MHz. This made it possible to use a one meter precision etalon and a I_2 stabilized HeNe to assign the final frequency of d/f=384 227 981.87 MHz with a 1σ accuracy of ±60 kHz.

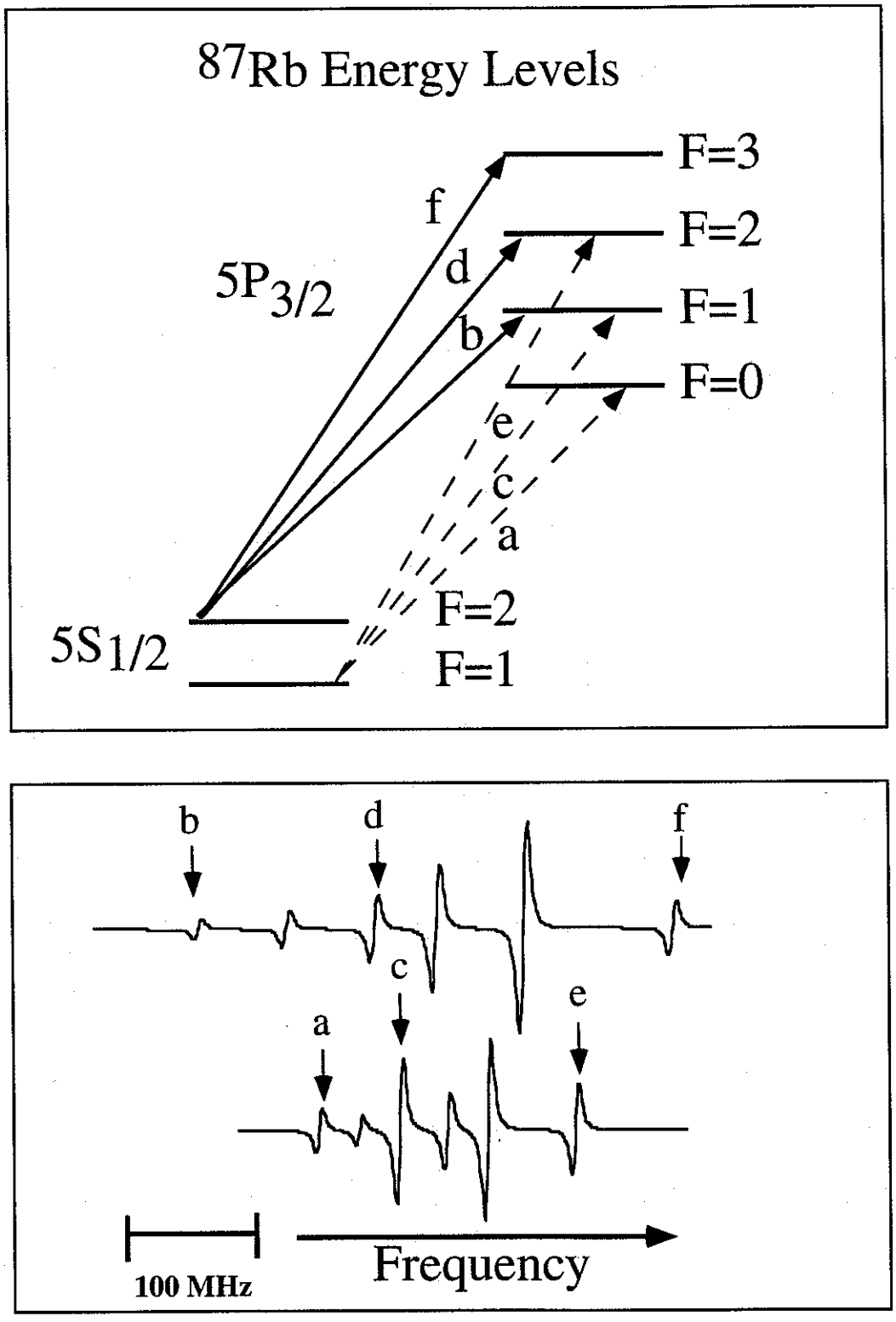

Figure 4-3 Designations for ^{87}Rb D_2 Hyperfine Lines

$5S_{1/2}$-$5D_{3/2}$ Two Photon Line as a Standard

The first studies of the two-photon transitions in Rb were carried out by Stoicheff, Yoshiaki and Harvey, who examined the range of 5S-nD transitions for n=11-124 [9,10]. The first determination of the absolute frequencies of the 5S-5D transitions was carried out in 1993 by Nez [11] at *Laboratorio Europeo di Spectroscopie Non-Lineari* (LENS). A schematic of the 5S-5D energy levels is shown in figure 4-4. The actual measurement was the by-product of an absolute frequency measurement of the 2S-8S/D two-photon transition in hydrogen that was already under way [12].

The hydrogen measurement took advantage of the fact that the difference frequency between the well studied HeNe 633/I_2 frequency standard and the HeNe/CH_4 standard lies only 88GHz from the frequency of the hydrogen transition of interest. Fortunately, the rubidium $5S_{1/2}$-$5D_{3/2}$ lines are also in near coincidence (δf=5 GHz) with this difference frequency, so their study was a natural follow on.

It is not difficult to understand that the **absolute** limit of accuracy for the European measurement was determined by the limit of accuracy of the reference sources. Fortunately, the LENS group had available a HeNe/I_2 laser (INM12) which had just been measured at *Laboratoire Primiare des Temps et des Frequences* (L.P.T.F)[8] to an accuracy of 3.4 kHz. The HeNe/CH_4 laser was one which came from BIPM and had a frequency uncertainty of one kilohertz. In their study of the stability and reproducibility of the two-photon locked laser it was found initially to have an Allan variance of $7*10^{-12}$ for 1 s integration time to $7*10^{-13}$ for 100 s. This matched closely to the measured values for the INM12 HeNe/I_2 laser, indicating that the Rb $5S_{1/2}$-$5D_{3/2}$ stabi-

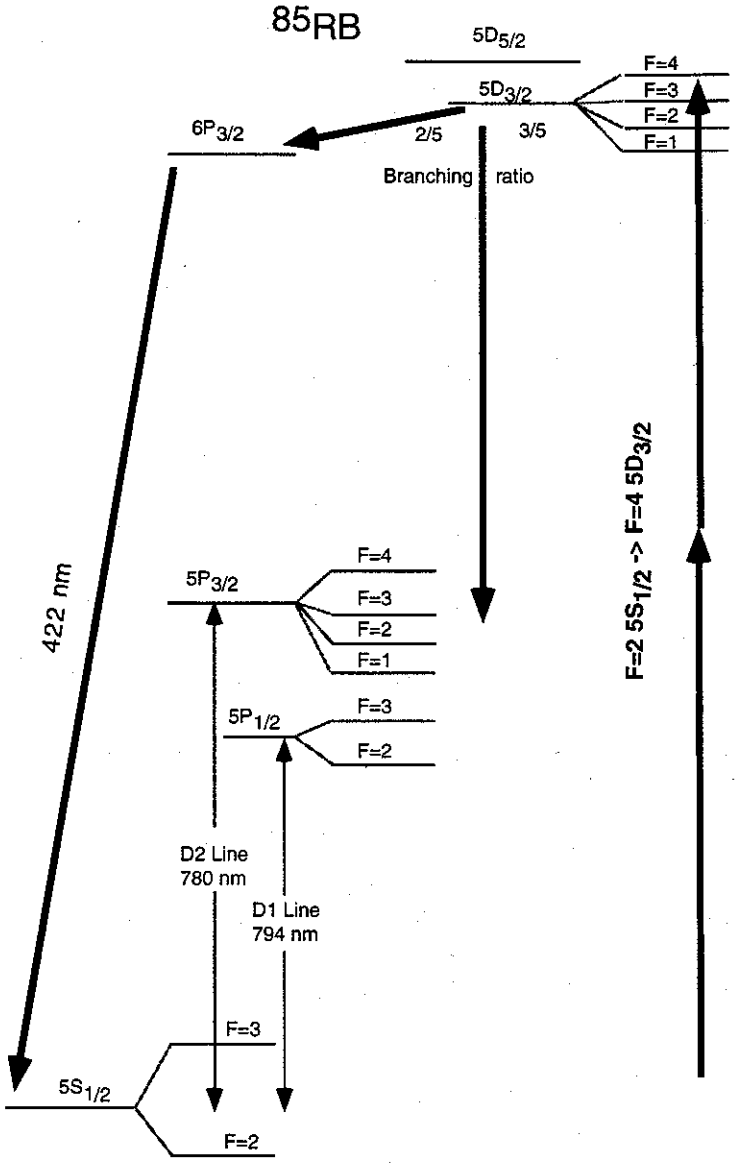

Figure 4-4 Energy Schematic for Two-Photon Transition

lized laser did not contribute significantly to the Allan variance. This indicates that the Rb $5S_{1/2}$-$5D_{3/2}$ transition could make an excellent frequency standard if it were not too sensitive to experimental conditions.

Nez reported that changes in the Rb cell temperature from 90° C to 50° C produced frequency variations of smaller then 300 Hz. And exchange with another cell produced only a 500 Hz change. The reported light shift for the $5S_{1/2}$-$5D_{3/2}$ transition was 2.4 kHz for the experimental conditions given (10mw/mm^2), this corresponds roughly to the expected light shift from the ground state alone. Day to day variations in the frequency of the two-photon measurement were conservatively estimated at 3 kHz. Overall, the initial reported uncertainty was 5 kHz.

Based on these encouraging results, Millerioux et al. built a pair of external cavity diode laser spectrometers [13]. These systems showed improved stability, an Allan variance of $3*10^{-13}$ at τ=2000 s and substantially improved day to day repeatability, δ frequency = 200 Hz. The difference frequency between the identical systems was only 1.7 kHz. Much of the improved result was believed by the authors to be do to the use of build-up cavities around the Rb cell, the improvements being due not to the increased intensity, but rather the guaranteed wave-front (mode) match between the counter propagating beams.

In order to more accurately determine the absolute frequency of the Rb two-photon transition LPTF has planned a frequency chain traceable to the Cs standard [14]. It is interesting to note that the chain relies on external cavity diode lasers using the same technology described earlier in this thesis.

Experimental Overview

Introduction

The measurement chain used to establish the absolute frequency of the a_{10} component of the R(56)32-0 line of I_2 at 532 nm consists of two parts. In the first, the frequency of the Rb/D_2 d/f crossover line is determined relative to the $5S_{1/2}$-$5D_{3/2}$ two-photon transition. In the second, the difference frequency between the Rb/D_2 transition and the a_{10} component of the I_2 R(56)32-0 ro-vibrational transition was measured. Both measurements rely on many interdependent elements. In this section is a description and demonstration of the proper operation of each critical part of the frequency chains and an explanation of how they determine the final absolute frequency and the confidence intervals of the measurements. A discussion of how on-going improvements in the measurement techniques and systems may improved accuracy.

I_2 Frequency Measurement, Overall Description

The absolute frequency measurement of the a_{10} component of the R(56)32-0 transition is accomplished using the frequency chain depicted in figure 4-5. The chain takes advantage of the fact that the sum of the 532 nm "green" I_2 frequency and the 780 nm Rb D_2 frequencies are only 263 GHz from twice the frequency of the 633 nm I_2 stabilized HeNe. This chain was selected because it had the overall smallest rf gap of any of the possible measurement chains

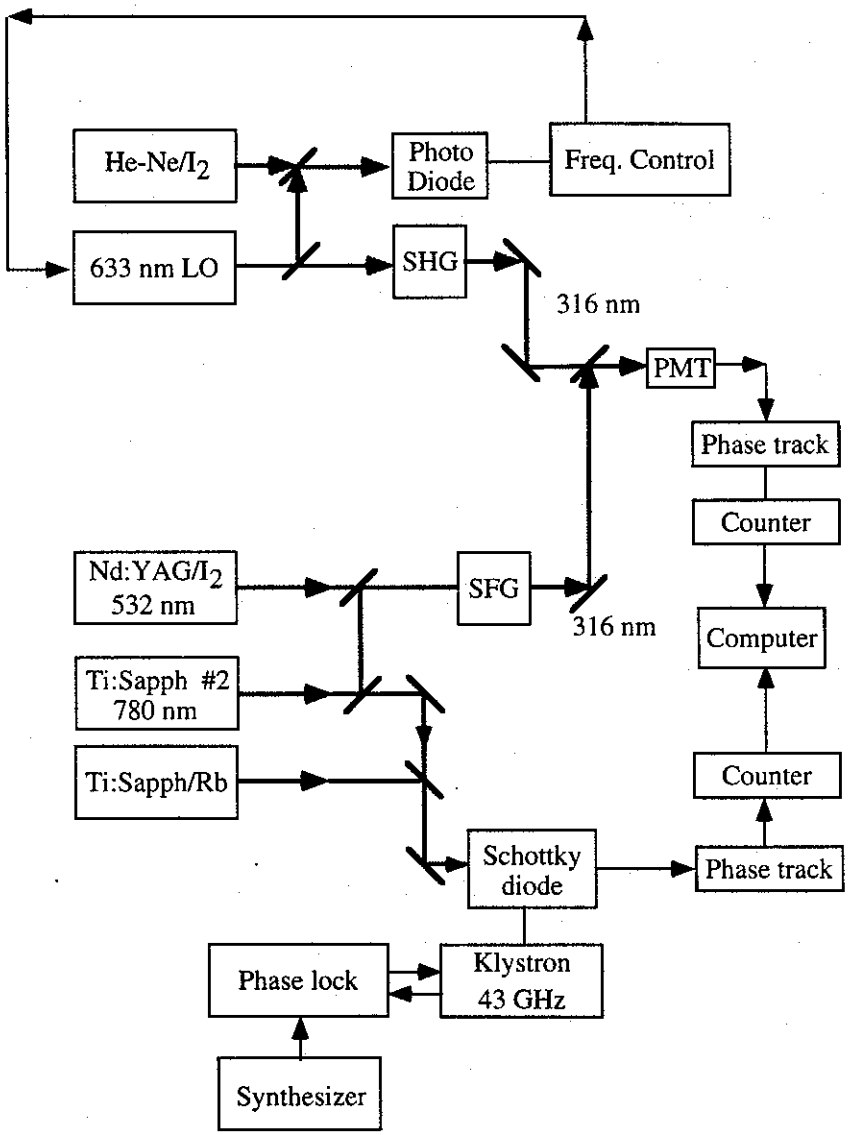

Figure 4-5 Experimental Overview of Frequency Chain

In the frequency chain the measurement is reduced to frequency counting of two heterodyne beat notes. One beat note measures the difference between two Ti-Sapphire lasers. One of the lasers is locked to the center of a Rb D_2 hyperfine transition and other Ti-Sapphire laser is tuned to a frequency approximately 263 GHz higher and locked to a stable Fabry-Perot cavity. The two beams are combined on a Farran-built Schottky photodetector. A stabilized klystron operating at 51 GHz is also injected into the detector. The output of the detector is equal to the laser difference frequency minus five times the klystron output frequency. A microwave phase locked loop is used to recover the signal for counting.

The second beat note measures the difference between two UV beams. One beam is derived by frequency doubling a HeNe laser, which obtains its long term frequency stability by offset frequency/phase lock from an I_2 stabilized HeNe laser. The other beam is generated by summing the "unknown" green laser and the higher frequency Ti-Sapphire laser. The resulting beat, which falls around 20 MHz, is detected with a photo-multiplier tube (PMT). As with the first beat note, an oscillator is phase locked to the beat to regenerate a "clean" high signal to noise version of the signal for counting.

633 nm I_2 Stabilized Laser

Introduction

A critical part of the frequency chain is the 633 nm HeNe/I_2 reference laser. The 633 nm transitions of I_2 have been recommended as secondary optical frequency standards for precision spectroscopy in the recent CCDM report[7]. Our reference laser was originally built by J-M Chartier and M. Winters. The design is described in great detail in the internal JILA report[15]. It follows the path of design laid down by Wallard[16] and Rowley[17]. Since its construction, the laser has undergone minor modifications to improve its mechanical performance. Because its output is frequency doubled, and because it is one of the two optical frequency standards used in our chain we were delighted that the lasers's correct operation could be verified by comparison with two of the portable transfer standards from BIPM (See section "HeNe/I_2 Calibration Results").

Design and Construction

Mechanical

The overall construction of the HeNe/I_2 is shown in Fig 4-6. The design uses a 43cm optical cavity corresponding to an FSR of 350 MHz. The length is defined by three 1.9 cm diameter invar rods with a glass disk at each end. The glass disks act as carriers for the end mirrors with attached PZT actuators. One PZT disk is used to achieve the 6 MHz peak to peak cavity modulation at a frequency of 5 kHz. A PZT

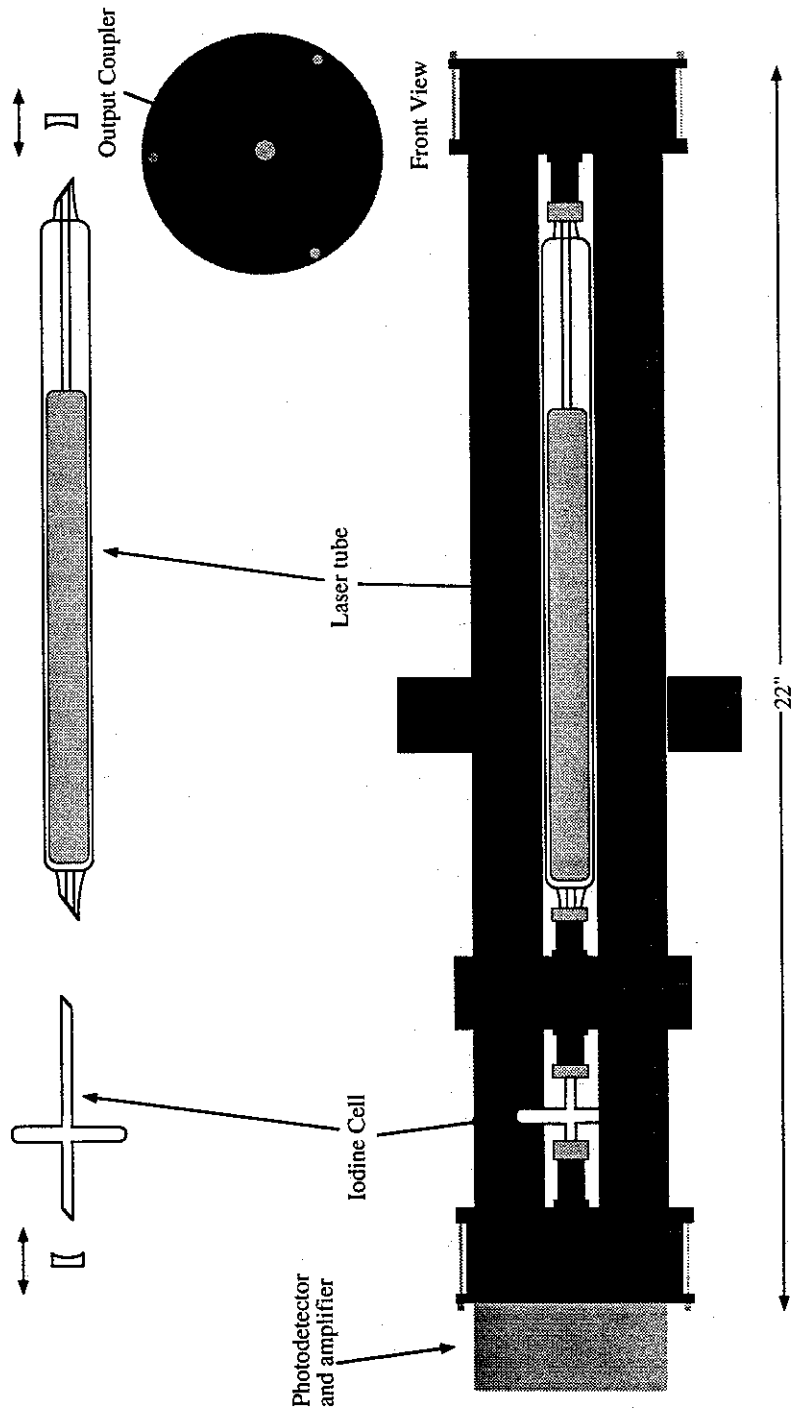

Figure 4-6 HeNe/I2 Stabilized laser

tube is used for cavity length corrections. About 100 V are needed for one cavity order. Around each of the invar rods is a layer of lead impregnated foam to act as an acoustic dampening agent. Around the lead foam and the invar rods are aluminum tubes. The glass end plates are protected by sealed cylinders. The cylinders also house the laser's photodetectors and preamplifiers. The entire laser is housed in a plexiglass box to isolate it from wind currents

Laser Gain Tube

The laser gain tube is an NEC model GLT-2040, which uses two compensating Brewster windows. The tube is 27.5 cm in length. The internal gas pressure is 333 Pa and the He-Ne ratio is 7:1 allowing a discharge current of 3-8 ma. Previous studies at BIPM have shown that these parameters result in a low level of plasma noise.

I_2 Absorption Cell

The length of the cell is 10 cm with an outside tube diameter of 1.5 cm. The cell was filled with $^{127}I_2$ in 1985 at BIPM (BIPM no.53). Before being installed in the present laser the cell was compared at BIPM to the BIPM2 reference laser. The result was:

Frequency(BIPM4,cell 53) - Frequency(BIPM2) = -2.5 ±1 kHz

For these tests the cell's cold finger was maintained at 15± 0.01° C.

Cavity Mirrors.

The I_2 laser uses two Spectra Physics mirrors with 0.775 cm diameter and a transmission of 0.9%. The side farthest from the I_2 cell uses a 60 cm radius of curvature and the other side uses a flat mirror.

Electronics

The output signal from the back of the I_2 laser is first detected by a fast photo-detector then amplified. Then, two 5 kHz notch filters are used to remove the modulation fundamental and a third notch filter at 10 kHz removes its second harmonic. Finally a 15 kHz bandpass filter reduces all other extraneous signals. A JILA designed lock-in amplifier is used to detect the 3rd harmonic signal, and a JILA designed high voltage PZT amplifier drives the laser PZT, completing the frequency servo. The sine wave oscillator for the laser system was tested and found to have second harmonic content of -65 db. The third harmonic was down by - 60db. So important systematic error from harmonic errors are not expected. Many thanks are owed T. Brown who built the lock-in, HV PZT amplifier and sine wave oscillator for this laser.

Iodine Spectrometers

Two separate I_2 spectrometers are used in the frequency chain measurements. For clarity, they will be referred to as E and W, indicating their location on the East or West side of the optical table. Each of the spectrometers has an independent source of light at 532 nm. These 532 nm sources each have their own 1.064 μm Nd:YAG laser pumping a second harmonic generator (SHG) with a build up cavity. In both cavities one of the mirrors is weakly dithered at about 50 kHz and first derivative detection is used to lock the cavity to the laser's output. Having two independent spectrometers makes it possible to evaluate their short and long term stability. The actual frequency measurements are conducted with the E spectrometer. The E spectrometer's layout is depicted in fig 4-7.

In the E frequency doubler a four mirror folded resonator is used. A crystal of MgO:$LiNbO_3$ is 90° phase matched at 110 °C to provide the second harmonic generation. The W frequency doubler used a less conventional 6 mirror, figure 8 cavity which had two foci. At one focus a KNO_3 crystal at 180 °C was used to generate 532 nm light. At the second focus a $LiIO_3$ crystal was angle tuned to sum the 532 nm light with additional 1064 nm light using type I phase matching to produce 355 nm UV radiation.

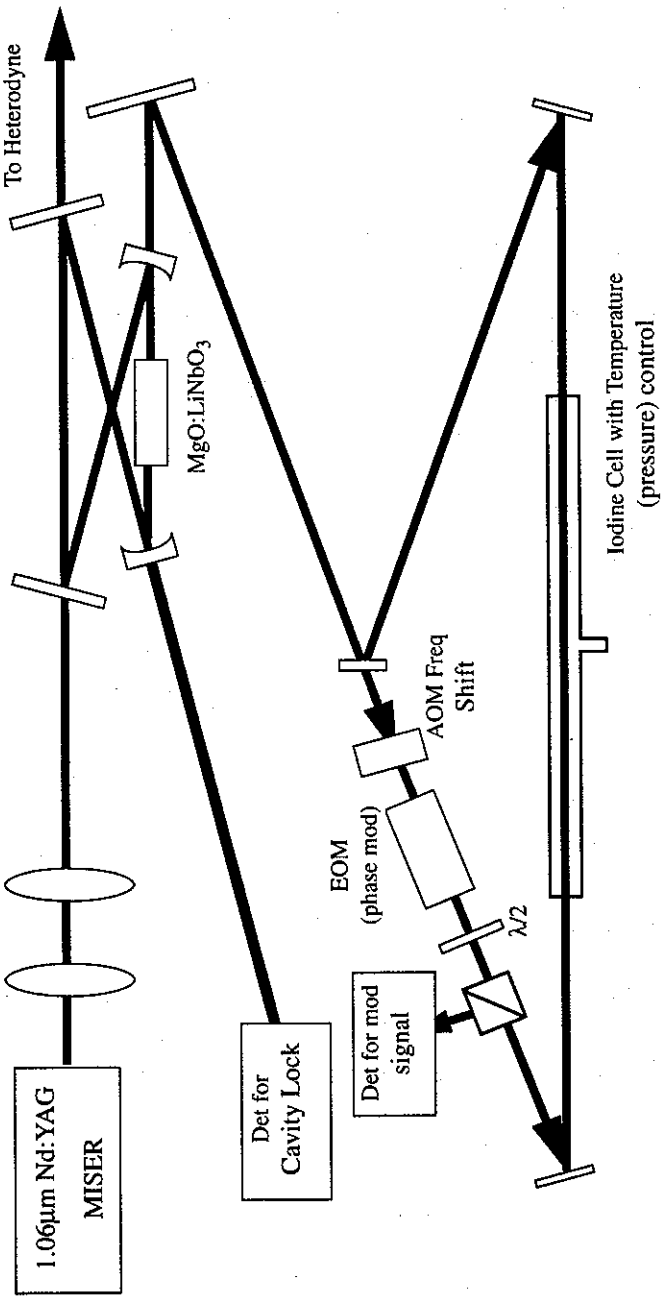

I_2 modulation transfer spectrometer.

Figure 4-7 Optical setup for I_2 Spectrometer

Light for these doubling cavities is provided by two Non-Planar Ring Oscillators (NPRO) from Lightwave Electronics model #122-1064-300F which produce about 300 mW each. These lasers can be coarsely tuned by changing the Nd:YAG temperature with the laser's built in controller. Smaller rapid frequency changes can be made using a piezo actuator attached to the laser crystal.

The iodine spectrometers are based on the technique of modulation transfer spectroscopy[18]. In both spectrometers, the laser beam is first split into a weak probe beam and strong pump beam. The pump beam is the then frequency shifted by 80 MHz with an AOM to eliminate interferometric interference effects[19]. The pump beam is then phase modulated with an EOM. In the W(E) spectrometer, the modulation frequency is 500(680) kHz and the modulation index is 2.1(1.0). A half-wave plate is then used to rotate the polarization of the beam by 90°. In the W spectrometer the beams interact with crossed polarizations in the 1.2 m long iodine cell. In the E spectrometer 45° Faraday rotators are placed in both beams so that they are parallel, after this the pump and probe beams are propagated through the 1.2 m Brewster cut cell. In both spectrometers the probe beam of either spectrometer is then picked off with a polarizing beam splitter and imaged onto a photodiode. The AC component of the signal is then amplified and demodulated in the standard way with a double balanced mixer(DBM). An adjustable phase shifter in the reference channel of the DBM allows either the in-phase or quadrature component of the signal to be detected. Vapor pressure in the I_2 cells is set with the temperature of a cold finger (T≈-10°C->1.4 Pa) that is under servo control.

Offset Phaselocked Laser

In order to generate the second harmonic of the 633 nm/I_2 reference for the frequency chain, two additional systems are employed. These are the offset frequency locked laser and the 633nm doubling cavity. The offset frequency locked laser (OFLL) is needed for two reasons. The first reason is simply that the HeNe-I_2 laser only emits 100-150 micro watts, which is insufficient for frequency doubling. The second is that the HeNe-I_2 laser has 5 MHz frequency dither. This dither would require other parts of the frequency chain to produce much higher signal to noise for counting than was available.

The OFLL is made from a commercial hard sealed HeNe laser tube which has a peak output power into one polarization of 700μW. Two methods are used in combination to tune the laser. The first is heat applied directly to the tube with heating tape causing it to expand and shrink. The second is a piezo electric tube which was glued to the body of the tube. The laser tube is enclosed in a sealed aluminum can to reduce susceptibility to acoustic pickup and temperature variations.

Frequency control for the OFLL is derived by heterodyning it with the HeNe-I_2 reference on an avalanche photo diode. The detected rf beat signal is amplified, limited and processed by a comparator which produces digital domain signals which are then divided by 88 and compared to a 1 MHz stable crystal oscillator with a Hall labs designed predecessor to the Motorola MC4044 phase/frequency detector.

The phase/frequency error signal from the detector is then filtered through a notch filter which removes the dither frequency of the HeNe/I_2 laser. Then it is routed to the input of a servo loop controller which sends slow, long term frequency corrections to the heater and faster corrections to the laser piezo. The result is the OFLL locks at a frequency 88 MHz from the HeNe-I_2 laser but without transferring its large dither. The spectral width of the offset-locked laser is about 20kHz.

During operation, the output of the phase detector can be observed. At no time does the output of the phase detector "wrap around", thus indicating that the maximum phase error is bounded by $\pm 88\pi$ rad, and the long term frequency stability of the OFFL laser is the same as the I_2 laser.

The output of the OFLL is coupled to a ring build-up cavity. The cavity is used to increase the intensity of the 633nm light to the Rubidium Dihydrogen Phosphate (RDP) crystal which was placed inside. Using the program "SH/SUM generation" written by Surendra P. Singh, the temperature for 90° phase matching was determined to be 65° C. The crystal, obtained from Inrad, has dimensions 10x10x30mm with brewster cut faces. The RDP crystal is housed in a small (10cm x 5cm) cylindrical oven made of copper and heated with three cartridge heaters from the HotWatt corporation. Temperature of the oven is controlled on the milli-degree scale with a JILA designed PID type servo controller.

UV Frequency Doubling Cavity

The cavity itself is of a slightly unusual configuration because the only mirrors which were available with appropriate coatings (highly reflecting at 633nm but transparent at 316nm were flat. See figure 4-8. Measurements showed that the cavity had a finesse of about ten and that about 20% of the light was coupled into the cavity, giving and approximate buildup of 1.2 mW which is 2 times more then the 600μW of pump from the OFLL.

The ring cavity was kept in resonance with the light from the OFLL by dithering one of the cavity mirrors at approximately three kilohertz. The change in the amplitude of the light built up inside the cavity is detected by imaging the red light which "leaked" through one of the curved mirrors onto a photo detector. The detector output is then demodulated with a lock-in amplifier to produce the appropriate signal for the cavity servo control.

The amount of UV light from the buildup cavity is estimated by measuring the dc current from the PMT. Light from a HeNe laser was then used to illuminate the PMT and the amount of light from HeNe adjusted until the same photo-current was obtained. The published responsivity of the cathode material at 633 and 316nm is used to estimate that the HeNe doubler was producing about 100nW of UV.

The UV light from the buildup cavity was combined with the UV output from the summing crystal (described below) on a beam-splitter and the heterodyne signal was detected with a RCA 4837 photo multiplier tube. The beam splitter reflects a large

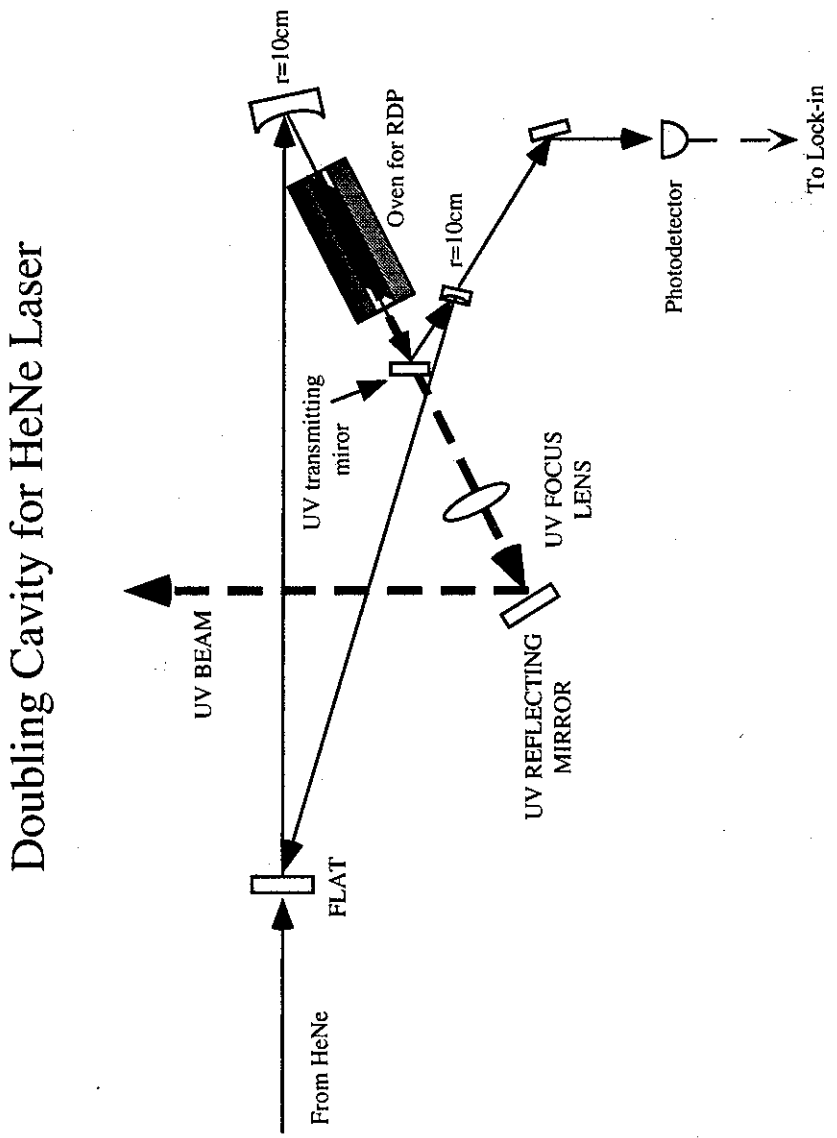

Figure 4-8 HeNe Doubling Cavity

portion of the light from the doubling cavity at the expense of the light from the summing cavity, but in practice the IR beam in the summing crystal still had to be miss-aligned to reduce amount of light from the summing crystal. This is because, in shot noise limited heterodyne detection systems, the S/N ratio is limited by the weaker of the two signals so no increase in signal to noise is obtained by increasing the strength of the stronger of the two beams. There is however, a penalty for the summing beam being too strong. According to the manufacturer, the DC current in the tube should not exceed 2 mA so the accelerating voltage on the tube must be adjusted downward, based on the sum of the power in both beams. This causes a different problem. When the voltage on the PMT falls below six or seven hundred volts, the high frequency (above a few MHz) response suffers dramatically. The reason for this behavior is not well understood, however at the 1000 volts usually employed the response was flat to beyond 50 MHz

General Configuration of Ti-saph Laser

The Ti-Sapphire laser used for the Rb spectrometer was designed in our lab at JILA and consists of a folded ring configuration similar to one that has proven to be successful in several dye laser designs. The Ti-Sapphire crystal is 20 mm long with doping of .04%, obtained from the Union Carbide company. The crystal has a guaranteed figure of merit of 210 and has Brewster cut faces. It rests in a JILA -designed custom mount, which provides water cooling and allows for 4 degrees of freedom of movement. The folding mirrors are of 10 cm radius and have coatings which are HR for the output wavelength and transmissive for the pump wave length. For these experiments the pump laser, either a Spectra physics model 2045 argon-ion laser or a Coherent Inova 200, was used. Operation on the single 514nm line was found to give lower frequency and amplitude noise than with all-lines operation.

The primary wavelength control for the laser comes from a Coherent 3-plate birefringent tuner which is used to manually set the coarse wavelength. A thin plate etalon is used for further wavelength selection. For the Rb-spectrometer's laser, the thin etalon has a free-spectral-range of 250 GHz and reflectance of 30%. Final mode selection is done with a JILA designed Mach-Zender-interferometer based on a design by J. Hall. The design results in negligible vertical displacement which makes it possible to remove and replace the interferometer without changing the beam path. Fine frequency control of the laser is accomplished with an electronically tunable Brewster plate. The plate has a thickness of 2 mm and is used in a double-pass configuration

with a narrow folding angle to give the laser a tuning range of 15 GHZ with the present limit being fixed by the PZT of the Mach-Zender. One of the laser mirrors is fitted to a piezo-ceramic actuator which gives it the ability to be used for fast frequency control or high frequency wavelength dithering

General Configuration Of Rb Spectrometers

Introduction

In order to measure the spectra of the Rb D_2 lines, a saturation spectrometer is used. The spectrometer uses a two step process to enable the resolution of sub-Doppler signals. First a "pump" beam excites a velocity population sub-group to the excited state leaving a "hole" in the corresponding velocity sub-group of the ground state, then a second weaker counter-propagating "probe" beam is used to measure the absorption in the ground state caused by the pump beam[a]. An examination of the details of the system show that only one velocity sub-group can interact with both the "pump" and the "probe" beam thus resolving below the doppler limit.

Light Path

In our experiment, the frequency control system of the laser and the microwave heterodyning system require single frequency (unmodulated)light to function properly. To achieve this, spectrometer light for both the pump and the probe beam is first transmitted through a double pass acousto-optic modulator (AOM), which allows us to put a controlled frequency dither on just the spectrometer's laser beam. The frequency

a. More accurately the probe measures the difference between the ground state and the excited state populations.

dither is generated by taking the AOM's 80MHz drive signal and dividing its frequency by ten. This signal is then compared to an FM modulated 8MHz signal which is generated by a Stanford DS345 DDS signal generator. A high speed (unity gain frequency about 100 kHz) phase locked loop uses these signals to steer the AOM's VCO so that it is equal to ten times the output of the generator. This assures that the frequency shifter has a frequency offset and dither amplitude which are well defined and precisely known and do not drift with time. As a side benefit, this system puts few harmonics of the primary modulation frequency on the AOM. This is important as the third harmonic detection scheme used in the spectrometer is sensitive to contamination by high order harmonics.

The beam then passes through a pin-hole mode cleaner which removes optical aberrations caused by the double pass AOM and associated optics.

The intensity fluctuations that would be caused by the strong frequency dependent efficiency of the double-pass AOM are reduced (>40db) with an intensity stabilizer. The stabilizer works by sampling the output intensity of the double-pass AOM and controling the amplitude its rf drive to it so as to keep the optical output constant.

The beam is then split into pump and probe beam. The pump beam's intensity can be adjusted with a variable neutral density filter (NDF) to achieve an optimum pump to probe ratio. The beam then passes through a second AO frequency shifter. This eliminates possible standing wave interference in the saturation spectrometer[19]. The fact that the pump beam and the probe beam are at different frequencies moves the apparent center frequencies of the Rb resonance by half the offset frequency. This offset is controlled by the crystal oscillator which drives the AOM and is measured at

the start of each day when data is taken. Experience has shown that it does not otherwise change on any scale that would affect the experiment. After passing through the AOM the pump beam is directed into the Rb cell where it interacts with the atomic Rb gas, depleting each hyperfine level at a specific velocity.

The probe beam is then directed into the Rb sample along a path that is anti-parallel to the pump. Before entering the Rb cell the pump and probe are passed thought individual polarizing beam splitters to establish definite polarizations. After sampling the velocity distribution as modified by the pump beam, the probe beam is reflected from a beam splitter to a photo detector. The system can be seen in figure 4-9

The detected signal from the photo detector is fed into a 15 kHz bandpass filter and then the a portion of the signal is split away for monitoring by a FFT spectrum analyzer (Stanford Model 760). Most of the signal is fed through a 10 kHz notch filter and then to a Stanford Instruments model 510 lock-in. The reference channel of this lock-in is fed the third harmonic of the modulation frequency. The dispersion-like output signal of the lock-in is then used to lock the spectrometer to the line center of the appropriate Rb transition for use as an intermediate frequency reference.

The choice of third harmonic detection, rather then the more commonly used first harmonic detection is made on the basis that the 3-H signal gives superior rejection of offsets from nearby lines and the Doppler background. Both FM sideband spectroscopy and modulation transfer spectroscopy were also considered, but there are questions about the ability to minimize offset errors[20] (see also discussion).

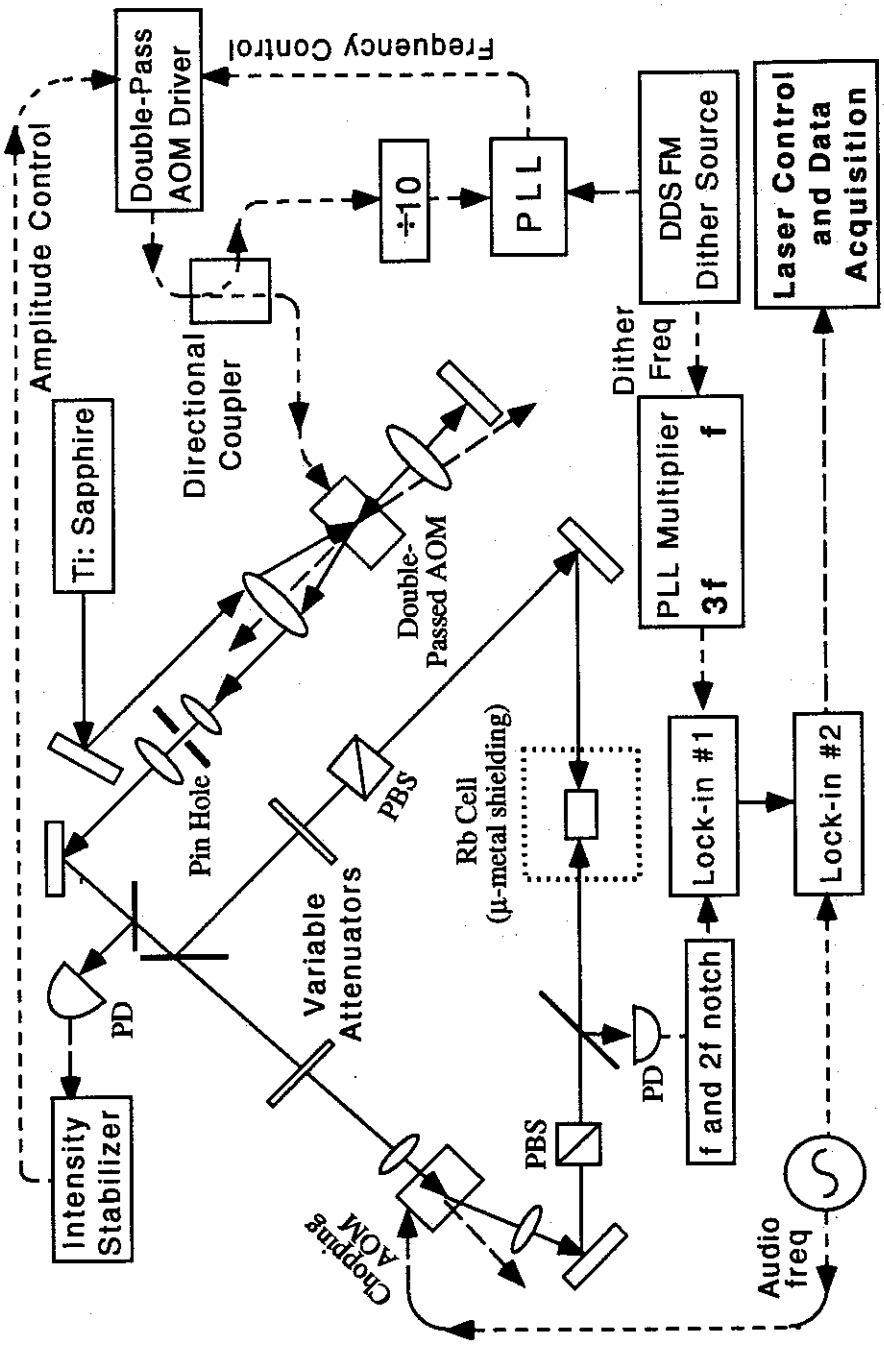

Figure 4-9 Schematic of Rb 3F Spectrometer

Preparation of Rb Cells

Several different Rb cells have been used during this experiment. Some have flat windows (with 5 degrees wedge) others have Brewster windows. Preparation of these cells follows along similar lines, with some particulars being changed depending on whether the cells were glass or quartz. An example preparation for a quartz Brewster cells starts with a washing of the cell body in a solution of sulfuric and chromic acid at 65° C. The cell bodies are then rinsed in distilled water, cleaned in an ultrasound machine then rinsed again in distilled water. Then they are rinsed again in double-distilled methanol. After cooling, the cell bodies are then heated to 800-900° C, just below the melting point of quartz. The cell bodies are then attached one by one to a foreline pump with a trap. The cell windows, which have been previously cleaned with double-distilled methanol are then fritted on. After all the cells have had their windows attached they are each attached to a manifold which is evacuated with an ion pump. The manifold and cells are then pumped for about 1 week at 350-400° C. The cells, now at a pressure of $\approx 10^{-9}$ Torr are then allowed to cool. At this point an ampoule of Rb is broken in the vacuum system and, after distilling the Rb into the system, the cells are tipped off at room temperature. The stems of the cells are made of pyrex and are attached to the quartz cell bodies by graded seals. This is to allow the cells to be tipped off at a lower temperature then would other wise be possible. The pressure with the tip-off region hot is $\approx 10^{-7}$ Torr.

Microwave System

Microwaves for the 263 GHz frequency differencing system (shown in figure 4-10) are generated in a OKI model 47v12 single reflex klystron. The klystron can output a maximum power of 300mW at 42 GHz. A Hewlett Packard (HP) V752D 20 db directional coupler splits the klystron output, sending the majority on towards a TRG V520 variable attenuator which is used to adjust the power to the Schottky diode (SD). Before reaching the SD the microwaves must pass through a polarization rotator and an E&H tuner which is used to achieve maximum coupling to the unusual load that the SD presents.

The fraction of the microwaves which are coupled out of the directional coupler feed an HP OPT H43 harmonic mixer. The mixer is also driven from an HP 8641 microwave synthesizer. The output of the harmonic mixer is:

$$\text{Harmonic\_Mixer}_{\text{Output}} = \pm\left|N\left(\text{Microwave\_Synth}_{\text{Output}} - \text{Klystron}_{\text{Output}}\right)\right|$$

In operation, the synthesizer is tuned to f≈3.5 GHz so that the output associated with the 12th harmonic of the synthesizer from the mixer is 60 MHz. This 60 MHz intermediate frequency is then amplified and used as the Rf input for the klystron frequency control system. Given the system topology, and that the microwave synthesizer uses a 10 MHz timebase, the multiplication error for that timebase is 26 kHz/Hz.

The servo system is shown in detail in figure 4-11. The 60 MHz local oscillator (LO) for this system is derived by multiplying a ten MHz Rb clock by six. The

Schematic of Microwave Generator System

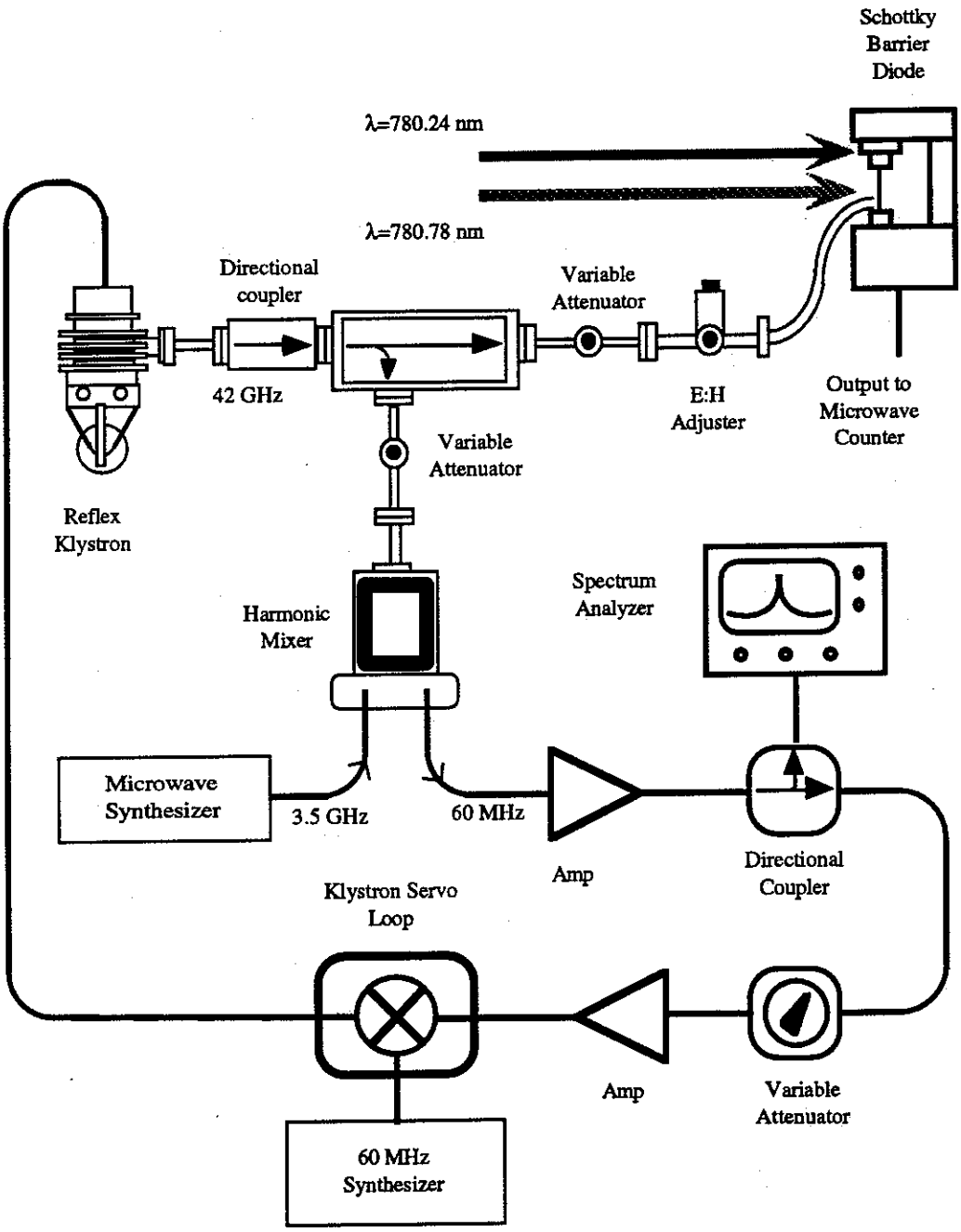

Figure 4-10 Schematic of Microwave System

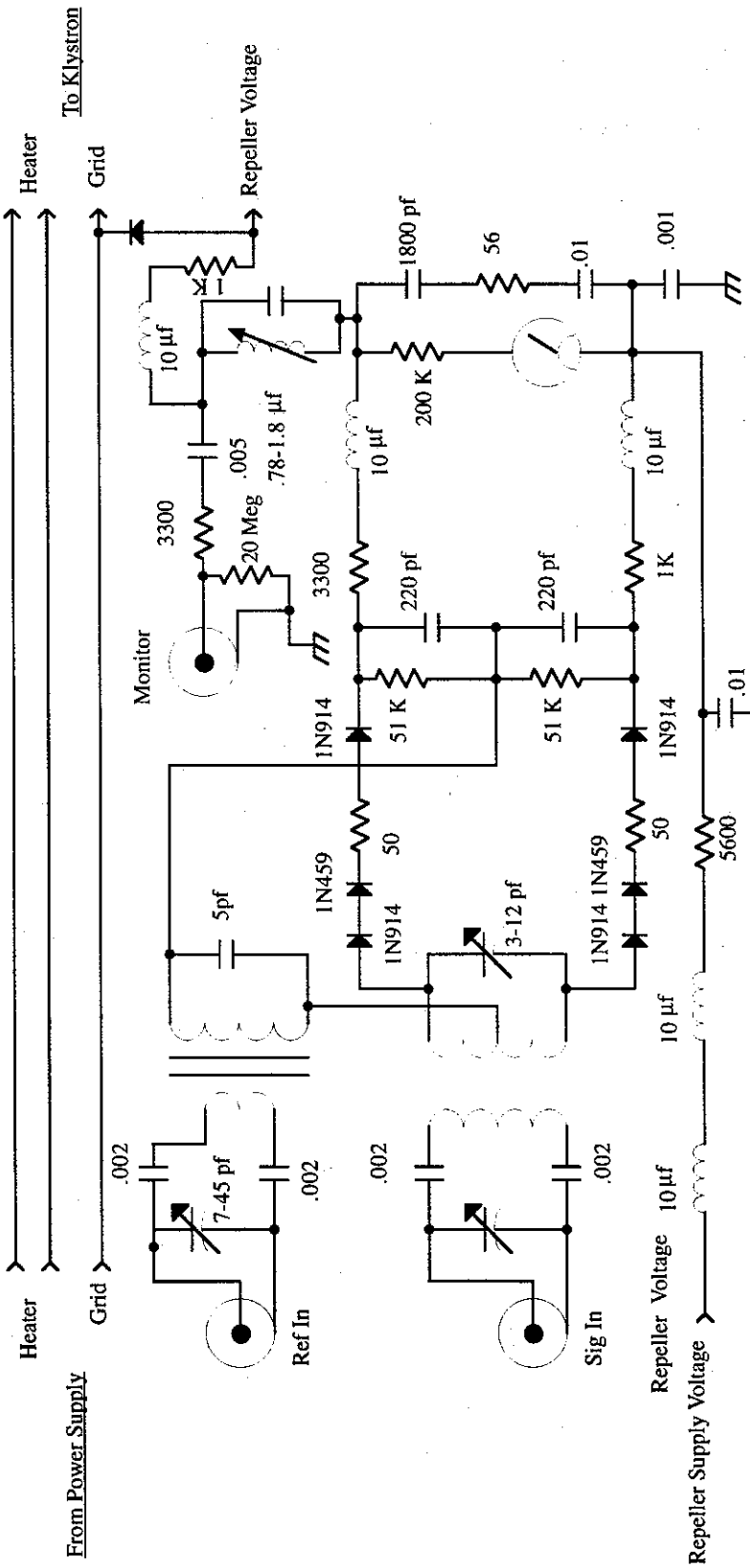

Figure 4-11 Klystron Frequency Servo controller

10 MHz reference is supplied by a Rb clock. The klystron frequency control voltage is derived by inductively coupling the LO and the output of the harmonic mixer to a single balanced mixer whose output is filtered and then impressed on the klystron repeller voltage. The result is a servo bandwidth for the klystron of about 200 kHz.

Microwave System Results

The output of the harmonic mixer can also be connected directly to a spectrum analyzer. If the frequency/phase stability of the mixing synthesizer is substantially better then the klystron (in this case it is), then the spectrum analyzer gives a picture of the klystron's frequency stability and spectral profile. This profile is shown in figure 4-12. With no frequency control, the klystron shows some slow frequency drift associated temperature changes and several MHz of fluctuations that are correlated to acoustic pick up. The spectral profile of the klystron is approximately Lorenzian with a half width of about 18 kHz. With feedback more then 90% of the klystron's energy appears in its carrier.

Summing Crystal for HeNe and "Green" YAG Beams

The Second Ti-Sapphire laser and the "Green" doubled YAG laser are combined together in a RDP crystal. The program "SH/SUM generation" written by Surendra P. Singh was used to determine that a matching temperature of 86 C° and a small angular tuning would be correct for producing 316.5nm from the combination of 532nm and 781nm in EEO configuration. The Inrad produced 5x5x30 mm crystal is

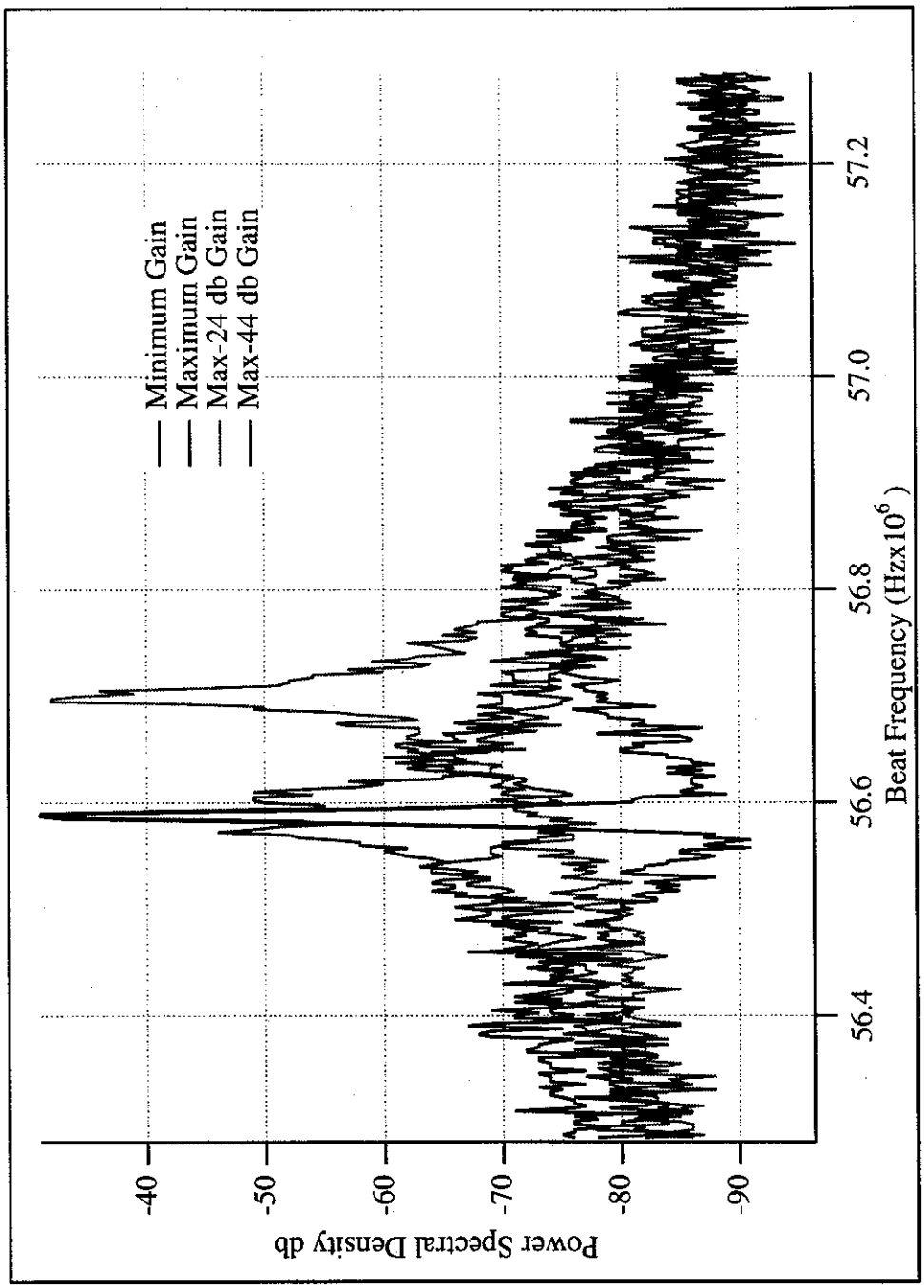

Figure 4-12 Power Spectral Density of Klystron Output

mounted in a copper oven of approximately 1.8X.8X1.1" size. The oven's temperature was controlled by a JILA designed temperature controller and the temperature oven was also monitored independently by a sensor based on the Analog Devices AD590 temperature-to-current converter.

References

[1]G.B. Barwood, P. Gill, and W.R.C Rowley, "Frequency Measuremnets on Opticaly Narrowed Rb-Stabilized Laser Diodes at 780 nm and 795nm," Appl. Phys. B 53, (1991): 142-147.

[2]G.B. Barwood, P. Gill, and W.R.C Rowley, "Optically Narrowed Rb-stabilized GaALAs Diode Laser Frequency Standards with $1.5*10^{-10}$ Absolute Accuracy," SPIE 1837, (1992): 262-270.

[3]S. Ezekiel and R. Weiss, "Laser-Induced Fluorescence in a Moleculer Beam Of Iodine," Phys. Rev. Lett. 20, (1968): 91-93.

[4]A.D. White, "Frequency Stabilization of Gass Lasèrs," IEEE J. of Quant. Electr. QE-1, (1965): 349-357.

[5]M.L. Skolnick and P.H. Lee, "Saturated Neon Absorption inside a 6238 A° Laser," Appl. Phys. Lett. 10, 11 (1967): 303.

[6]G.R. Hanes and Dalhstrom C.E., "Iodine Hyperfine Structure Observed in Saturated Absorption at 633 nm," Appl. Phys. Lett. 14, 11 (1969): 362-364.

[7]T.J. Quinn, "International Reports, Mise en pratique of the definition of the metre 1992," Metrologia 30, (1993/1994): 523-541.

[8]O. Acef et al., "A CO_2 to visable optical frequency synthesis chain: accurate measurement of the 473 THz HeNe/I_2 laser," Opt. Commun. 97, March (1993): 29-34.

[9]Kato Yoshiaki and B.P. Stoicheff, "Two-Photon absorption to highly exicted D states of Rb atoms," JOSA Letters 66, 5 (1976): 490-492.

[10]K.C. Harvey and B.P. Stoicheff, "Fine Structure of the n^2D Series in Rubidium near the Ionization Limit," Phys. Rev. Lett. 38, 10 (1977): 537-540.

[11]F. Nez et al., "Optical frequency determination of the hyperfine components of the 5s1/2-5D3/2 two-photon transitions in rubidium.," Optics Commun. 102, (1993): 432-438.

[12]F. Nez et al., "Precise Frequency Measurement of the 2S-8S/8D Transitions in Atomic Hydrogen: New Determination of the Rydberg Constant," Phys. Rev. Lett. 69, 16 (1992): 2326-2329.

[13]Y Millerioux et al., "Towards an accurate frequency standard at λ=778 nm using a laser diode stabilized on a hyperfine component of the Doppler-free two-photon transitions in rubidium," Opt. Commun. 108, May (1994): 91-96.

[14]D. Touahri et al., "LPTF Frequency Synthesis Chain: Results and Improvement for the Near Future," IEEE Trans. Instrum. Meas. 44, 2 (1995): 170-172.

[15]J.-M Chartier and M. Winters, "Design of an Iodine Stabilized He-Ne Laser at 633 nm," (Joint Institute of Laboratory Astrophysics, 1982).

[16]Andrew J. Wallard, "A Practical Aproach to the Design and Construction of Iodine Stabilized Lasers.," (National Physical Laboratory, 1979).

[17]W.R.C. Rowley, "Frequency Dependence of a 633 nm He-Ne laser stabilized by $^{127}I_2$, upon iodine pressure, modulation amplitude, and wall temperature.," (National Physical Laboratory, 1981).

[18]J.H. Shirley, "Modulation transfer process in optical heterodyne saturation spectroscopy," Opt. Lett. 7, 537-539 (1982).

[19]J.J. Snyder et al., "High-sensitivity nonlinear spectroscopy using a frequency-offset pump," Opt. Lett. 5, 4 (1980): 163-165.

[20]H.R. Xia et al., "Phase shifts and intensity dependence in frequency-modulation spectroscopy," JOSA B 11, 5 (1994): 721-730.

Chapter V: INTERMEDIATE RESULTS.

Experimental Results

Introduction

In the optical domain, there are no "simple" frequency counters into which a beam can be propagated and a precision measurement obtained. Optical frequencies can be measured by any one of several methods, which have varying degrees of accuracy and precision.

The most accurate available systems are frequency chains in which the measured frequency can be compared directly to some (usually large) integer of the Cs standard at 9 GHz. Such systems are very large and complex to operate[a] and only provide a small number of frequency markers. In practice, such systems are designed around measuring one or two special atomic or molecular transition frequencies. Such transitions are chosen for a combination of utility such as, they are near frequencies of physical interest or are easy to generate. Or they are robust, in that their center frequencies are not easily perturbed. For many optical standards, narrowness and ease of obtaining good signal to noise are what makes them attractive. This is helpful in reducing the effort needed to find the center of the transition in a repeatable manner.

---

a. As an example see the frequency chain of Evenson et al. as described in [1] or Laser Spectroscopy IV edited by Walther and Rothe (Springer Verlag 1979 New York)

Once a standard frequency has been measured it would be natural to assume that building an oscillator (in our case a laser) with sufficient care and locking it to the center of a known transition will ensure that it will be operating at a known frequency to within a measured statistical limits. The term "with sufficient care" in this case indicates that an adequate prescription for preparation of the sample, method of detecting the transition, and servo controlling the oscillator to the line center has been followed. Attention to the physics of what external forces (temperature, magnetic field, etc.) affect the transition are obviously also important. Our measurement of the Rb/D_2 transition frequencies are in this class of measurement as they rely on the known frequency and reproducibility of the Rb $5S_{1/2}$-$5D_{3/2}$ two-photon transition.

As an alternative to frequency measurements which are tied directly to the Cesium standard or, indirectly through a molecular transition, a frequency measurement can be made interferometrically. The original measurement by Barwood et al[2] of the Rb/D_2, which we have used, falls into this category. This involves starting with a known frequency (as previously discussed) and counting orders of a calibrated interferometer such as a high finesse cavity. This type of measurement is often substantially less accurate then direct frequency measurement. There are several reasons for this. One is the difficulty in precisely measuring the free spectral range (FSR) of an interferometer. Other reasons may include understanding the systematic changes in FSR of the interferometer with shifts in wavelength, temperature or polarization. Total input power and mode matching effects also complicate the measurement process. In our example measurement of the R(56)32-0 I_2 transition the uncertainty of the Rb/D_2 frequency (which is an interferometric measurement) is the dominant source of uncer-

tainty.

Measurements of transition wavelengths can also be done to a much lower degree of accuracy using a λ–meter. While the utility of this may seem limited, it is often the case that knowing a laser's frequency to ±10 MHz is more then enough. In our experiment two different λ–meters were used, one to roughly verify the frequency of the doppler broadened R(56)32-0 ro-vibrational transition as measured by FTIR spectroscopy, the other to ensure that all possible offset errors had been eliminated from the measurement (this type of error is typically on the order of some tens of MHz).

Results from Nd:YAG/I_2 Measurement

The difficulty of building and operating frequency chains means they can not be used in all experiments involving candidate transitions. A great deal of information can, however, be obtained by intercomparisons between similar test systems. Before deciding to build our frequency chain, the Nd:YAG/I_2 transition at 532 nm had already been investigated first by Arie et al[3]. Eickhoff and Hall [4] later made improved measurements of the relative splitting of more then six Doppler broadened transitions and demonstrated the system's excellent potential frequency stability. For each hyperfine transition within the Nd:YAG laser's tuning range, the splittings fit well to a four term Hamiltonian.

One of these transitions, R(56)32-0, because of its strength and large splittings from nearby neighbors, was chosen as the candidate for a possible frequency standard.

Within this ro-vibrational group the hyperfine component a_{10} was chosen as the main reference line because it is well isolated and near the center of the Doppler curve. The hyperfine splitting with respect to this transition are summarized in Table 5-2. The splittings were fit with a four term Hamiltonian, which included the nuclear electric quadrupole, spin-rotation, tensor spin-spin and scalar spin-spin interactions. The standard deviation of 1.3 kHz is quite good indicating that the precision of locking is high.

$$\hat{H}_{hfs} = eqQ\hat{H}_{NEQ} + C\hat{H}_{SR} + d\hat{H}_{TSS} + \delta\hat{H}_{SSS} \qquad \text{Eq 5-1}$$

Table 5-1 Fitting of hyperfine constants to four part Hamiltonian[5]

eqQ'	-544.1896(26) MHz	eqQ"	-2452.5837(16) MHz
C'	0.089519(3) MHz	C"	0.003162(8) MHz
d'	-0.04281(16) MHz	d"	0.00158(5) MHz
δ'	-0.000670(18) MHz	δ"	0.00366(3) MHz

'= Hyperfine constants for the excited state derived from this measurement

"=Hyperfine constants of the ground state (v"=0,J"=13) given by Yokezeki and Munter

Table 5-2 Fitting of splittings from a_{10} ref[5]

Component	F	I	Measurement (MHz)	Calculated (Mhz)	Meas.-Calc. kHz
a_1	57	2	-571.546774	571.545724	-1.052
a_2	53	4	-311.848288	-311.847728	-0.560
a_5	58	2	-260.176900	-260.1766045	-0.855
a_6	56	2	-170.066022	-170.064365	-1.657
a_7	61	4	-154.551039	-154.548713	-2.326
a_8	54	4	-131.915891	-131.915011	-0.880
a_9	55	4	-116.199435	-116.197377	-2.058
a_{10}	59	4	0.000000	0.000000	0.000
a_{11}	60	4	126.513402	126.512815	0.587
a_{12}	57	4	131.210847	131.212825	-1.978
a_{13}	55	2	154.490700	154.489932	0.768
a_{15}	56	4	286.410404	286.413056	-2.652

RMS 0.001091 MHz

sdev 0.001336MHz

Measurement Made 6/17/03

9:00-12:20 PM

By fitting to the measured lineshapes of the Nd:YAG/I_2 spectra, the slope of the frequency shift is found to be -1.3 kHz/Pa. This slope is much smaller then frequency shifts that have been measured for other I_2 lines (-10 kHz/Pa for the 633 nm transition[6] and -7 kHz/Pa for the transition at 612 nm[7]). In contrast, the power shift of 2.1 kHz/mW is of the same order as the 633 nm HeNe/I_2 laser's (-1.4 kHz/mW of estimated intercavity power[8]).

The Allan-Variance of the two laser/absorber systems was also measured (see figure 5-1). As can be seen for short time periods (τ< 1 ms), $<\sigma(\tau)>^2$ is about $6*10^{-12}$. This is the intrinsic noise of the laser as the time scale is too short for the servo electronics to have any effect. From $<\sigma(\tau)>^2=1*10^{-12}$ at τ=1 ms the variance drops quickly to $<\sigma(\tau)>^2 \approx 5*10^{-14}$ at $\tau \approx 3$ s. This is better than currently attainable with our HeNe/I_2 laser but not as good as the NIST-7 Cs clock[9].

HeNe/I_2 Calibration Results

In order to establish that our HeNe/I_2 laser works correctly, we were fortunate enough to have temporary access to two portable standard lasers from BIPM (BIPM P1, P3). These lasers had recently been tested against BIPM's master laser (BIPM4). This enabled us to compare the HeNe/I_2 laser's absolute frequencies with the "as maintained" value of BIPM 4. The comparison (See table 5-3) indicated that our laser was 5 kHz to the red of the accepted value. This value is obtained by fitting the values in the table with a least-squares fitting program to get the best fit offset, then removing the known 80 MHz AOM offset and 2 kHz offset between BIPM P3 and BIPM4.

Table 5-3 Comparison of JILA HeNe/I2 and BIPM I2 Laser

BIPM→ JILA↓	d	e	f	g
d	79.9942±1.6	92.8572±1.9	106.2213±1.0	119.4204±1.1
e	67.1269±0.9	79.9926±3.3	93.3561± 2.1	106.5544±1.6 or 106.2215±1.7
f	53.7648±0.7	66.6291±0.6	79.9925±2.0	93.1902±1.0
g	40.5636±0.4	53.4291±1.6	66.7925±1.7	79.9917±0.4 or 79.9915±1.4

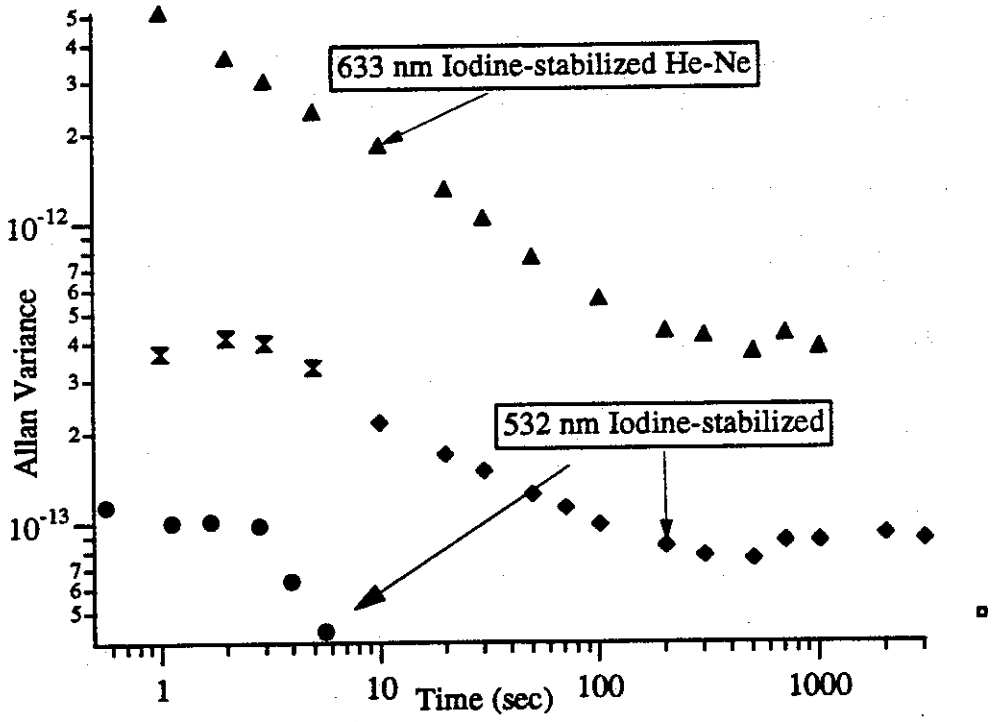

Figure 5-1 Allan Variance of Nd:YAG/I_2 and HeNe/I_2system

A measurement of the Allan Variance for our laser (see figure 5-1) was as also made at this time. The figure clearly shows that the Nd:YAG/I_2 system has much lower Allan-Variance then the HeNe/I_2 system at all time scales.

At shorter times scales this is due to the monolithic nature of the Nd:YAG NPRO laser. While at longer times it arises because of the more favorable S/N of the R(56)32-0 transition. This inherent stability is one of the primary reasons that I_2/532 nm system is of significant interest.

Rb/D_2 3F Spectrometer Measurements

No equivalent reference for the Rb/D_2transition was available in our lab, so two Rb/D_2 spectrometers were built (referred to as number 3F and FM for their detection methods). The 3F spectrometer, described earlier, was made to resemble as closely as possible the Rb/D_2 spectrometer at NPL which was used to establish the absolute frequency of the Rb/D_2 d/f crossover. The other, FM spectrometer was based on FM sideband spectroscopy [10]. All absolute frequency measurements were conducted using the 3F spectrometer. Using intercomparisons of the two spectrometers, upper limits on the sensitivity of the 3F spectrometer to several parameters have been measured and an upper limit for its Allan-Variance has also been determined. An experimental investigation of the splittings of the hyperfine components of the Rb/D_2 transition is also underway.

One of the parameters to which the Rb/D_2 spectrometer transition is sensitive is mag-

netic field. At low fields the primary effect is through a combination of Zeeman splitting of the magnetic sublevels and optical pumping. In order to reduce the sensitivity of the spectrometer the Rb cell axis is placed parallel to the earth's magnetic field. The spectrometer also uses an appropriate combination of linear-polarized beams that strongly favors $\Delta m_f=0$ transitions, reducing any optical pumping. This is especially important for the 3F spectrometer which uses 4 mm beams that can potentially allow many interactions on cycling transitions such as the F"=2 ->F'=3 line. To test for the effects of magnetic fields a bar magnet is held close to the Rb cell in several different positions while the inhomogenious field is monitored with a Gaussmeter. When the Gaussmeter shows a significant perturbation from the background field, the beat frequency with the other spectrometer is measured, in this manner an upper limit of the frequency shift due to the earth's magnetic field is estimated to be < 5 kHz.

Shifts in line center with optical power are another significant effect in the Rb/D_2 spectrometer. Fortunately, they are also one of the easiest to control. Figure 5-2 is a graph showing the measured power shift for three lines the f,d, and d/f crossover. For each point the probe power is kept at a constant 10μW while the pump power is varied. Notice that the f line shows a substantial power shift. This may be due to a combination of factors, an important one is that the f line arises from the F"=2 ->F'=3 transition which is "closed". This allows the Rb atom to accumulate a large velocity shift as it passes through the pump beam repeatedly absorbing photons from one direction but emitting them spontaneously in random directions. The result is the appearance of an asymmetric component in the line shape which contributes a power dependent offset when the 3rd harmonic detection converts the absorptive feature to a

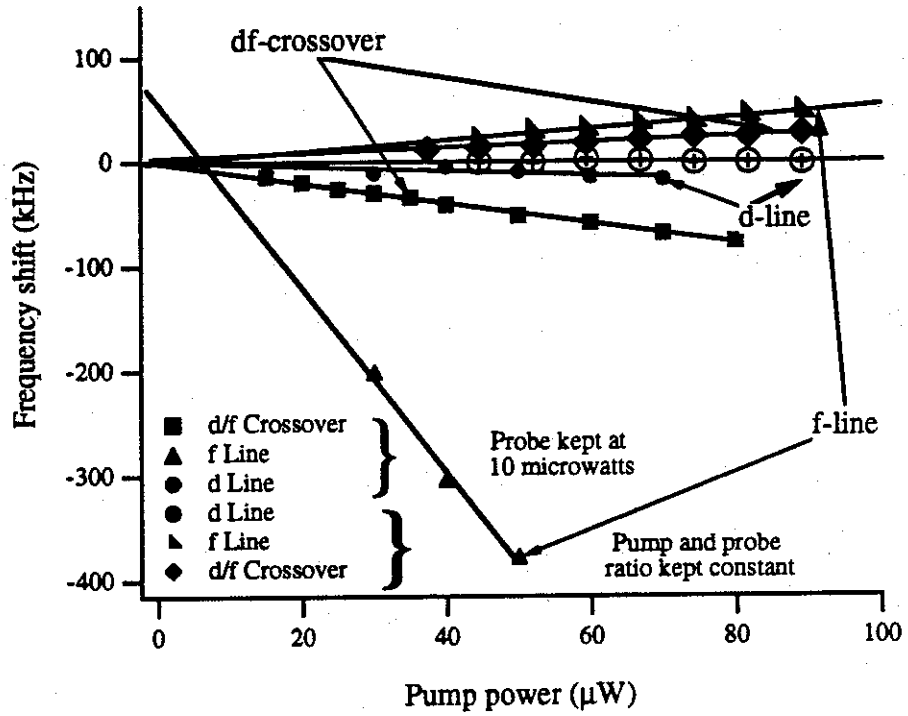

Frequency shift vs. power for d,f, and d/f crossover. Note that lines where the probe power was kept at 10 μw have smaller and reversed slope. In spite of this the zero power extrapolation for all but one of the "f" line is quite good (Ideal performance would be slope-intercept at -5kHz).

Figure 5-2 Power shift of f,d and d/f Rb lines

discriminator signal. The phenomenon has been studied by Grimm and Mlynek[11,12,13].

Another important factor is optical pumping. An explanation is provided by Schmidt et al.[14] for some of the odd behavior of the cycling transition. At low magnetic fields the lin||lin polarized light used in both JILA spectrometers excites only $\Delta m=0$ transitions. The Clebsh-Gordon coefficients for the cycling transition's spontaneous decay lead to optically pumping of atoms into the m=0 state. This state has a larger dipole moment then a statistical distribution of m states. The result is that at low optical powers the saturation spectrometer makes the "f" line more absorptive instead of more transmissive. Given enough optical power, saturation can finally be observed and the line "flips" over to transmissive, but first it goes through several intermediate stages showing a sharp transmissive feature against a broader absorptive feature.

The d line, which arises from the F"=2 -> F'=2 transition is relatively free from this problem as the Rb atom may decay from F'=2 ->F"=1 and thus cease interacting with the pump light. The d/f crossover is an intermediate case. At constant probe power it shows about -40 kHz/μW shift but, because it is quite strong and well isolated from nearby lines, it still a reasonable choice for a reference.

The choice of how the power shift is measured also plays an important role in its determination. In later experiments the pump and probe power were simultaneously varied so that their proportion stayed a constant. In these experiments the slope of the d/f line changed from -40 kHz/μW to 0.3 kHz/μW. This changed the extrapolated zero power point for the d/f transition by 370 Hz. The quality of the Rb cells used in the spectrometer is another possible limiting factor in obtaining good precision in the Rb/D_2 system. Barwood[15] pointed out that background gas may cause pressure-dependent

frequency shifts as it does in iodine and tellurium cells. Two tests were performed to ensure the quality of our cells. First we measured the absolute frequency shift obtained by exchanging our cells with two cells of pure ^{87}Rb made at NIST by Hugh Robinson with a completely different vacuum system. These shifts were all less then 10 kHz. As a second test, the linewidth of our Rb cells was also checked against the known natural linewidth of 5.9 MHz based on the Hanle-effect [16] (see figure 5-3). The extrapolated linewidth is approximately 7 MHz, of this <500 kHz is Zeeman broadening. This leaves about 600 kHz for all experimental uncertainties including background gas. It may be reasonably asked whether the gamma versus intensity curve for an unusual transition such as a cross-over which includes a cycling transition would be expected to follow the usual formula

$$\gamma = (\gamma_r (1 + \sqrt{1 + G})) / 2 \qquad \text{Eq 5-2}$$

The question was studied by Akulshin et al[17] who concluded after studying the equivalent transition to the d/f but in ^{85}Rb:

> "In spite of the fact that many levels and different mechanisms of optical pumping are involved in the saturation, the dependences are found to fit well the simple formula, obtained for a two level system with a phenomenologically defined saturation parameter"

λ-Meter Measurement

The wavelength of an unknown laser may also be compared against a known reference in a wave-meter[18,19]. Wave meters have demonstrated precisions of nine or even ten digits in our lab, however, their accuracy has not been tested to this level. Even though they lack the highest level of precision, two λ-meters were used as "real-

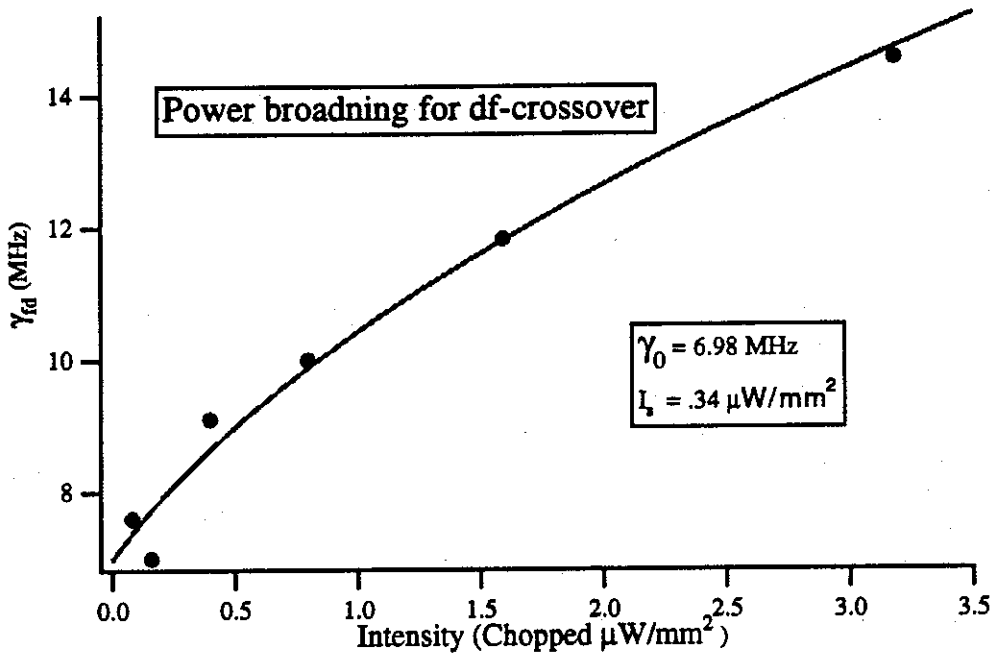

Figure 5-3 Gamma vs. Intensity for d/f crossover

ity checks". For the green Nd:YAG/I_2 system, it is possible to confirm the choice of ro-vibrational group based on FTIR measurements (80 MHz) accuracy with a λ-meter calibrated to the Na D_2 line[20]. The Rb/D_2 system was also checked for possible errors (accuracy 40 MHz) by cross calibration with a λ-meter that is calibrated to the Rb $5S_{1/2}$-$5D_{3/2}$ two-photon transition.

Results of Frequency Chain Measurement

Experimental Procedure

Once the individual parts of the chain are tested and found to be in working order, "all" that remains is to conduct the experiment. Since the frequency chain consisted of multiple servo-locked and cross-connected systems, their orderly activation is the primary difficulty of the actual experiment. First the Nd:YAG/I_2 laser doubling cavity is brought on resonance so that it generates green light which is used in the I_2 spectrometer. Then the laser/doubler system is brought into resonance with the apropriate hyperfine components of the I_2 R(56)32-0 transition and locked to the line center using modulation transfer spectroscopy as discussed. The spectrometer uses only a few milliwatts of green light and the rest (50-60 mW) is sent via a fiber optic cable to be summed with the output of a frequency stabilized Ti-Sapphire laser in an RDP crystal thus producing a small amount of UV at 316.5 nm

At the same time, the 633 nm HeNe/I_2 laser is locked to its I_2 reference line. Then the offset-frequency-phase locked loop laser is locked 88 MHz above the HeNe reference. The HeNe doubling cavity is then locked to this laser, and the result is a pre-

cise frequency of 316.5 nm light. This light along with the UV from the Ti-Sapphire/ Nd:YAG sum frequency generator is heterodyned in a PMT and the beat frequency of ≈ 20 MHz is input to an rf phase-locked-loop which provides an oscillator-out port for counting the UV beat frequency.

Simultaneously, a second Ti-Sapphire laser is locked to a tunable reference cavity. The cavity is then tuned so that the laser is on resonance with the d/f cross-over of the Rb/D_2 transition. The Rb spectrometer previously described is then used to detect the transition and provide the discriminator signals needed to lock the laser/cavity system to the Rb line center. This Ti-Sapph laser is then heterodyned against the first-mentioned one on the Shottky diode. Their difference frequency is about 263 GHz. This frequency when mixed against a harmonic of the klystron produces a signal in the 900 MHz region. A microwave tracking oscillator is then used to bring this weak signal up to a countable level. A computer is used for the triggering and recording of the output from the two counters, and later analysis.

At the end of each day all the oscillators in the various synthesizers and counters were tested by counting against a portable Cesium frequency standard. Other crystal oscillators such as the ones in EOMs and AOMs which are not frequency multiplied were tested once to obtain absolute value, and thereafter tested only occasionally to be sure their drift was only on the few Hz scale.

Experimental Results

In figure 5-4 A is an example of 40 minutes of data. It can be seen that individually the UV and microwave beatnotes drift at a hefty 450 Hz/Sec due to the thermal drift of the locking cavity of the 2nd Ti-Sapphire laser. In the calculation for the Nd:YAG/I_2 frequency they appear as a sum, and it can be seen that the drift for this sum is only -1.8 Hz/S showing that the cancellation is quite good. The standard deviation for this data record is ≈10 kHz as is the half-width at half maximum. This is well below the actual uncertainty in the published value for the Rb/D_2 line center. In figure 5-4 B is shown the power spectral density of this data after removing the 1026 MHz offset. It shows a rise for frequencies below $(50 \text{ seconds})^{-1}$ but no other serious anomalies indicating system oscillations. A closer view of the data and its Allan variance is given in Figure 5-5(note the arbitrary offset has changed). The first eight points of the Allan variance fit with a function of $A \approx \tau^{-0.46}$, which is in excellent agreement with the prediction of $A \approx \tau^{-0.5}$ for systems dominated by measurement noise. Sadly, the point of where the variance ultimately goes flat and then turns upward was never reached, but the reader is reminded that the measurement requires simultaneous operation of no less then 5 lasers (7 if you count the pump lasers for the Ti-Sapphire lasers) and several microwave PLL's. Figure 5-6 is a histogram plot of several sets of data taken at widely separated times. As can be seen the individual widths of the histograms from any given day are smaller than the bulk displacements of their centers. This leads to the suspicion that there are systematic effects which are in need of correction.

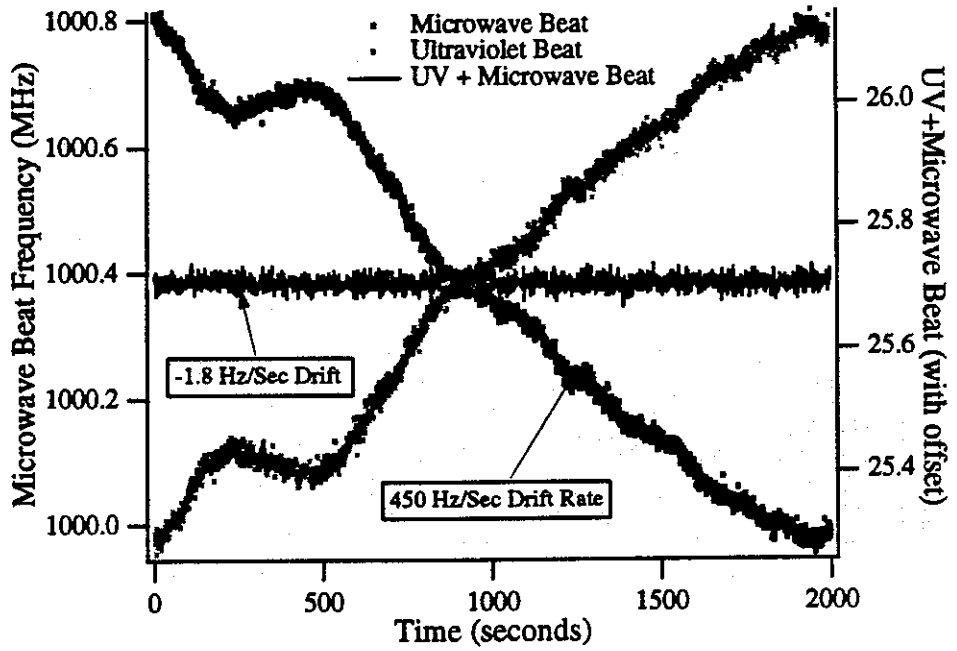

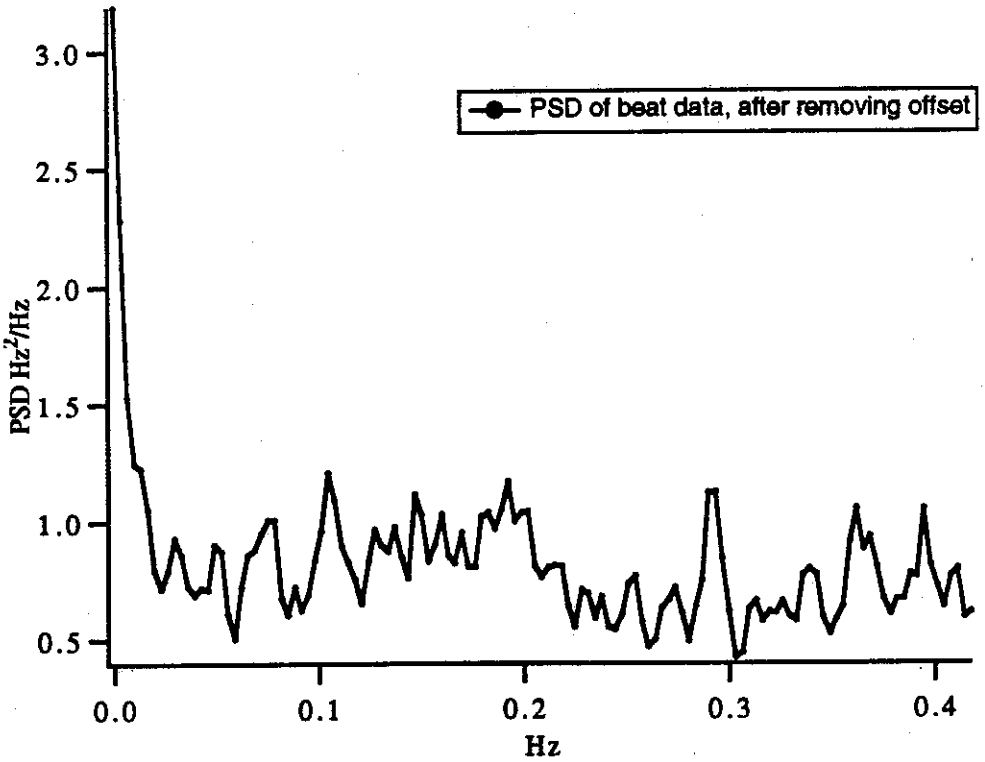

Figure 5-4 A&B Example data from I2 Frequency measurement

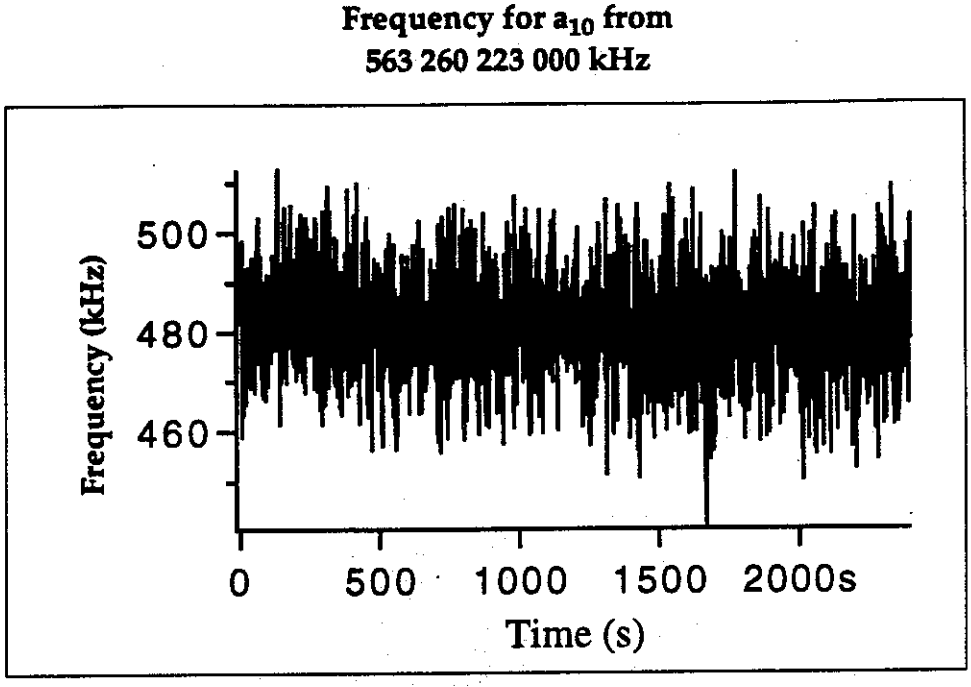

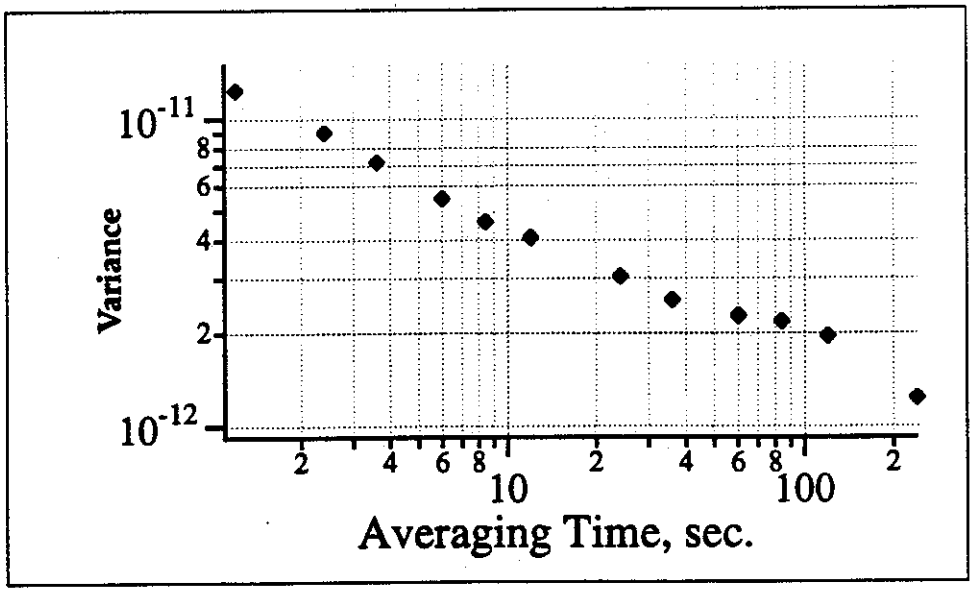

Figure 5-5 Data and Allan Variance from Nd:YAG/I_2 Frequency Measurement

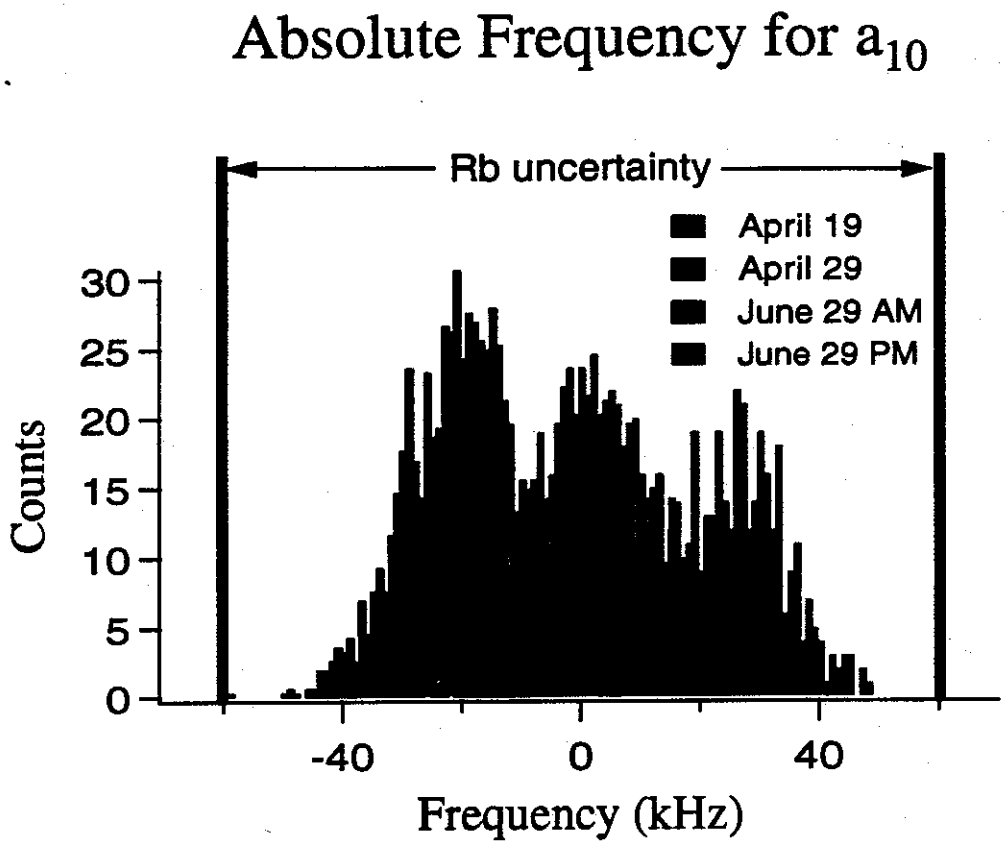

Center frequency = 563 260 223.480 MHz

Interferometric meas. = 563 260 223 ± 10 MHz

I_2 Atlas = 563 260 250 ± 60 MHz

Figure 5-6 Histogram of Beat Data for Different Data Runs

Major Source of Systematic Problems

A further investigation showed that much of those systematic effects were due to amplitude modulation generated in the double-pass AOM used in the 3F Rb/D_2 spectrometer. In particular the AM which is generated at the third harmonic of the modulating frequency is problematic. This is because third harmonic detection was used and so 3rd harmonic AM is converted to an offset in the spectrometer lock-in detector. This was always known and so adjustment of this double-pass frequency-shifter was always done while monitoring it's AM 3rd harmonic content. Unfortunately, although a skilled pair of hands could almost completely null out the 3rd harmonic AM, the adjustment was **extremely** sensitive to temperature and mechanical alignment and was therefore not stable over time.

Error Estimates

Based on the data the following errors are estimated, no attempt has been made to classify their sources as being of a technical or fundamental nature. Also included are the estimates for the hypothetical Two-Photon direct measurement (with 1.2 THz frequency gap) and for the Two-Photon+CH_4 systems.

Table 5-4 Error Estimates

	1 Photon	2 Photon	2Photon +CH_4
Reproducibility	± 25 kHz	?	?
Rb-reference	± 60 kHz	± 5 kHz	± 5 kHz
HeNe I_2	± 5 kHz	± 5 kHz	NA
CH_4	NA	NA	± 0.3 kHz
Green I_2	± 1 kHz	± 1 kHz	± 1 kHz
Total Error	± 70kHz	≈ 7.1kHz	≈ 5kHz

References

[1]K. Evenson et al., Appl. Phys. Lett. 20, (1972): 133.

[2]G.B. Barwood, P. Gill, and W.R.C Rowley, "Frequency Measuremnets on Opticaly Narrowed Rb-Stabilized Laser Diodes at 780 nm and 795nm," Appl. Phys. B 53, (1991): 142-147.

[3]Ady Arie and Robert L. Byer, "Laser Heterodyne Spectrosocpy of 127I2 Hyperfine Structure near532 nm," JOSA B 10, 11 (1993): 1990-1997.

[4]M.L. Eickhoff and J.L. Hall, " Optical Frequency Standard at 533 nm," IEEE Trans. Instrum. Meas. 44, 2 (1995): 155-158.

[5]M.L. Eickhoff, "Two New Methods for Real-Time Precision Refractometery and Precise Test of the Hyperfine Hamiltonian via Modulation Spectroscopy of Moleculer Iodine at 532 nm" (Phd Thesis, University of Colorado, 1994).

[6]W.R.C. Rowley, "Frequency Dependence of a 633 nm He-Ne laser stabilized by $^{127}I_2$, upon iodine pressure, modulation amplitude, and wall temperature.," (National Physical Laboratory, 1981).

[7]M. Glaser, "An improved He-Ne at λ= 612 nm, stabilized by means of an external absorbtion cell," Metrologia 23, (1986): 45-53.

[8]T.J. Quinn, "International Reports, Mise en pratique of the definition of the metre 1992," Metrologia 30, (1993/1994): 523-541.

[9]W.D. Lee et al., "Accuracy Evaluation of NIST-7," IEEE Trans. Instrum. Meas. 44, 2 (1995): 120-123.

[10]J.L. Hall et al., "Optical heterodyne saturation spectroscopy," Appl. Phys. Lett. 39, 9 (1981): 680-682.

[11]Rudolf Grimm and Jurgen Mlynek, "Light-pressure-induced nonliner dispersion in a Doppler-broadened medium: theory and experimental proposal," JOSA B 5, 8 (1988): 1655-1660.

[12]Rudolf Grimm and Jurgen Mlynek, "Light-Pressure-Induced Line-Shape Asymmetry of the Saturation Dip in an Atomic Gas," Phys. Rev. Lett. 63, 3 (1989): 232-235.

[13]Rudolf Grimm and Jurgen Mlynek, "The Effect of Resonant Light Pressure in Saturation Spectroscopy," Appl. Phys. B 49, (1989): 179-189.

[14]O. Schmidt et al., "Cesium saturation spectroscopy revisited: How to reverse peaks and observe narrow resonances," Appl. Phys. B 59, (1994): 167-178.

[15]G.B. Barwood, P. Gill, and W.R.C Rowley, "Optically Narrowed Rb-stabilized GaALAs Diode Laser Frequency Standards with $1.5*10^{-10}$ Absolute Accuracy," SPIE 1837, (1992): 262-270.

[16]Alan Gallagher, "Resonance broadening of the Hanle-effect signals in rubidium," Phys. Rev. A 10, 1 (1974): 231-241.

[17]A.M. Akulshin et al., "Power Broadening of the Absorption Resonance on the D_2 Line of Rubidium," Opt. Commun. 77, 4 (1990): 295-298.

[18]J.L. Hall and S.A. Lee, "Interferometeric real-time display of cw dye laser wavelength with sub-Doppler accuracy," Appl. Phys. Lett. 29, 6 (1976): 367-369.

[19]J. J. Snyder et al., "LambdaMeter Resolution Enhancement using a novel Frequency Meter," Conf. on Laser Engineering & Optics (CLEO) , (1981).

[20]P. Juncar et al., "Absolute determination of the wavelengths of the sodium D_1 and D_2 lines by using a cw tunable dye laser stabilized on iodine," Metrologia 17, (1981): 77-79.

Chapter VI: DIRECT MEASUREMENT OF Rb/D_2 TRANSITION FREQUENCY AND SPLITTINGS

Introduction

We were also able to directly compare the output frequency of our Rb/D_2 spectrometer to the $5S_{1/2}$-$5D_{3/2}$ two photon transition in Rb by frequency difference methods[1]. The absolute frequency for this two photon transition has recently been measured by Nez et al [2]. This made it possible to verify the absolute frequency of our Rb/D_2 setup and reduce the Rb/D_2 measurement from an interferometric one to one based on frequency difference methods. This measurement required the use of our Rb/D_2 3F spectrometer, a different microwave generation system and some additional equipment whose description follows.

Extra Equipment Description

Second Microwave Oscillator System

A second microwave system was designed in order to measure the laser beat frequency of 1.014 THz. This is nearly four times the 263 GHz measured in the previous experiment. Measurements with the 47GHz klystron showed that, considering the harmonic number needed (21), there would not be sufficient signal to noise available. Beat notes of this high frequency have previously been measured using 90 GHz sources so it was decided to build a stabilized 90GHz Gunn Oscillator system (see figure 6-1) to drive the Schottky diode. Substantial care was taken to avoid the problem of loss of carrier energy into the phase-noise pedestal [3].

Physical Realization

About fifty milliwatts of 91.7 GHz radiation are generated in a Osctek Gunn diode. The diodes output is coupled into a MODCM110 integrated 10 dB coupler and harmonic mixer. Most of microwaves are then fed through an isolator and an E & H tuner to the Schottky diode where they are used to down-convert the 1 THz optical beat note to rf frequencies for processing and counting. The isolator is needed to reduce the effect of the loading caused by the Schottky diode on the Gunn oscillator's stability.

A portion of the Gunn's energy which does not go to the Schottky diode is combined with the 10.6 GHz output from the Microwave Oscillator Corp. MOC110/17 dielectric resonant oscillator (DRO) in the integrated harmonic mixer. The output of the harmonic mixer is the difference between nine times the DRO's output and the 90.7 GHz output of the Gunn diode. This difference frequency, which falls near 3.6

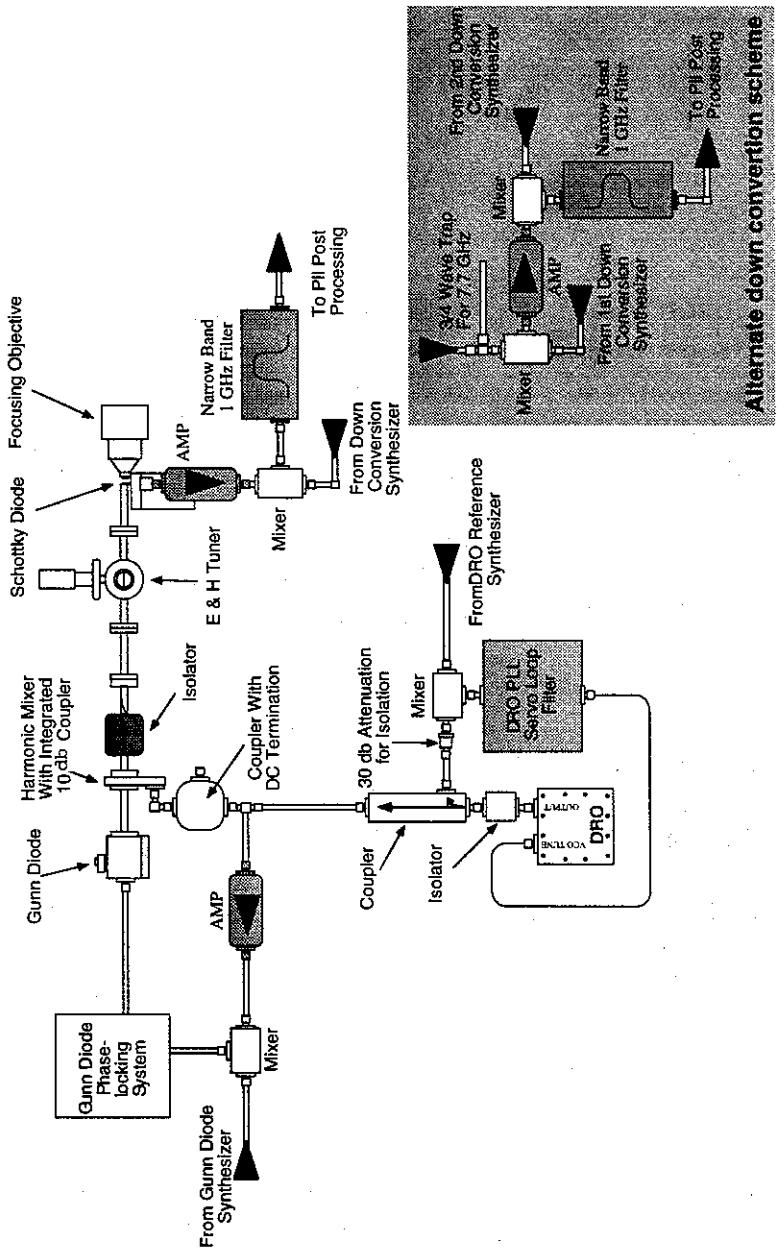

Figure 6-1 Gunn diode synthesis chain

GHz in the microwave region, is then mixed with the output of an HP 8672A synthesizer to achieve a final frequency of 55 MHz. This 55 MHz signal is then amplified and lowpass filtered before being input to a high speed phase locked loop based on the Analog Devices AD 9901 FPL. This PLL provides correction signals to phase lock the Gunn diode's frequency. It is interesting to note that this last PLL stage is based on a box originally built by Linda D'Evelyn for the purpose of phase locking diode lasers, and required only a slight modification gain coefficients and time constants for this job.

Dielectric Resonator Oscillator Stabilization

While the previously described system may sound somewhat complex it is still not sufficient to uniquely fix the frequency of the Gunn oscillator. This is because the DRO frequency is subject to frequency drifts due to changes in its dielectric resonator. In order to stabilize the frequency of the DRO a fraction of its output power is mixed with the output of a Gigatronix 1018 microwave synthesizer. The resulting signal is used by a phase-locked loop circuit to control the DRO's frequency. The loop parameters of the PLL are chosen such that the PLL's unity gain bandwidth is below 200 Hz. This is so that only the long term frequency stability of the DRO is determined by the synthesizer and the excellent phase noise characteristic of the DRO will not be disturbed.

Processing and Counting

Because of the availability of a narrow band 1 GHz microwave filter, counting for many of the 1 THz beatnotes was chosen to fall near 1 GHz. For other transitions the limited tuning range of the Gunn oscillator dictated a 5.7 GHz beat note and two-mix down conversions were used. In this case, ahead of the first mixer was placed a 3/4 λ stub which removed noise in the region of 7.7 GHz so that it would not lower the signal to noise ratio. The first mix down was to 1 GHz so the narrow microwave filter could be used. In either case after passing through this filter the signal was mixed down again to 18-22 MHz. Even under the best conditions this results in a signal to noise ratio of no better then 15 db in a 30 kHz band width.

In order to reliably count this difference signal it was necessary to regenerate it at higher S/N with a phase locked oscillator. Over the course of the experiment additional signal processing elements were slowly added to this phase locking system to improve its reliability, figure 6-2 shows the final form of the system which has additional filtering, amplification and limiting. Additionally, in order to be sure that the phase-locked oscillator was not skipping cycles a system of oscilloscopes was used for monitoring the output of the PLL mixer as well as the zero crossings of the signal with respect to the slave oscillator. The counting of the output of the phase locked oscillator was then done with a HP 53132a counter under computer control.

$5S_{1/2}$-$5D_{3/2}$ Two Photon Spectrometer

Our two photon spectrometer was designed to resemble as closely as possible the one which was used by Nez[2] et al to measure the absolute frequency of the $5S_{1/2}$-$5D_{3/2}$ transition. Light for the spectrometer was generated by a Ti-Sapphire laser. The

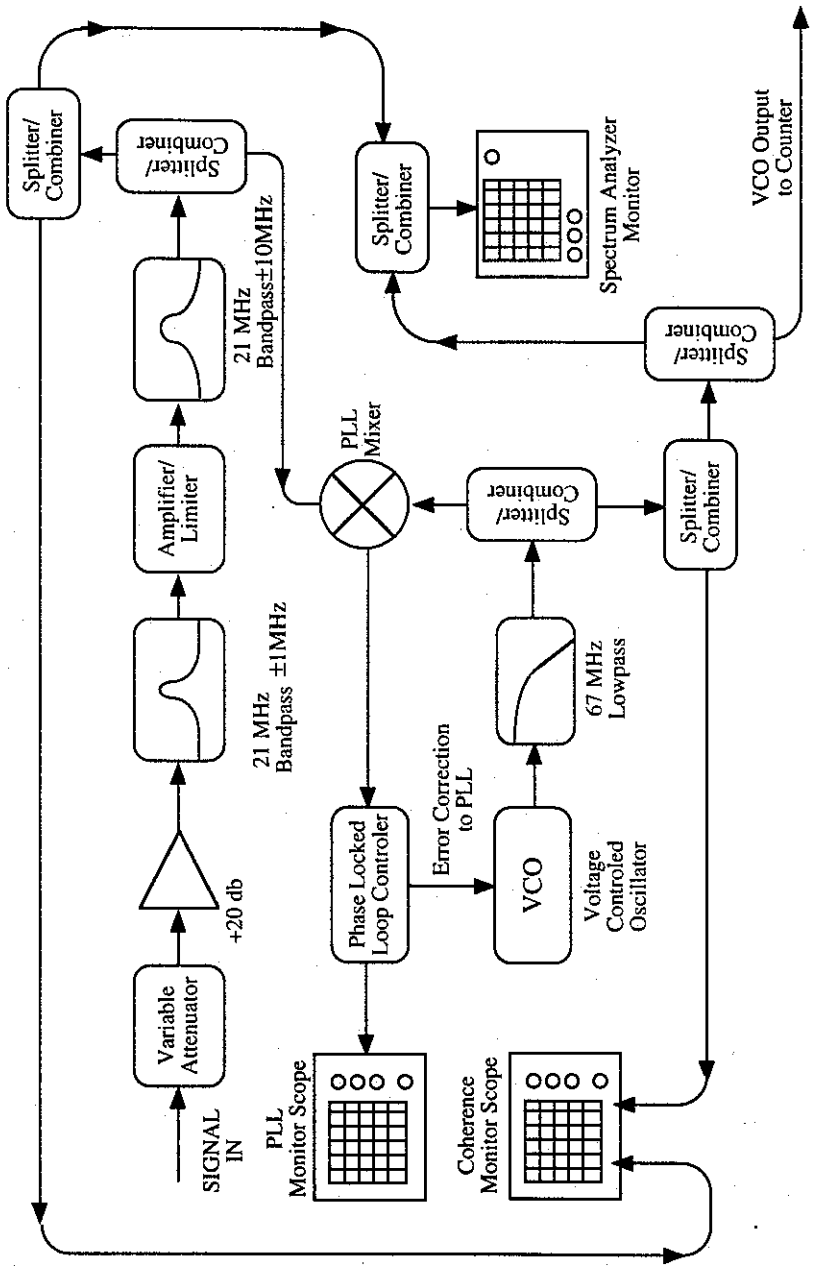

Figure 6-2 Post Processing System for PLL Regenerator

laser beam was split to accomplish three functions: frequency stabilization for the laser, input to the Schottky diode detector and light for the spectrometer.

Frequency Control System

The two photon resonance is relatively narrow and so a moderately exotic method was used to keep the laser servoed to the transition line center. Before reaching a temperature-controlled Zerodur cavity, the laser beam was first frequency shifted in a double-pass AOM. The laser was frequency locked by FM sideband technique to this cavity with a loop bandwidth of about 110 kHz. This yields a initial laser linewidth of $\approx$ 1 kHz estimated from the loop error signal. A computer was used to constantly monitor the error signal from the two-photon spectrometer. The computer implemented a servo algorithm (double integrator plus proportional) to keep the laser locked on line center by changing the frequency of the digital synthesizer which drove the double-pass AOM. The bandwidth for this servo was about 2 Hz, but it should be remembered that it only has to correct for the slow drift of the cavity.

Two Photon Spectrometer

Light for the spectrometer was delivered by a polarization maintaining fiber with a built in divergence reducing lens (output divergence of .7 mrad) made by Oz optics. Final collimation was accomplished with a curved mirror. The laser beam at 778 nm was then propagated through a double pass AOM set up which was used to put FM modulation on the beam. The modulation frequency was 500 Hz and the modulation width was 500 kHz pk-pk after the double pass AOM. The beam was then directed into the spectrometer which consists of a telescope, the Rb oven, and a retro-reflecting mirror. The Rb oven consists of a copper parallelepiped with dimensions of approxi-

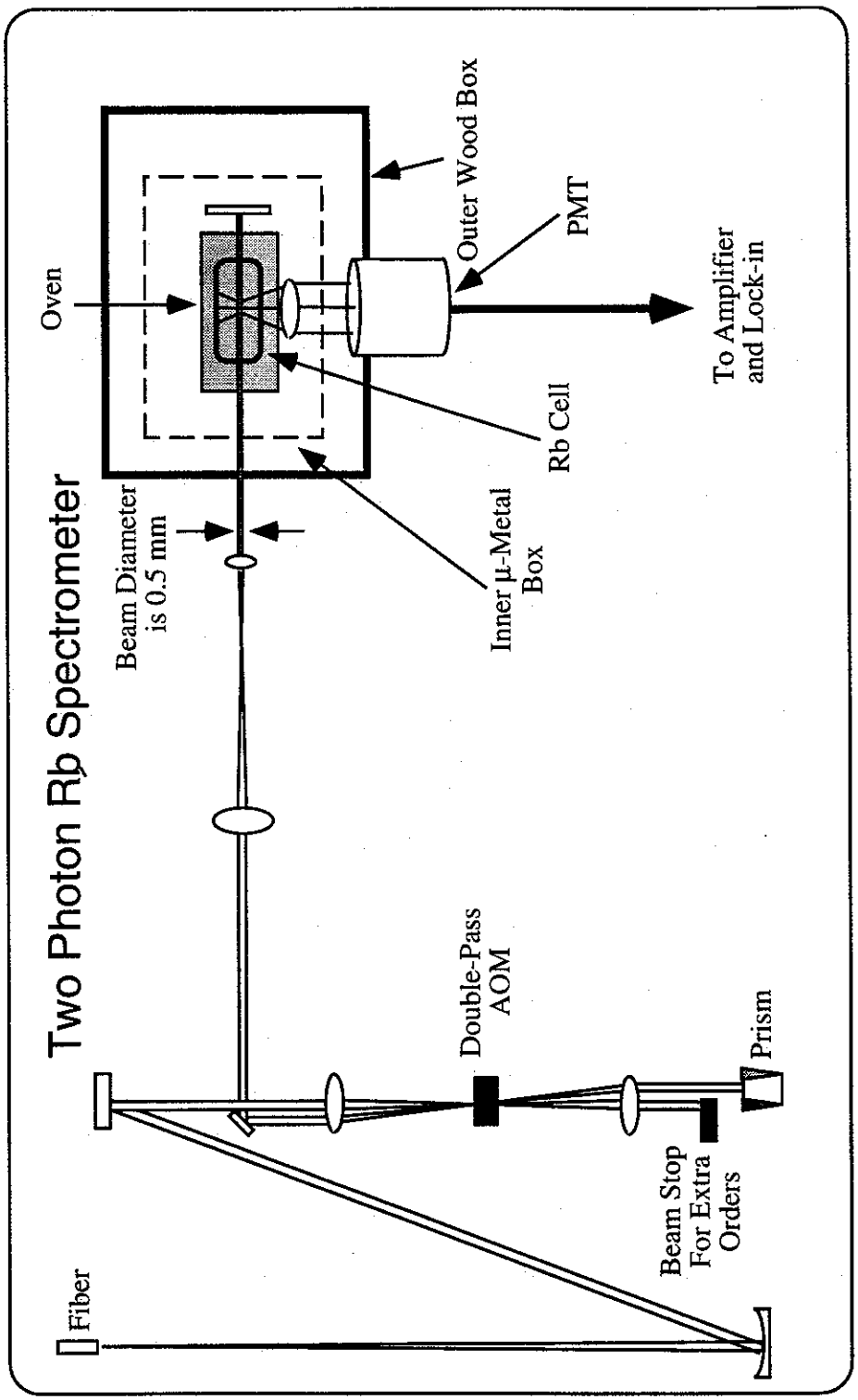

Figure 6-3 Two Photon Spectrometer

mately 3x1x1". Inside the oven is the Rb cell which is approximately 5 cm long and 1 cm wide with flat windows (5° wedge). The cell contains Rb with a natural abundance of isotopes (73% ^{85}Rb, 27% ^{87} Rb). The oven has three openings, one at either end for the laser beam to pass thought, and one on the side to allow fluorescence decay light to pass through. At each opening is also a window and a copper overlay piece. These were found to be necessary; otherwise cool zones on the Rb cell would form at the openings and subsequently Rb condensation onto these zones would severely hamper light propagation. On the bottom of the oven were carbon composition resisters used to heat the oven, and a "chimney" to keep the Rb reservoir cool. Wiring to the resistors was done with care so as to avoid generating stray magnetic fields. The oven core was surrounded by a μ-metal shield. Typical operating temperatures were 90°-110° C. The diameter of the laser beam after collimation in the telescope was 0.5 mm.

Detection of the two photon signal was done via the 422 nm radiation from the transition of $6^2P_{3/2}$->$5^2S_{1/2}$ which lies in a decay branch of the $5^2D_{5/2}$ upper state. The radiation was collected by a lens and focused on a RCA 4837 photomultiplier tube (PMT). A filter which passes the 422nm blue light but not the 778nm pump was used to allow a maximum of PMT gain to be used. After further electronic amplification the two-photon signal is processed using a Stanford model SR-510 lock-in. The voltage output of this lock-in was then digitized into a computer and processed as described earlier to maintain the servo lock.

Improved Rb Spectrometer

We were also able to make improvements in the long term stability of our Rb spectrometers. First a double layer of μ–metal was placed around each of the Rb cells. In order to estimate the residual field inside the μ-metal can, a magnetometer was placed in the can and the residual field plotted as the top of the can was slid closed (finite size of the magnetometer and cables kept to top from being completely closed). Using these measurements a residual field of less than 20 milli-Gauss was estimated.

Then the pump and probe beams were carefully aligned and mode matched. Finally, and perhaps most important, the pump beam was chopped on and off at a frequency near 610 Hz (chosen so that its harmonics did not fall near the 5000 Hz FM dither frequency) and another lock-in placed after the first (JILA designed built by ERBTEC). The detection scheme then had the signal from the photodetector going through a bandpass filter at 15 kHz, and two notch filters (one at 5 kHz the other at 10 kHz.) The first lock-in demodulated the 3rd harmonic of the 5 kHz drive. This signal was then passed through a bandpass filter centered at 610 Hz and demodulated by the Stanford SR510 lock-in. The important feature of this second lock-in it that is suppresses the first order sensitivity to the 15 kHz AM from the AOM double pass modulator.

The output of this lock-in was input to a JILA designed servo loop filter. The output of the filter drove the frequency steering electronics of the composite Ti-Saph laser and locking cavity system, thus closing the frequency control loop.

References

[1]P. Jungner et al., "Stability and absolute frequency of moleculer iodine transitions near 532 nm," (San Jose California: SPIE-The Society for Optical Engineering, 1995) V 2378, 22-34.

[2]F. Nez et al., "Optical frequency determination of the hyperfine components of the 5s1/2-5D3/2 two-photon transitions in rubidium.," Optics CommunicationsJap. J. Appl. Phys. 102, (1993): 432-438.

[3]F.L. Walls and DeMarchi A., "RF spectrum of a signal after frequency multiplication. Measurement and comparison with a simple calculation.," IEEE Trans. Instrum. Meas. IM-24, (1975): 210-217.

Chapter VII: EXPERIMENTAL CONCLUSIONS

Introduction

Measurements made of the frequencies of the Rb/D_2 transitions fall into two classes. First are the frequency measurements made by determining the frequency difference between the two-photon transition and the D_2 lines. These are intended to refine our knowledge of the D_2 line and thus reduce its dominant contribution to the uncertainty of the R(56)32-0 I_2 measurement.

The second class of measurements involves measuring the frequency splittings and environmental sensitivities of the hyperfine components of the Rb/D_2 transition. These measurements were accomplished with our FM and 3F spectrometers. It is possible to obtain these measurements using the two-photon spectrometer, but, the added problems associated with detecting and counting the 1 THz beatnote would only make their interpretation more difficult.

There is a minor philosophical point that should be clarified before the data on the frequency differences is presented. It is clear that the actual quantity which was measured in some experiments is the frequency difference between the ^{85}Rb $5S_{1/2}$-$5D_{3/2}$ two-photon transition and the ^{87}Rb/D_2 transition. What is not obvious is whether this represents only a frequency difference measurement or whether it is an absolute frequency measurement for the ^{87}Rb/D_2 transition. The point may seem

trifling, but consider the Allan variances of the difference beat signal as measured. In one case it should be normalized by 1 THz in the other case 385 THz. For the purpose of this thesis we will adopt the standard that all frequency difference measurements are absolute frequency measurements. This is because a great deal of the frequency stability data available is normalized in this way and thus it will be easier to compare this data with published material.

The alert reader will also note that most of absolute and frequency difference measurements discussed involve the ^{87}Rb D/F crossover or the ^{87}Rb E line. The heavy emphasis on the D/F line comes from the fact that this was used as the NPL reference line in their absolute frequency measurement. The E line was chosen because it has a different ground state (F=1 instead of F=2, see figure 4-3) then the D/F line. This allows for the possible study of ground state dependent effects.

The E line is also important because it allows for a check of the accuracy of the two spectrometer system. The is done by comparing the splitting between the E and D lines which share the F=2 upper state. This make their frequency difference equal to the ground state splitting, which is the well known microwave clock transition at 6834.682 614 (1) MHz [1].

Improved Rb/D_2 Stability Measurements

In figure 7-1 is an example of the beat signal between our 3F and FM spectrometer before and after modifications. Theses included addition of two layers of magnetic shielding and a more sophisticated modulation and detection scheme to suppress sensitivity to AM in the spectrometer. Notice that the "before" signal has a 2.1 Hz/s drift. Also notice the Allan variance for this signal shows that it is approximately

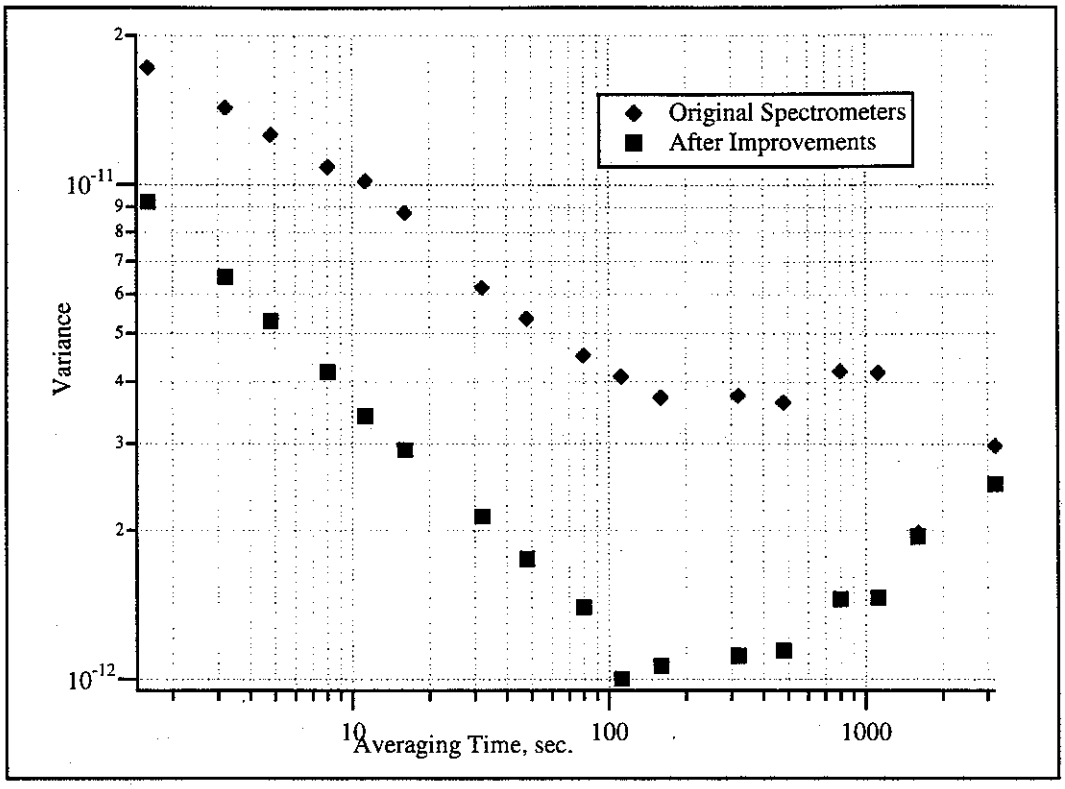

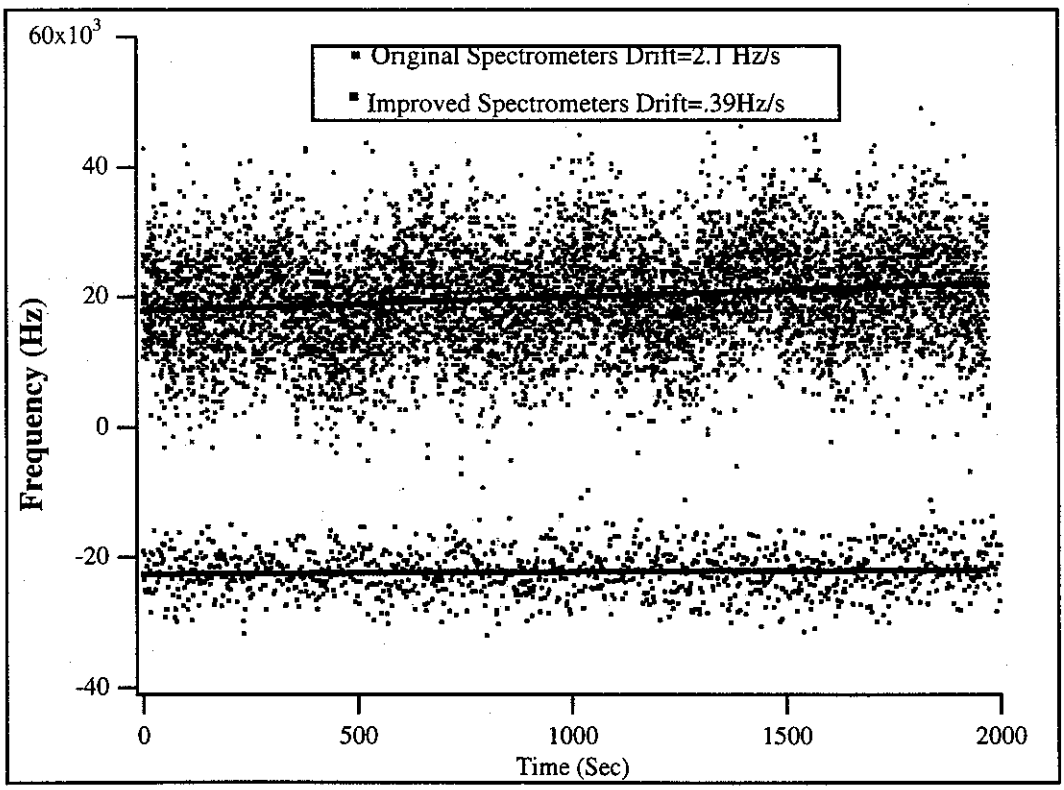

Figure 7-1 Beatnote and Allan Variance Between FM and 3F Spectrometers

An arbitrary offset has been added to both data records in 7-1b for plotting purposes

the same magnitude as the composite I_2 measurement. This leads to the conclusion that the stability of the Rb/D_2 spectrometer was the limiting factor in the long term stability of the I_2 line[a].

While both spectrometers were configured for locking to the Rb/D_2 transitions, the relative splittings between different lines of the D_2 F=2->F=3 hyperfine group were measured. This was done by simply locking one spectrometer to a reference line while the other was locked alternately to the members of the hyperfine series. This was done with both the FM and the 3F spectrometers. A comparison with the published values for those splittings was then done. The results are summarized in figure 7-2.

A surprising feature of comparing this measurement to the measured splittings of Barwood,Gill, and Rowley[2] is that all the splittings differ by approximately 100 kHz! This seems quite large considering that the both experiments place the absolute frequency of the d/f crossover to within 10 kHz of each other. The "a,c,e" lines of Barwood et al. have splittings about 100 kHz larger then measured in our lab while the "d" and "b" lines have splittings that are 100 kHz smaller then our measurement. A self consistent picture of this is possible, but, it is only conjecture. It requires Barwood et al to have one "good" (agreeing with our's) Rb cell/spectrometer combination which was used for the absolute frequency measurement of the d/f crossover. It also supposes that they used another Rb cell/spectrometer combination which was systematically shifted 100 kHz to the **blue** which was used when making the measurements of the line splittings. This combination results in our measurement of the absolute frequency

a. The record for the "improved" signal is over 8000 s long only the first 2000s are shown for brevity.

Measured Splitting between 3rd Harmonic Detection and FM Sideband Spectrometers

(all splittings in MHz)

3f \ FM	e	c	a	f	d/f	d	b
e					-6701.370 ±0.003		
c					-6544.428 ±0.004		
a					-6472.210 ±0.003		
f							
d/f	6701.363 ±0.003				-0.001 ±0.003	-133.280 ±0.004*	-290.268 ±0.006
d					133.320 ±0.004	0.039 ±0.007**	
b					290.268 ±0.008		

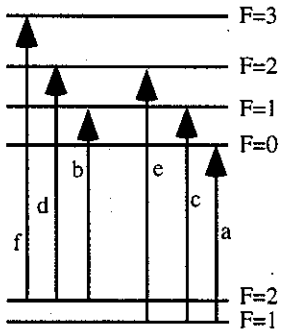

*Corrected for 60 kHz "pulling" effect of nearby lines
Both (e-d) and (c-b) give the ground state splitting
Optically measured value 6834.691±0.004 MHz
μ–wave measured value 6834.683 MHz

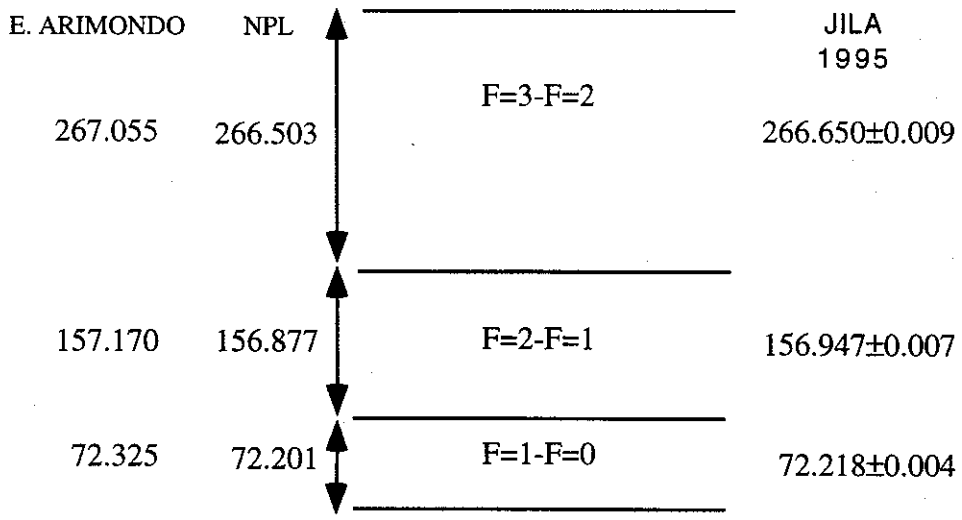

Figure 7-2 Measured Frequency Splittings

of the d/f crossover being in good agreement with theirs. It also results in all their measured splittings to transitions with energies higher then the d/f crossover being too large and all the frequency splittings to transitions with energy levels below d/f being too small. A similar but conjugate explanation would also have the "good" spectrometer cell being used for the absolute frequency measurement, thus still producing agreement with the JILA experiment. Then the "bad" spectrometer which is in this case is shifted **red** by 100 kHz would be locked to the d/f crossover and the "good" spectrometer locked to separate lines to make the splitting measurements. This scenario has the advantage that what would be expected from cell contamination is frequency shiting to the red. Using the figure of -6.2 MHz/Torr for N_2 (taken only as an example) obtained by Tetu[3] we see that 16 millitorr of N_2 would be needed to cause this size of shift. Barwood states that the NPL cells showed a linewidth of ten MHz after accounting for laser jitter, modulation, and power broadening. This is much wider then the accepted value of ≈6 MHz as the width of the Rb/D_2 lines and adds credence to the possibility that the discrepancies between the NPL measurement and the JILA measurement are due to cell contamination at NPL.

Based on the measured frequency splittings, the strength of the hyperfine interaction energy for the magnetic dipole and the electronic quadrupole were calculated, and the values A=84.7185±0.002 MHz and B=12.4965±.0037 MHz. The A and B coefficients are defined as in Arimondo et al.[1] as:

$$W_f = \frac{1}{2}hAK + hB\frac{\frac{3}{2}K(K+1) - 2I(I+1)J(J+1)}{2I(2I-1)2J(2J-1)}$$

Where: $K = F(F+1) - I(I+1) - J(J+1)$

These results are compared with other measurements of these constants and summarized in figure 7-3.

As discussed already the measurement of the frequency difference between the Rb/D_2 hyperfine group and the $5S_{1/2}$-$5D_{3/2}$ two-photon line was restricted to a small subset of the possible combinations. The d/f crossover and the e lines were the only members of the D_2 hyperfine group to be investigated. In the two-photon transition only the $5S_{1/2}$-$5D_{3/2}$ F_g=2-F_e=4 component at 385 242 216 362.9(5) kHz [4] was used as a reference. It is the strongest of the hyperfine group in which it lies, and is sufficiently isolated to make a good frequency reference. Also mentioned previously was that the 6834 MHz difference in down conversion frequency between the d/f and the e line leads to a significantly different signal to noise in the beatnote of the two signals.

Particularly interesting was the extreme variability of the d/f crossover signal. Figures 7-4 and 7-5 show the beatnote for this splitting and a histogram of the data accumulated from a period of several weeks. Much of the data has a signature of drifting between two limits. This is especially evident for the Sept. 18 data set. It is worth noting that over time, as more sophisticated signal processing techniques were employed, the center of mass of the histograms shifts $\approx$ 25 kHz toward lower frequencies.

No certain cause for the irregularity in the data was ever determined. Drift in the Rb/D_2 spectrometer were eliminated as a possibility because the beats between the two D_2 spectrometers never show this characteristic bi-stable irregularity.

In an informal test, a beat signal with frequency noise similar in characteristics to the Rb/D_2- two-photon signal was synthesized. Noise was then added to it and

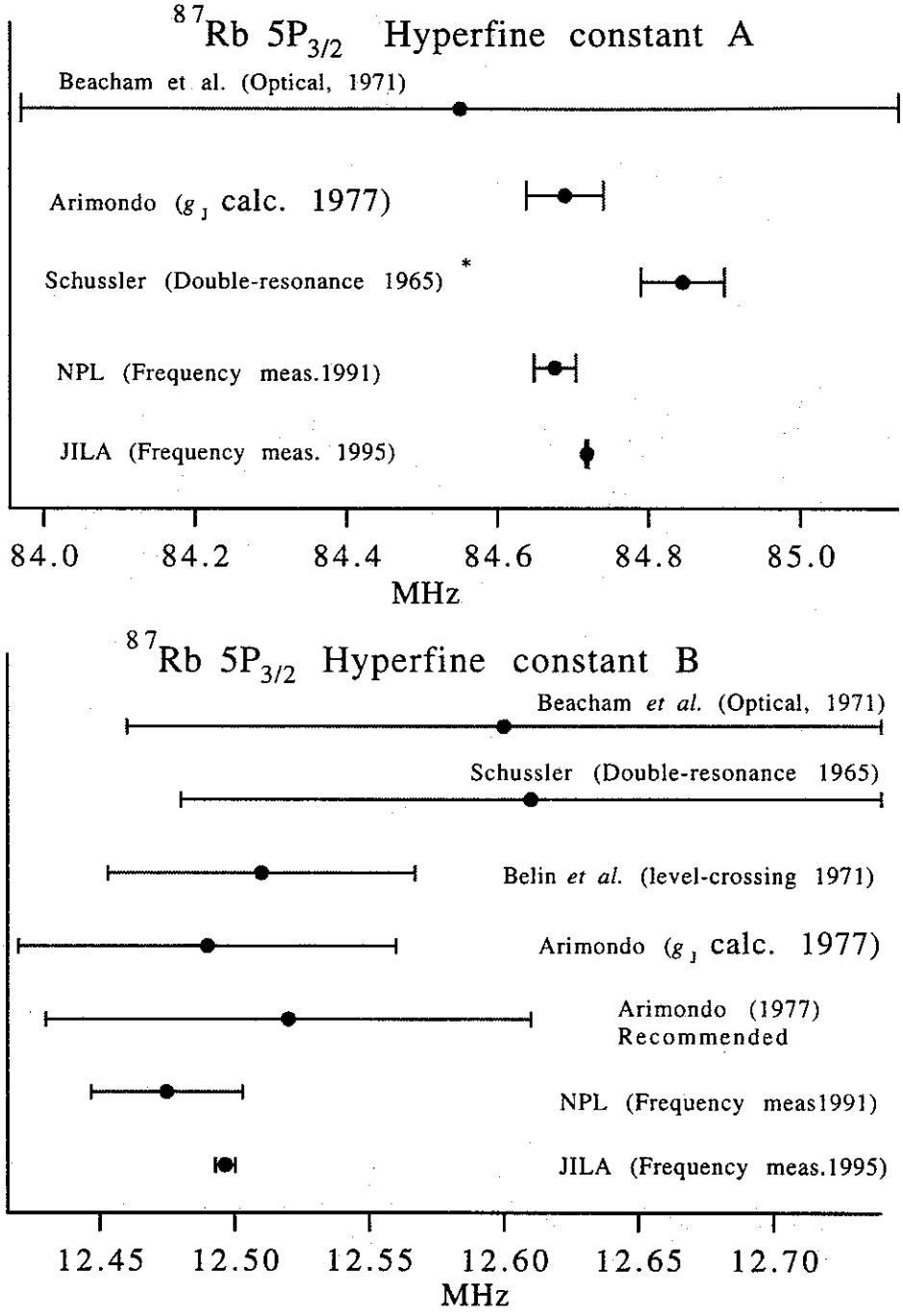

Figure 7-3 Summary of A and B Coefficients for ^{87}Rb D_2 F=2->F=3

Rb 2-photon @ 778 nm vs.
Rb D_2 df-crossover @ 780 nm

Beat frequency offset by 1 014 234.4929 MHz

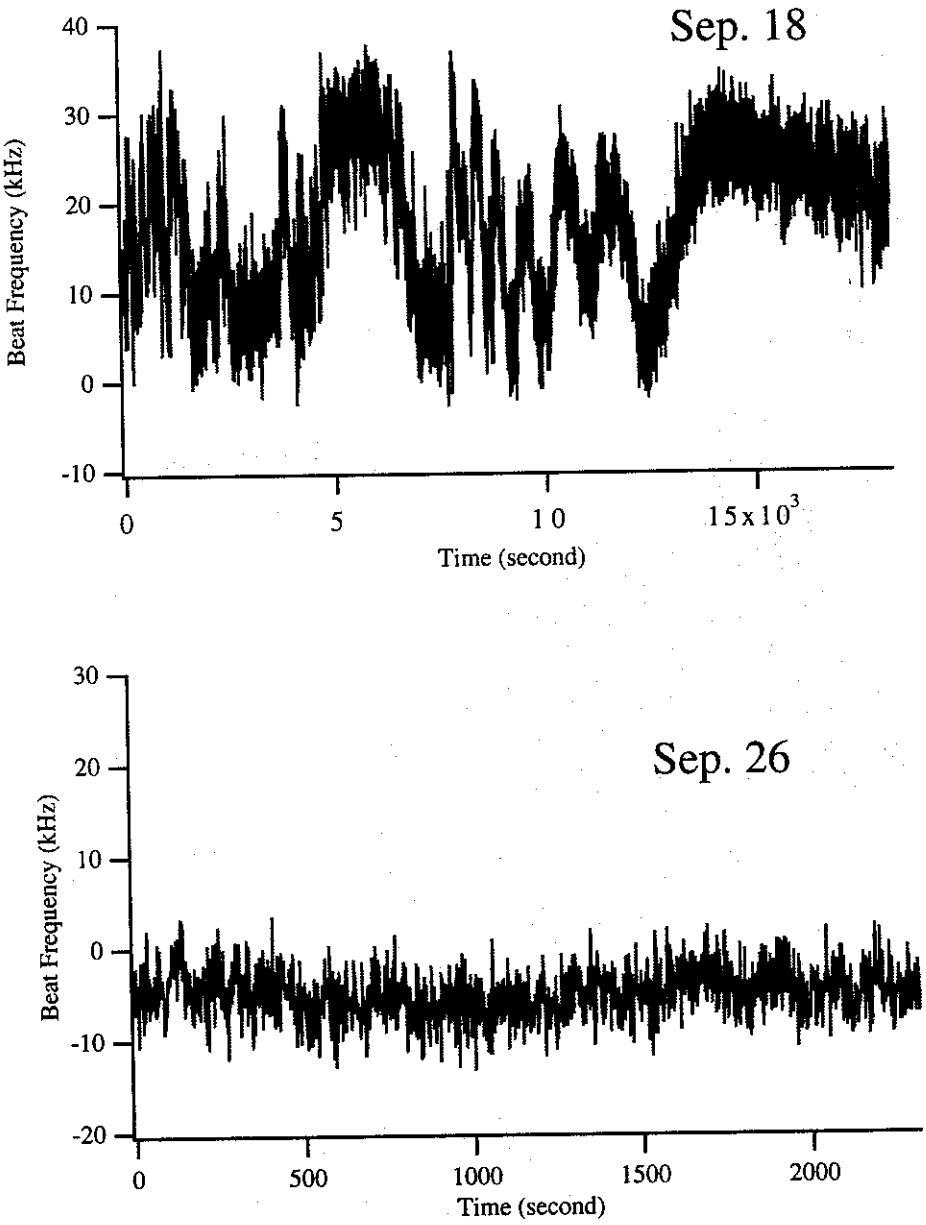

Data from two separate days of measuring d/f crossover frequency.

Note the substantial difference between the quality of data.

Figure 7-4 Beatnote showing variability of the quality of the d/f signal

Histogram of Data for Frequency Difference Measurements

of ^{87}Rb D_2 d/f Crossover

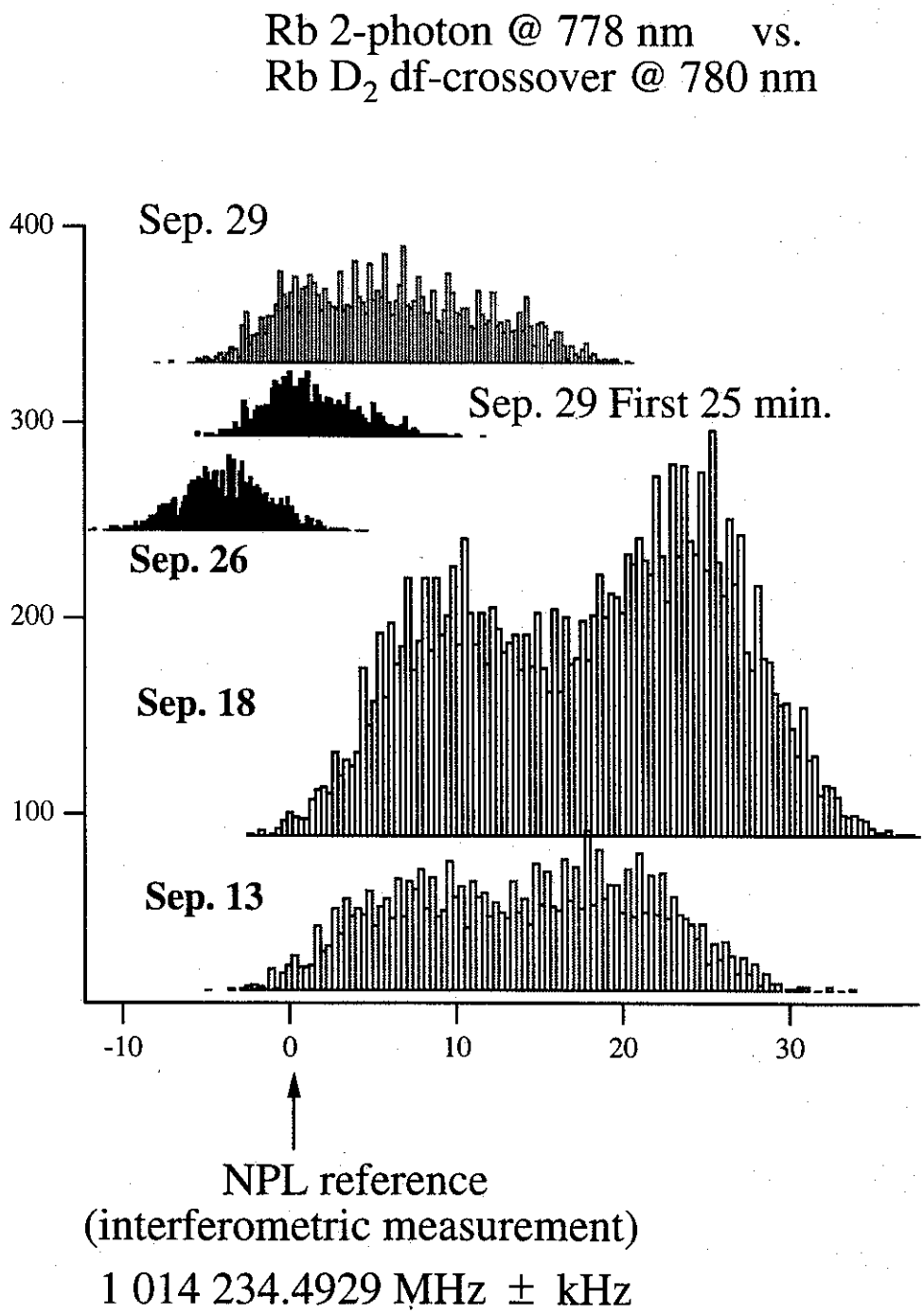

Figure 7-5 Histogram of data from d/f frequency difference measurements

the signal was then recovered and counted with our processing electronics. The accuracy of the recovered beatnote count showed a sensitivity on the ± 1 db scale to the amount of injected noise. The noise level at which counting became less reliable was nearly the same signal-to-noise that was actually observed in the experiment. This is far from conclusive proof that S/N is the sole source of the data irregularity and further experiments are planned. Taken as a whole the data show an average frequency of 13.6 kHz higher than the frequency marked as "NPL reference" and have a 9.6 kHz standard deviation. The usefulness of these numbers is minimal since the distribution is far from statistical. Most interesting in these data sets are runs like those which occurred on Sept. 26 which can be fit well with a Gaussian and show a HWHM of 3.6 kHz. This seems to hold out the promise that with some more work to isolate and eliminate the cause of the bounded drifting that the uncertainty of the ^{87}Rb D_2 d/f crossover could be reduced below the uncertainty of the HeNe I_2 reference at 633 nm.

The measurement of the ^{87}Rb D_2 e line is, in contrast, much better behaved. A similar histogram of the data indicating its conduct is shown in figure 7-6. The data for September can all be reasonably fit with Gaussian distributions having HWHM values between 9 and 6 kHz. The centers of these distributions fall between -12 and -6 kHz relative to the NPL-JILA zero frequency except for the data from September 14 which has an unexplained shift to 8 kHz. Taking the data from each day as an ensemble of 6 data points with each day's data being weighted according to the number of data points in it we find the zero of the data to be at -7.3 ± 2.3 kHz from the frequency predicted by NPL. This frequency 1014234.493 MHz is based on using the NPL value for the d/f crossover, but the JILA value of the splitting between the d/f and e lines. This is

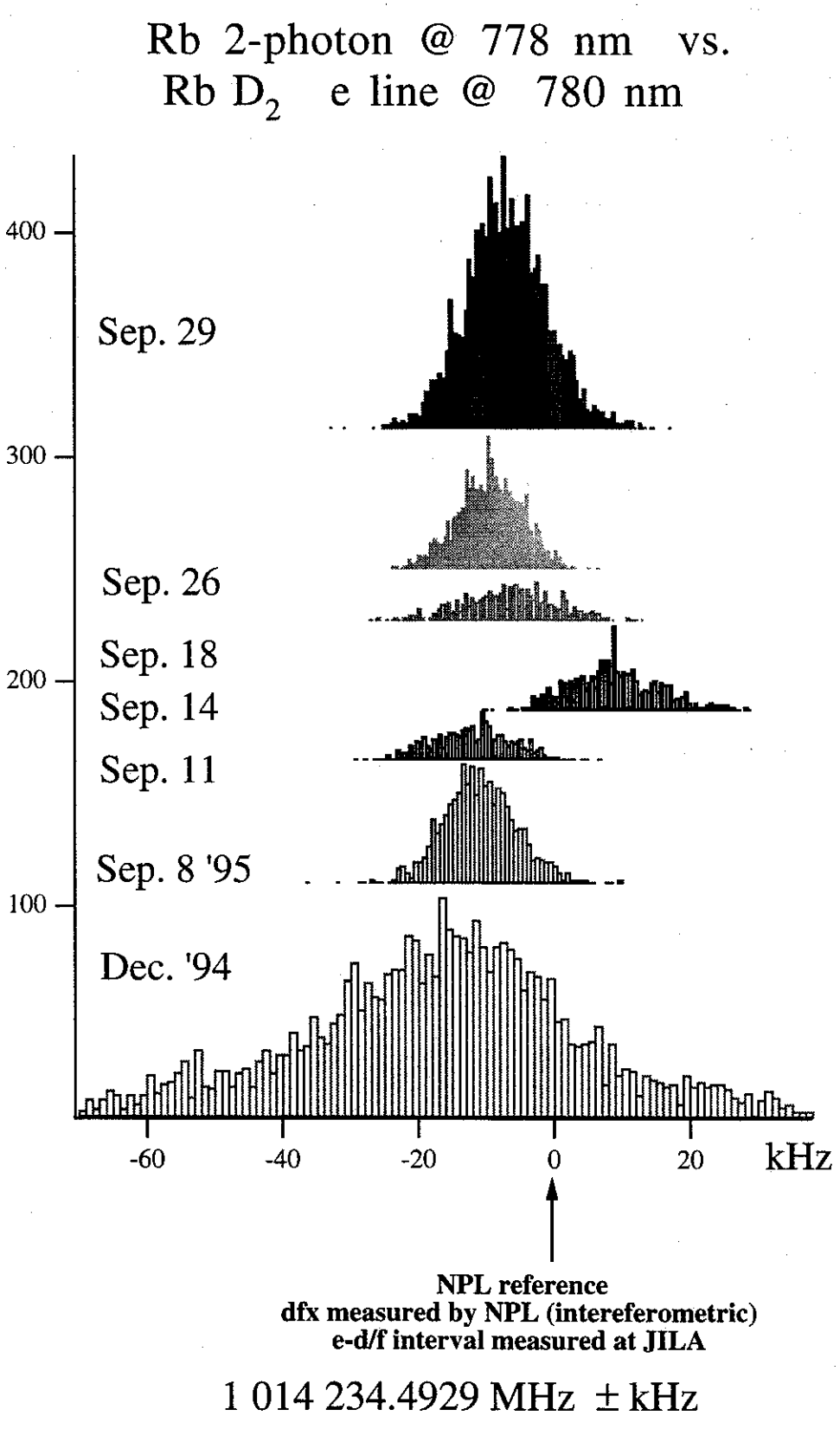

Figure 7-6 Histogram of data from e line frequency difference measurements

derived from the well known ground state splitting plus half the F=2 to F=3 splitting as measured here in JILA. The December data was not used for this average due to the large number of changes made in the spectrometers made in the intervening time period. In spite of this there is good agreement with the earlier December measurement of -15.9 kHz with a HWHM of 17.25 kHz. This consistency indicates that the technique and the Rb cell have a good "inherent" stability.

Discussion

Lineshape Detection

The alert reader will have noticed that four different methods of detection of the transition/lineshape have been used in these experiments. These are

1: FM sideband spectroscopy[5] on one of the Rb/D_2 spectrometer

2: Dither modulation with first harmonic recovery of decay fluorescence in the case of the two-photon spectrometer [6]

3: Dither modulation with third harmonic recovery for the "standard" Rb/D_2 spectrometer [6]

4: Modulation transfer spectroscopy for the I_2 spectrometer.

The use of modulation transfer spectroscopy for the I_2 spectrometer is discussed extensively in [7] and will not be covered here again. While conducting frequency comparisons between the 3F and FM Rb spectrometers it was noticed that although agreement between the spectrometers was excellent, the "d" component of the FM spectrometer appeared shifted from its expected position. It was suspected that the "wings" of nearby lines might be "pulling" it slightly (≈50 kHz or about $5*10^{-3}$ of the 10MHz linewidth of the power-broadened Rb line). To test this hypothesis the effect of nearby transitions on the "d" line was estimated using the theoretical lineshapes for FM sideband spectroscopy.

In FM sideband spectroscopy a phase modulator is used to apply sidebands to the laser beam which will probe the sample. The modulation index is chosen to be low

so the all but the first few sidebands and the carrier are negligible. The E field impinging on the sample is considered to have the form:

$$\tilde{E}_2(t) = E_0 \sin(\Omega t + m\sin\omega t) = E_0 \sum_{n=0}^{\infty} J_n(m)\sin(\Omega t + \sin n\omega t) + E_0 \sum_{n=1}^{\infty} (-1)^n J_n(m)\sin(\Omega t - \sin n\omega t) \ ,$$

where m is the modulation index, Ω is the carrier frequency of the optical field and ω is the frequency on the modulator. The sample is assumed to have a length L and a real absorption coefficient α and an index of refraction *n*. Using the notation of Hall, Hollberg , Baer and Robinson [8] it is convienient to define:

$$\Omega^* = \Omega_0 \pm \Delta/2$$

$$\omega^{\pm} = \Omega - \Omega^* \pm (\omega/2) \qquad \omega^{*} = \Omega - \Omega^* \qquad \text{Eq 7-1}$$

$$\omega^{++} = \Omega - \Omega^* + 2(\omega/2) \qquad \omega^{--} = \Omega - \Omega^* - 2(\omega/2)$$

Where Ω^* is the line center shifted by $\pm \Delta/2$ the AOM frequency as determined by whether the plus or minus order is used: The $\omega^{\pm}$ and ω^{*} are the components from the upper and lower sidebands and the carrier, and the ω^{++} and ω^{--} are from the second order upper and lower sidebands.The real absorption and dispersion are then defined as:

$$L^{\pm} \equiv \frac{\Gamma^2}{\Gamma^2 + (\omega^{\pm})^2} \qquad D^{\pm} \equiv \frac{\Gamma\omega^{\pm}}{\Gamma^2 + (\omega^{\pm})^2} \qquad \text{Eq 7-2}$$

Taking $A=\alpha_0 L$, where α is the unsaturated absorption coeffient and L is the cell length, for the in-phase case with m<1 and A<<1 (small absorption limit), the in-phase signal is:

$$\text{Sig}_{\text{in phase}} = BA\left([J_1(m)(J_0(m) + J_2(m))(L^- - L^+)] - [J_2(L^{++} - L^{--})] \right)\cos\omega t$$

$$\text{Sig}_{\text{quadrature phase}} = -CAJ_1(m)[(J_0(m) - J_2(m))(D^+ - 2D^* + D^-) + J_2(m)(D^{++} - 2D^* + D^{--})]\sin\omega t \qquad \text{Eq 7-3}$$

For our typical experiments m was set to m=.85 and ω fixed at $\omega=2\pi*3.75$

MHz. A measurement of the absorption at the center of the Doppler curve showed it to be less then 0.1%. Thus it is expected that the experiment meets the appropriate criterion for this formalism.The saturation parameter was estimated as being ≈ 1, so the coefficients B and C were treated as approximately equal. Example data from the FM spectrometer was fitted with equation 7-3 and a detection phase of approximately 22° was recovered. Using the example data, the relative strengths of the transitions in the hyperfine group were obtained. Using these strengths and the "known" splittings of lines the sum of the values of all the lines at the location of the "d" line was calculated. This is then divided by the slope of the "d" line to obtain the apparent shift. In our case this was -60 kHz. Both the sign and the magnitude of the shift are dependent on accurate knowledge of the detection phase. A graph of the shift verse detection phase is shown in figure 7-7. As a check, the same calculation was done for the "b" line which showed 5 kHz of shift, a relatively small value.

For dither modulation with first harmonic recovery used in the two-photon spectrometer, the line profile recovered owes its name to Wahlquist[5]. The line shape is derived by the Fourier integration of the expected Lorentzian

$$\lambda(\omega, h_\omega, h_d, h_m) = \int_{-\pi/\tau}^{\pi/\tau} \frac{\left(\frac{h_d}{2}\right)^2 \cos\omega\tau}{\left(\frac{h_d}{2}\right)^2 + (h_\omega + h_m \cos\omega\tau)^2} d\tau$$

While Wahlquist gives a solution to this integral it is interesting to find another one. First the integration is changed from over $\cos\omega\tau$ to over $\sin\omega\tau$ and then the half width removed from the integrand

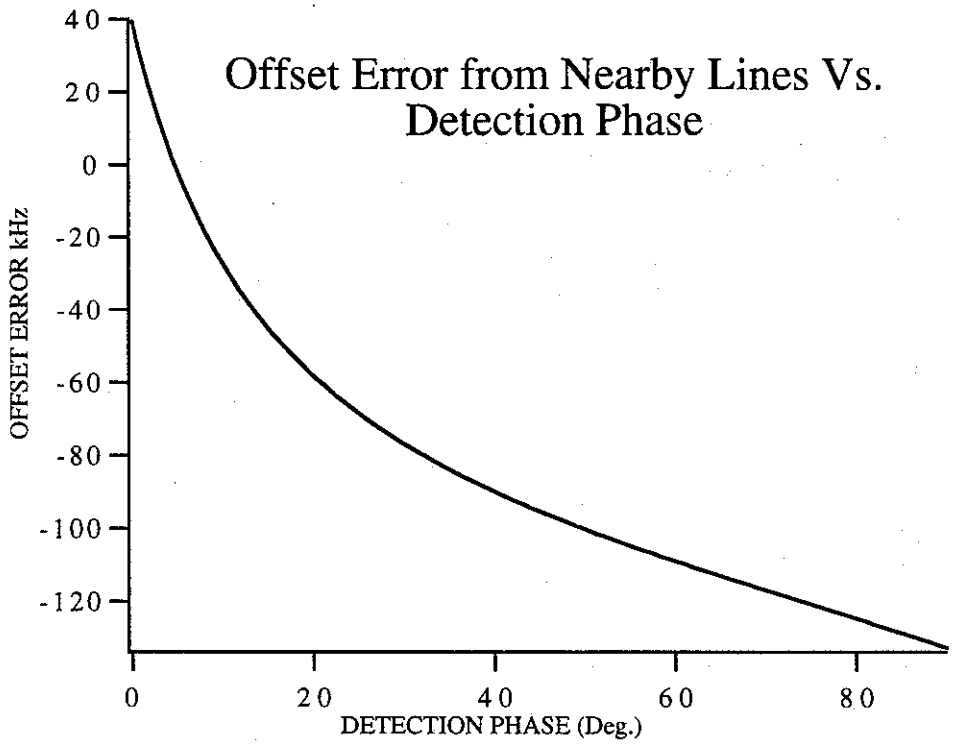

Figure 7-7 Offset Error verses Detection Phase for "d" Line

$$\lambda(\omega, h_\omega, h_d, h_m) = \int_0^{2\pi} \frac{\sin\omega\tau}{1+\left(\frac{h_\omega + h_m(\sin\omega\tau)}{h_d/2}\right)^2} d\tau = \int_0^{2\pi} \frac{\sin\omega\tau}{1+(\alpha+\beta(\sin\omega\tau))^2} d\tau \qquad \text{Eq 7-4}$$

where α and β are obviously equal to $2h_\omega/h_d$ and $2h_m/h_d$. Mathematica offers the solution:

$$-4\pi i \cdot \frac{\sqrt{\frac{(\alpha-i)^2}{(\alpha-i)^2-\beta^2}} - \sqrt{\frac{(\alpha+i)^2}{(\alpha+i)^2-\beta^2}}}{\beta} \qquad \text{Eq 7-5}$$

Noting that this has the form $C-C^*=2\mathrm{Im}(C)$, we get

$$-4\pi i \cdot \frac{\sqrt{\frac{(\alpha-i)^2}{(\alpha-i)^2-\beta^2}} - \sqrt{\frac{(\alpha+i)^2}{(\alpha+i)^2-\beta^2}}}{\beta} = -8\pi \frac{\mathrm{Im}\left[\sqrt{\frac{(\alpha-i)^2}{(\alpha-i)^2-\beta^2}}\right]}{\beta}$$

The method of detection by 3rd harmonic leads naturally to the integral

$$\lambda_3(\omega, h_\omega, h_d, h_m) = \left(\frac{2}{h_d}\right)^2 \int_0^{2\pi} \frac{\sin 3\omega\tau}{1+(\alpha+\beta(\sin\omega\tau))^2} d\tau \qquad \text{Eq 7-6}$$

Which by same method yields:

$$\left(\frac{-4}{\beta^2} - \pi i \frac{\sqrt{\frac{(\alpha+i)^2}{(\alpha+i)^2-\beta^2}} \cdot (4 - 8i\alpha - 4\alpha^2 + 3\beta^2)}{\beta^3} + \pi i \frac{\sqrt{\frac{(\alpha-i)^2}{(\alpha-i)^2-\beta^2}} \cdot (4 + 8i\alpha - 4\alpha^2 + 3\beta^2)}{\beta^3} + \frac{4(\beta+4\alpha\pi)}{\beta^3} \right)$$

Which can be simplified:

$$\left(\frac{-4}{\beta^2} + \frac{4(\beta+4\alpha\pi)}{\beta^3} - \pi i \frac{\sqrt{\frac{(\alpha+i)^2}{(\alpha+i)^2-\beta^2}} \cdot ((2-2i\alpha)^2 + 3\beta^2)}{\beta^3} + \pi i \frac{\sqrt{\frac{(\alpha-i)^2}{(\alpha-i)^2-\beta^2}} \cdot ((2+2i\alpha)^2 + 3\beta^2)}{\beta^3} \right)$$

As before:

$$\mathrm{Wal}_3(\alpha, \beta) = \frac{4(4\alpha\pi)}{\beta^3} + 2\pi \mathrm{Re}\left(\frac{\sqrt{\frac{(\alpha-i)^2}{(\alpha-i)^2-\beta^2}} \cdot ((2+2i\alpha)^2 + 3\beta^2)}{\beta^3}\right) \qquad \text{Eq 7-7}$$

These three functions are compared in figure 7-8 for conditions similar to what

is used in our experiments. As can be see the 3rd harmonic detection has the least "bleed-over" into nearby lines

Temperature Effects

During the course of these experiments there was no attempt to control the temperature of the Rb cells. This stands in stark contrast to I_2 cells in both the 633 nm HeNe laser and the 532 nm I_2 spectrometer which where controlled by active servos. The reason for this can be seen in figure 7-9 which shows the pressure vs temperture curve and its derivitive for Rb.As can be seen at room temperature dp/dT is of order 10^{-8} torr/K. Taking the usual figure off 10 MHz/torr pressure/frequency change it can be seen that the likely shift of .1 Hz/K is unimportant on the scale of the few degrees change in room temperature.

is used in our experiments. As can be see the 3rd harmonic detection has the least "bleed-over" into nearby lines

Temperature Effects

During the course of these experiments there was no attempt to control the temperature of the Rb cells. This stands in stark contrast to I_2 cells in both the 633 nm HeNe laser and the 532 nm I_2 spectrometer which where controlled by active servos. The reason for this can be seen in figure 7-9 which shows the pressure vs temperture curve and its derivitive for Rb.As can be seen at room temperature dp/dT is of order 10^{-8} torr/K. Taking the usual figure off 10 MHz/torr pressure/frequency change it can be seen that the likely shift of .1 Hz/K is unimportant on the scale of the few degrees change in room temperature.

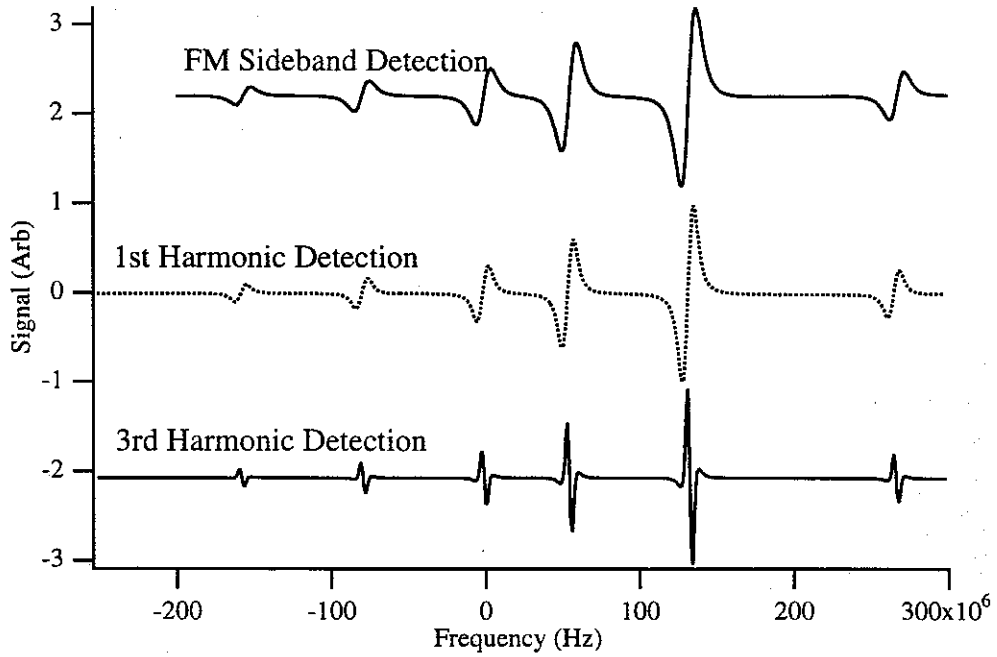

Figure 7-8 FM, 1st Harmonic and 3rd Harmonic detection for comparison

Synthesized data for comparison of FM, 1st Harmonic and 3rd Harmonic detection method. Signal amplitudes are all arbitrarily set to max signal equals one.

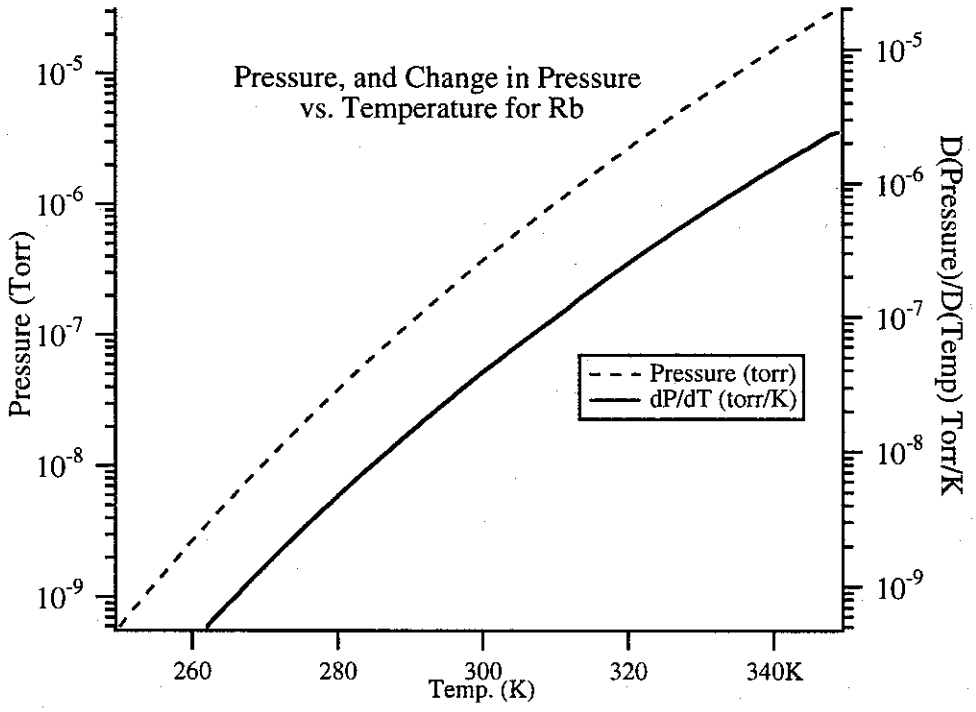

Figure 7-9 Pressure and dP/dT for Rb

Concluding Remarks

In this thesis it has been detailed how the frequency of the a_{10} I_2 hyperfine line in the transition R(56)32-0 of the Iodine molecule was measured. The measurement was referenced to the working standard for the Rb/D_2 d/f crossover line as measured at the National Physical Laboratories(NPL) and the CCDM standard for the absolute frequency of the $HeNe/I_2$ laser at 633nm. The measured frequency of the a_{10} component was determined to be 563,260,223.471 MHz ± 40 kHz. This provides a secondary frequency standard within the tuning range of a doubled Nd:YAG laser. Excellent stability for two independent spectrometers locked on this line have been observed ($<10^{-13}$ for $\tau>1$s).

The the largest source of uncertainty in this measurement was the uncertainty of the Rb/D_2 d/f line. In order to improve the measurement of the absolute frequency of the $Nd:YAG/I_2$ line, the accuracy of the measurement of the Rb/D_2 d/f frequency needed to be improved. This was accomplished in two steps. First a two-photon Rb spectrometer was built, and frequency difference measurements were made between the ^{85}Rb $5S_{1/2}$-$5D_{3/2}$ two photon line and the Rb/D_2 transitions. Next improvements were made to our 3F Rb/D_2 reference spectrometer. Although the difference frequency was large (≈1.014 THz) the overall reduction in the uncertainty of the absolute frequency of the Rb/D_2 transition was from ±60 kHz to ±2.3 kHz and the reproducibility from ±25 kHz to ±8 kHz (the size of the largest shift in the

two-photon to "e" line measurement). This demonstrates the possibility that the uncertainty in the a_{10} Nd:YAG/I_2 could be reduced to ±13 kHz with the majority of the error then coming from the frequency doubled HeNe/I_2 laser at 633nm. This should come as no surprise since its linewidth is about the same as the Rb/D_2 transitions and it is considered to be a "weak" transition due to predissociation.

An unfortunate side effect of the modifications to the 3F spectrometer is that the new frequency assignment for the Rb/D_2 d/f crossover cannot be directly transferred to the Nd:YAG/I_2 measurement. To honestly use the newer frequency and uncertainty values, the entire frequency chain will have to be reactivated and absolute frequency of the a_{10} R(56)32-0 transition re-evaluated. Given this, one has to ask if this is still the best available strategy. Since the Nd:YAG/I_2 laser has shown the possibility of having kilohertz level reproducibility it seems to beg to have its frequency measured to better than the 13 kHz proposed. Another reality of modern laboratory life is that before (re)-starting an experiment which requires two ion argon pump lasers it is best to check all possible alternatives.

It requires no use of imagination to simply replace both Ti-Sapphire lasers with external cavity diode lasers and repeat the experiment using the existing topology. Diode lasers are low enough in cost that, if needed, extra ones can be used in frequency bridges. They can also be used as frequency power-regenerators by either phase-lock as described early or optical injection locking. As stated earlier a duplication of the existing frequency chain would likely lead to a measurement uncertainty of ≈13 kHz.

Examining figure 4-1, the predicted uncertainty of the frequency chain based on:

$$2*\text{HeNe@633nm}+1.2\text{THz} \approx \text{Nd:YAG}/I_2+^{85}\text{Rb Two-photon}$$

is about ±13kHz so there does not seem to be any immediate reason to use it other then it would require only a small change in the existing frequency chain.

This may not be the case for long. As mentioned previously, the repeatability for the diode laser pumped ^{85}Rb two-photon transition is already at the ±2kHz level. Another factor which is just over the horizon is the possibility of a significantly better $633/I_2$ reference. As discussed in the section on the Iodine stabilized laser, the transition used for the existing $HeNe/I_2$ laser is broadened by its proximity to an unbound state at the bottom of the excited state potential well. It is also weakly populated due to the fact it originates in the fifth vibrational band. Just one gigahertz away from this transition lies the P(33)6-3 transition which is better with regards to these problems. In the past it would have been considered as unusable as a frequency standard because no simple[a] lasing system could approach it. Now, red diode lasers which are tunable over several nanometers, and can be frequency narrowed by methods already described, will make access to this and many other nearby I_2 lines possible. If they have similar strengths and linewidths as the R(56)32-0 "green" transition it is quite possible that similar frequency repeatabilities and stabilities will be achievable. Thus in the not too distant future this chain may be capable of ±3-4 kHz accuracy.

---

a. The dye laser can, of course, easily tune to this wavelength.

Another frequency chain which is an excellent candidate for further research is based on the relation:

$$\text{Nd:YAG/I}_2 \approx \text{HeNe/I}_2@633\text{nm} + \text{HeNe/I}_2@3.39\mu\text{m} + 1.27\ \text{THz}$$

When previously considered, this chain was considered impossible to execute. This was because there was no way to measure or make up the 1.27 THz gap. Now, a pair of new technologies make this possible. One is the tunable red laser diode as discussed earlier. To build the frequency chain the red diode will be tuned 1.27 THz blue of the 633nm HeNe/I_2 standard and frequency summed in a nonlinear crystal with radiation from a HeNe/I_2@3.39μm laser. The resulting green light will then be heterodyned against the Nd:YAG/I_2 light to obtain its exact frequency.

Considering that our obtainable signal-to-noise ratio at a difference frequency of 1.014 THz was marginal, it is legitimate to ask how to measure a frequency difference of 1.27 THz. For this we rely on the second piece of new technology, the optical comb frequency generator [8]. This novel device works by placing a traveling wave electro-optic-modulator inside a resonant cavity which is pumped with laser light. The cavity resonance is chosen so that the optical sidebands generated in the EOM are also resonant. The laser carrier and the sidebands bounce back and forth over and over, generating addition sidebands with each pass. Soon a comb of sidebands is present, all with a precisely known frequency shifts from their neighbors. Combs over 1 THz wide have already been generated [9] and the dispersion limited range of the optical comb generator has been estimated at 16 nm in the region of 780 nm[10]. Large optical frequency differences can be measured by simply heterodyning the unknown lasers with components of the comb.

The expected uncertainty for this frequency chain is dominated by the 633nm HeNe/I_2 standard which is currently ≈ 7 kHz. The same comments regarding the possible improvement available from the P(33)6-3 I_2 transition apply to this frequency chain as well.

The last of the frequency chains considered is based on the relation:

Nd:YAG/I_2 ≈ ^{85}Rb Two-photon+2*HeNe@3.39μm+1.22THz

This frequency chain's main advantage is that it will achieve an uncertainty of approximately ±5kHz based on **current** measurements. Also, as the uncertainty in the ^{85}Rb two-photon transition frequency is reduced, this frequency chains uncertainty will follow to below 1kHz. The disadvantage is that HeNe@3.39μm source does not generate much power and is at a frequency where their are no convenient higher power lasers to lock to it.

One realization of this chain could be made by first using an optical comb frequency generator to lock an ECLD 1.22 THz above the ^{85}Rb two-photon transition. The output of this diode could then be frequency summed with the 3.39μm radiation from the HeNe/I_2 laser. This generates an output frequency which falls in the region can be reached by red laser diodes. One of these diodes could use phase-lock techniques to regenerate the sum frequency at higher power. The output of this diode would then be frequency summed with the 3.39μm radiation again to yield "green" light that could then compared to the Nd:YAG/I_2.

As can be seen, there are any number of alternatives for re-measuring the frequency of the a_{10} R(56)32-0 transition. Some are "sure things" others are "long shots," but none of them require the continued use of a Ti-Sapphire laser, thus potentially lowering their cost substantially. No matter what choice (of frequency chain) is eventually made, it is clear that the recently developed technology of frequency controlled laser diodes and optical comb frequency generator will play a key role.

References

[1]E. Arimondo, M. Inguscio, and P. Violino, "Experimantal determinations of the hyperfine structure in the aklali atoms," Rev. Mod. Phys. 49, No 1 January (1977).

[2]G.B. Barwood, P. Gill, and W.R.C Rowley, "Frequency Measuremnets on Opticaly Narrowed Rb-Stabilized Laser Diodes at 780 nm and 795nm," Appl. Phys. B 53, (1991): 142-147.

[3]M. et al. Tetu, "Multiwavelength Sources Using Laser Diodes Frequency-Locked to Atomic Resonances," IEEE J. Lightwave Technol. 7, (1989): 1540-1548.

[4]F. Nez et al., "Optical frequency determination of the hyperfine components of the 5s1/2-5D3/2 two-photon transitions in rubidium.," Optics CommunicationsJap. J. Appl. Phys. 102, (1993): 432-438.

[5]G.C. Bjorklund et al., "Frequency Modulation (FM) Spectroscopy: Theory of Line-shapes and Signal-to-Noise Analysis," Appl. Phys. B 32, (1983): 145-152.

[6]Hugo Wahlquist, "Modulation Broadening of Unsaturated Lorentzian Lines," The J. of Chem. Phys 35, 5 (1961): 1708-1710.

[7]M.L. Eickhoff, "Two New Methods for Real-Time Precision Refractometery and Precise Test of the Hyperfine Hamiltonian via Modulation Spectroscopy of Moleculer Iodine at 532 nm" (Phd Thesis, University of Colorado, 1994).

[8]J.L. Hall et al., "Optical heterodyne saturation spectroscopy," Appl. Phys. Lett. 39, 9 (1981): 680-682.

[9]M. Kourogi, K. Nakagawa, and M. Ohtsu, "Wide span optical frequency comb generator for accurate optical frequency difference measurement," IEEE J. of Quant. Electr. 29, 10 (1993): 2693-2701.

[10]M. Kourogi et al., "Limit of Optical-Frequency Comb Generation Due to Material Dispersion," IEEE J. of Quant. Electr. 31, Dec. (1995): 2120-2126.

BIBLIOGRAPHY

Joan Lisa Bromberg, "The Birth of the Laser," Physics Today , October (1988): 26-33.

W.E. Lamb,"Theory of an Optical Maser," Phys. Rev. 134, (1964): 1429.

John L. Hall, "Frequency Stabilized Lasers - A Parochial Review," in Frequency-Stabilized Laser and Their Applications, ed. M. Ohtsu, Leo Hollberg, and Chung (Boston: SPIE, 1992), Vol 1837, 2-15.

W.R. Jr. Bennett and J.W. Jr Knutson, Pro. of the IEEE 52, (1964): 861.

P.H. Lee and M.L. Skolnick, "Satuarated Neon Absorbtion Inside a 6328 A Laser," Appl. Phys. Lett. 10, (1967): 303-305.

V.N. Lisityn and V.P. Chebotayev, ZH. Eksper. Teor. Fiz. 54, (1968): 419.

J.L. Hall, "P-1 The Absolute Wavelength Standard Problem," IEEE J. of Quant. Electr. 4, 10 (1968): 638-631.

R.L. Barger and J.H. Hall, "Pressure Shift and Broadening of Methane Line at 3.39 micron Studied by Laser Saturated Absorbtion," Phys. Rev. Lett. 22, (1969): 4-8.

S.N Bagaev et al., IEEE J. of Quant. Electr. 4, (1968): 868.

Yu G. Rastorguev and A.N. Titov, "Increase in Frequency Stability and Reproducability of HeNe Standard using E component of Methane.," Sov. J. Quantum Electron. 21, (1991): 348-351.

G.R. Hanes and C.E. Dahlstorm, "Iodine Hyperfine Structure Observer in Saturated Absorption at 633 nm," Appl. Phys. Lett. 14, (1969): 362-364.

R.L. Byer and et al, "Optical Pumped Moleculer Iodine Vapor Phase Laser," Appl. Phys. Lett. 20, (1972): 463-466.

R.W.P. Drever et al., "Laser phase and frequency stabilization using an optical resonator," Appl. Phys. B B31, (1983): 97-105.

J. Hough et al., "Dye- Laser Frequency Stabilization Using Optical Resonators," App. Phys. B 33, (1984): 179-185.Zhu Miao and John L. Hall, "Stabilization of Optical phase/frequency of a laser system: application to a commercial dye laser laser with an external stabilizer.," JOSA B 10, May (1993): 802-816.

T. Day, E.K. Gustafson, and R.L. Byer, "Active frequency stabilization of a 1.062 mm Nd:GGG, diode-laser-pumped nonplaner ring oscillator to less than 3 Hz linewidth," Opt. Lett. 15, 4 (1990): 221-223.

Moler, K. Weis, D. Kasevich, M., Chu, S, "Theoretical analysis of velocity-selective Raman transistions," Phys.Rev. A 45, 1 (1992): 342-348

R.C. Steele, "Optical Phase-Locked Loop Using Semiconductor Laser Diodes," Electron. Lett. 19, 2 (1983).

B. Dahmani, L. Hollberg, and R. Drullinger, "Frequency Stabilization of Semiconductor Lasers by Resonant Optical Feedback," P-Opr. Lett. , (1987).

P. H. Laurent, A. Clairon, and CH. Breant, "Frequency Noise Analysis of Optically Self-Locked Diode Lasers," IEEE J. of Quant. Electr. 25, June (1989): 1131-1142.

Carl E. Weiman and Leo Hollberg, "Using diode lasers for atomic physics," Rev. Sci. Instrum. 62, January (1991): 1-19.

J.L. Hall, Ma Long-Sheng, and G. Kramer, "Principles of Optical Phase-Locking: Application to Internal Mirror He-Ne Lasers Phase-Locked via Fast Control of Discharge Current.," IEEE J. of Quant. Electr. QE-23, 427-437 (1987).

John L. Hall and Zhu Miao, "An Introduction to Phase-Stable Optical Sources.," in Proceedings of the International School of Physics 'Enrico Fermi', ed. E. Arimondo, W.D. Philips, and F. Strumia (North Holland, 1992), 671-701.

D.S. Elliot and S.J. Smith, "Experimantal Synthsis of phase-diffusing optical fields," JOSA B 5, Sept (1988): 1927-1939.

Michael Philip Winters, "Correlated Spontaneous Emission in Zeeman Laser and High Resolution Optical Spectroscopy" (PH.d, University of Colorado, 1990).

Gardner Floyd M., Phaselock Techniques , 2nd ed. (New York:John Wiley & Sons,1979).

Ronald N. Bracewell, The Fourier Transform and Its Applications, 2nd ed. (New York: McGraw-Hill Book Company, 1986).

M.W. Flemming and A. Mooradian, "Fundamental line broadening of single-mode (GaAs)As diode lasers," Appl. Phys. Lett. 38, (1981): 511.

Charles H. Henry, "Theory of the Linewidth of Semiconductor Lasers," IEEE J. of Quant. Electr. QE-18, Feb (1982): 259-264.

Motoichi Ohtsu, Highly Coherent Semiconductor Lasers, 1st ed. (Boston: Artech, 1991).

K. Kikuchi, "Effect of 1/f -type FM Noise on Semiconductor Laser Linewidth Residual in High-power Limit," IEEE J. Quant. Electr. 25, #4, April 1989 (1989): 684-688.

Motoichi Ohtsu and Shinichi Kotajima, "Derivation of Spectral Width of a 0.8 micron AlGaAs Laser Considering 1/f Noise," Jap. J. Appl. Phys. 23, 6 (1984): 760-764.

F.L. Walls and DeMarchi A., "RF spectrum of a signal after frequency multiplication. Measurement and comparison with a simple calculation.," IEEE Trans. Instrum. Meas. IM-24, (1975): 210-217.

Roland Dr. Best, Phase-Locked Loops: Theory Design & Applications, 1st ed. (New York: McGraw-Hill Book Company, 1984).

Motorola, MECL DEVICE DATA (1985).

D. Welford and S.B. Alexander, "Magnitude and phase characteristics of frequency modulation in directly modulated GaAlAs semiconductor diode lasers," J. Lightwave Technol. LT-3, (1985): 1092-1099.

Masaaki Imai and Koji Kawakita, "Measurementt of direct frequency modulation characteristics of laser diodes by Michelson Interferometry," Appl. Opt. 29, 3 (1990): 348-353.

S.B. Alexander, D. Welford, and D.L Marquis, "Passive Equalization of Semiconductor Diode Laser Frequency Modulation," J. Lightwave Technol. 7, Jan (1989): 11-23.

William Egan, "Sampling Delay- Is it Real?," RF Design , Febuary (1991): 114-116.

Linlin Li, "The Optimal Loop Gain for the Spectral Linewidth Reduction in an Electrical Feedback Simeconductor Laser," IEEE J. of Quant. Electr. 27, 8 (1991): 1975-1980.

Allen Hill and Jim Surber, "The PLL Dead Zone and How to Avoid it," RF Design , March (1992): 131-134.

D. Hils and J.L. Hall, "Ultra-Stable Cavity-Stabilized Lasers with Subhertz Linewidth," in Frequency Standards and Metrology, ed. A. DeMarchi (Berlin,Hiedelberg: Springer-Verlag, 1989).

M.H. Anderson et al., "Observation of Bose-Enstein Condensation in a Dilute Atomic Vapor," Science 269, 14 July (1995): 198-201.

Y Millerioux et al., "Towards an accurate frequency standard at λ=778 nm using a laser diode stabilized on a hyperfine component of the Doppler-free two-photon transitions in rubidium," Opt. Commun. 108, May (1994): 91-96.

M. Kourogi, C.H. Shin, and M. Ohtsu, "A 134 MHz Bandwidth Homodyne Optical Phase-Locked Loop of Semiconductor Lasers," IEEE Photon. Techol. Lett. 3, 3 (1991): 270-272.

Y. Kotani et al., "Tunable DBR Laser with Wide Tuning Range," Electron. Lett. 24, 8 (1988): 503-505.

Peng, En T. et al.,"Properties of an external-cavity traveling-wave semiconductor ring laser" Opt. Lett 17, 1 (1992): 55-57

M.S. Wu, "Tunable micromachined vertical cavity surface emitting laser," Electron. Lett. 19, (1995): 1671.

"Stimulated Emission from Current Injected InGaN/AlGaN Diode," Coumpound Semiconductor Nov/Dec, (1995): 8.

J. Faist et al., "Quantum Cascade Lasers," Science 264, 22 April (1994): 553.

J. Faist et al., "Quantum Cascade Lasers: Temperature Dependence of the Performance Characteristics and High T0 Operaction," Appl. Phys. Lett. 65, 23 (1994): 2901.

G.B. Barwood, P. Gill, and W.R.C Rowley, "Frequency Measuremnets on Opticaly Narrowed Rb-Stabilized Laser Diodes at 780 nm and 795nm," Appl. Phys. B 53, (1991): 142-147.

G.B. Barwood, P. Gill, and W.R.C Rowley, "Optically Narrowed Rb-stabilized GaALAs Diode Laser Frequency Standards with $1.5*10^{-10}$ Absolute Accuracy," SPIE 1837, (1992): 262-270.

S. Ezekiel and R. Weiss, "Laser-Induced Fluorescence in a Moleculer Beam of Iodine," Phys. Rev. Lett. 20, (1968): 91-93.

A.D. White, "Frequency Stabilization of Gas Lasers," IEEE J. of Quant. Electr. QE-1, (1965): 349-357.

M.L. Skolnick and P.H. Lee, "Saturated Neon Absorption inside a 6238 A° Laser," Appl. Phys. Lett. 10, 11 (1967): 303.

G.R. Hanes and Dalhstrom C.E., "Iodine Hyperfine Structure Observed in Saturated Absorption at 633 nm," Appl. Phys. Lett. 14, 11 (1969): 362-364.

T.J. Quinn, "International Reports, Mise en pratique of the definition of the metre 1992," Metrologia 30, (1993/1994): 523-541.

O. Acef et al., "A CO_2 to visable optical frequency synthesis chain: accurate measurement of the 473 THz HeNe/I_2 laser," Opt. Commun. 97, March (1993): 29-34.

Kato Yoshiaki and B.P. Stoicheff, "Two-Photon absorption to highly exicted D states of Rb atoms," JOSA Letters 66, 5 (1976): 490-492.

K.C. Harvey and B.P. Stoicheff, "Fine Structure of the n^2D Series in Rubidium near the Ionization Limit," Phys. Rev. Lett. 38, 10 (1977): 537-540.

F. Nez et al., "Optical frequency determination of the hyperfine components of the 5s1/2-5D3/2 two-photon transitions in rubidium.," Optics CommunicationsJap. J. Appl. Phys. 102, (1993): 432-438.

F. Nez et al., "Precise Frequency Measurement of the 2S-8S/8D Transitions in Atomic Hydrogen: New Determination of the Rydberg Constant," Phys. Rev. Lett. 69, 16 (1992): 2326-2329.

D. Touahri et al., "LPTF Frequency Synthesis Chain: Results and Improvement for the Near Future," IEEE Trans. Instrum. Meas. 44, 2 (1995): 170-172.

J.-M Chartier and M. Winters, "Design of an Iodine Stabilized He-Ne Laser at 633 nm," (Joint Institute of Laboratory Astrophysics, 1982).

Andrew J. Wallard, "A Practical Aproach to the Design and Construction of Iodine Stabilized Lasers.," (National Physical Laboratory, 1979).

W.R.C. Rowley, "Frequency Dependence of a 633 nm He-Ne laser stabilized by $^{127}I_2$, upon iodine pressure, modulation amplitude, and wall temperature.," (National Physical Laboratory, 1981).

J.H. Shirley, "Modulation transfer process in optical heterodyne saturation spectroscopy," Opt. Lett. 7, 537-539 (1982).

J.J. Snyder et al., "High-sensitivity nonlinear spectroscopy using a frequency-offset pump," Opt. Lett. 5, 4 (1980): 163-165.

H.R. Xia et al., "Phase shifts and intensity dependence in frequency-modulation spectroscopy," JOSA B 11, 5 (1994): 721-730.

K. Evenson et al., Appl. Phys. Lett. 20, (1972): 133.

Ady Arie and Robert L. Byer, "Laser Heterodyne Spectrosocpy of 127I2 Hyperfine Structure near532 nm," JOSA B 10, 11 (1993): 1990-1997.

M.L. Eickhoff and J.L. Hall, " Optical Frequency Standard at 533 nm," IEEE Trans. Instrum. Meas. 44, 2 (1995): 155-158.

M.L. Eickhoff, "Two New Methods for Real-Time Precision Refractometery and Precise Test of the Hyperfine Hamiltonian via Modulation Spectroscopy of Moleculer Iodine at 532 nm" (Phd Thesis, University of Colorado, 1994).

M. Glaser, "An improved He-Ne at λ= 612 nm, stabilized by means of an external absorbtion cell," Metrologia 23, (1986): 45-53.

W.D. Lee et al., "Accuracy Evaluation of NIST-7," IEEE Trans. Instrum. Meas. 44, 2 (1995): 120-123.

J.L. Hall et al., "Optical heterodyne saturation spectroscopy," Appl. Phys. Lett. 39, 9 (1981): 680-682.

Rudolf Grimm and Jurgen Mlynek, "Light-pressure-induced nonliner dispersion in a Doppler-broadened medium: theory and experimental proposal," JOSA B 5, 8 (1988): 1655-1660.

Rudolf Grimm and Jurgen Mlynek, "Light-Pressure-Induced Line-Shape Asymmetry of the Saturation Dip in an Atomic Gas," Phys. Rev. Lett. 63, 3 (1989): 232-235.

Rudolf Grimm and Jurgen Mlynek, "The Effect of Resonant Light Pressure in Saturation Spectroscopy," Appl. Phys. B 49, (1989): 179-189.

O. Schmidt et al., "Cesium saturation spectroscopy revisited: How to reverse peaks and observe narrow resonances," Appl. Phys. B 59, (1994): 167-178.

Alan Gallagher, "Resonance broadening of the Hanle-effect signals in rubidium," Phys. Rev. A 10, 1 (1974): 231-241.

A.M. Akulshin et al., "Power Broadening of the Absorption Resonance on the D_2 Line of Rubidium," Opt. Commun. 77, 4 (1990): 295-298.

J.L. Hall and S.A. Lee, "Interferometeric real-time display of cw dye laser wavelength with sub-Doppler accuracy," Appl. Phys. Lett. 29, 6 (1976): 367-369.

J. J. Snyder et al., "LambdaMeter Resolution Enhancement using a novel Frequency Meter," Conf. on Laser Engineering & Optics (CLEO) , (1981).

P. Juncar et al., "Absolute determination of the wavelengths of the sodium D_1 and D_2 lines by using a cw tunable dye laser stabilized on iodine," Metrologia 17, (1981): 77-79.

P. Jungner et al., "Stability and absolute frequency of moleculer iodine transitions near 532 nm," (San Jose California: SPIE-The Society for Optical Engineering, 1995), 22-34.

E. Arimondo, M. Inguscio, and P. Violino, "Experimantal determinations of the hyperfine structure in the alkali atoms," Rev. Mod. Phys. 49, No 1 January (1977).

M. et al. Tetu, "Multiwavelength Sources Using Laser Diodes Frequency-Locked to Atomic Resonances," IEEE J. Lightwave Technol. 7, (1989): 1540-1548.

G.C. Bjorklund et al., "Frequency Modulation (FM) Spectroscopy Theory of Lineshapes and Signal-to-Noise Analysis," Appl. Phys. B 32, (1983): 145-152.

Hugo Wahlquist, "Modulation Broadening of Unsaturated Lorentzian Lines," The J. of Chem. Phys 35, 5 (1961): 1708-1710.

M. Kourogi, K. Nakagawa, and M. Ohtsu, "Wide span optical frequency comb generator for accurate optical frequency difference measurement," IEEE J. of Quant. Electr. 29, 10 (1993): 2693-2701.

M. Kourogi et al., "Limit of Optical-Frequency Comb Generation Due to Material Dispersion," IEEE J. of Quant. Electr. 31, Dec. (1995): 2120-2126.

Appendix A: $S_\phi(\omega)$ FOR TWO POLES AT ZERO

For the double pole high pass filter we take $S_v(\omega) = 2D\left(\omega^2 / \left(1 + \frac{b^2}{\omega^2}\right)^2\right)$:

which when plugged into the WK equation yields the need to do the first integral:

$$\text{integral} = 4D \cdot \int_0^\infty \frac{\omega^2 \sin\left(\frac{\omega\tau}{2}\right)}{(\omega^2 + b^2)^2} d\omega \qquad \text{Eq 1-1}$$

This results in

$$P_E(\omega) = \frac{1}{2\pi}\int_{-\infty}^{\infty} e^{-i\omega\tau} \exp\left[\frac{-D}{2b}\left(1 + e^{-b|\tau|} + b|\tau| e^{-b|\tau|}\right)\right] d\tau \qquad \text{Eq 1-2}$$

which is done by splitting the integral so that :

$$P_E(\omega) = \frac{1}{2\pi} e^{\frac{-D}{2b}} \int_{-\infty}^{\infty} e^{-i\omega\tau} e^{\frac{-D}{2b}\left(e^{-b|\tau|}\right)} e^{\frac{-D}{2b}\left(b|\tau| e^{-b|\tau|}\right)} d\tau \qquad \text{Eq 1-3}$$

Notice that P(ω) is the transform of the product of two functions which means that it is the convolution of the individual transforms. The first looks like the results from the previous one-pole problem except the common factor in the exponential is -D/2b instead of -D/b. Thus by analogy :

$$P_{E1}(\omega) = e^{\frac{-D}{2b}}\left\{\delta(\omega) + \frac{1}{2\pi}\left[\frac{2}{1!}\left(\frac{D}{2b}\right)\frac{b}{b^2 + \omega^2} + \frac{2}{2!}\left(\frac{D}{2b}\right)\frac{2b}{(2b)^2 + \omega^2} \cdots\right]\right\} \qquad \text{Eq 1-4}$$

The second part of the original integral:

$$P_{E2}(\omega) = \frac{1}{2\pi} e^{\frac{-D}{2b}} \int_{-\infty}^{\infty} e^{-i\omega\tau} \exp\left[\frac{-D}{2}|\tau| e^{-b|\tau|}\right] d\tau \qquad \text{Eq 1-5}$$

is done by first expanding the first exponential

$$P_{E2}(\omega) = \frac{1}{2\pi} e^{\frac{-D}{2b}} \int_{-\infty}^{\infty} e^{-i\omega\tau} \left(1 + \sum_{n=1}^{\infty} \frac{\left[\frac{-D}{2}|\tau| e^{-b|\tau|}\right]^n}{n!}\right) d\tau \qquad \text{Eq 1-6}$$

Then exchanging the summation and integration. It is worth evaluating the n=0 term at this point. Since 0!=1 the n=0 term evaluates to 1.

$$P_{E2}(\omega) = \frac{1}{2\pi} e^{\frac{-D}{2b}} \sum_{n=1}^{\infty} \frac{\left(-\frac{D}{2}\right)^n}{n!} \int_{-\infty}^{\infty} \left(e^{-i\omega\tau} \left([|\tau|^n e^{-bn|\tau|}] + 1\right) d\tau\right) \qquad \text{Eq 1-7}$$

We take advantage of the fact that both $P_E(\omega)$ and $R(\tau)$ are defined to be real and symmetric about their origins. This allows us to remove the absolute value signs on τ and change the limit of integration on the transform.

$$P_{E2}(\omega) = \frac{1}{\pi} e^{\frac{-D}{2b}} \sum_{n=1}^{\infty} \frac{\left(-\frac{D}{2}\right)^n}{n!} \int_{0}^{\infty} e^{-i\omega\tau} \left([\tau^n e^{-bn\tau}] + 1\right) d\tau \qquad \text{Eq 1-8}$$

The integration is done by *MATHEMATICA* assuming that b, D are greater then zero and the n is an integer. It should also be noted that $\Gamma(1+n)$ is n! and that the integral transform of 1 is $\delta(\omega)$

$$\int_0^{\infty} e^{-i\omega\tau} [\tau^n e^{-bn\tau}] d\tau = \frac{1}{\left(1 + \left(\frac{\omega}{bn}\right)^2\right)^{\frac{n+1}{2}}} \cdot \frac{\left(\cos\left[(1+n)\operatorname{atan}\left(\frac{\omega}{bn}\right)\right] \cdot \Gamma(1+n)\right)}{(bn)^n} \qquad \text{Eq 1-9}$$

This leads to the result that second part of the integration is :

$$P_{E2}(\omega) = \frac{1}{\pi} e^{\frac{-D}{2b}} \left\{ \delta(\omega)\pi + \sum_{n=1}^{\infty} \left(-\frac{D}{2}\right)^n \left(\frac{\left(\cos\left[(1+n)\,\mathrm{atan}\left(\frac{\omega}{bn}\right)\right]\right)}{\left(1+\left(\frac{\omega}{bn}\right)^2\right)^{\frac{n+1}{2}} \cdot (bn)^n} \right) \right\} \qquad \text{Eq 1-10}$$

$$P_{E2}(\omega) = e^{\frac{-D}{2b}} \left\{ \delta(\omega) + \frac{1}{\pi} \sum_{n=1}^{\infty} \left(-\frac{D}{2b}\right)^n \left(\frac{\left(\cos\left[(1+n)\,\mathrm{atan}\left(\frac{\omega}{bn}\right)\right]\right)}{\left(1+\left(\frac{\omega}{bn}\right)^2\right)^{\frac{n+1}{2}} \cdot (n)^n} \right) \right\} \qquad \text{Eq 1-11}$$